2017

Energy efficient planning and operation models for wireless cellular networks

Ahmad Alsharoa
Iowa State University

Energy efficient planning and operation models for wireless cellular networks

by

Ahmad Alsharoa

A dissertation submitted to the graduate faculty

in partial fulfillment of the requirements for the degree of

DOCTOR OF PHILOSOPHY

Co-majors: Electrical Engineering; Computer Engineering

Program of Study Committee:
Ahmed E. Kamal, Major Professor
Zhengdao Wang
Sang W. Kim
Daji Qiao
Mingyi Hong

The student author and the program of study committee are solely responsible for the content of this dissertation. The Graduate College will ensure this dissertation is globally accessible and will not permit alterations after a degree is conferred.

Iowa State University

Ames, Iowa

2017

DEDICATION

I would like to dedicate this thesis to my big family; my father, mother, brother and sisters. Specially to my father who inspired me with his thoughts and wisdom, who gave me a good example on how to live with respect in this life and to my mother who brought me virtue, and from her I learned the principles of modesty, tolerance, and kindness to all people.

I would also like to dedicate this thesis to my small family; to my wife for her constant love, support, and patience and to my children, Mustafa and Ghina, you have made me stronger and more fulfilled than I could have ever imagined.

I would also like to thank my friends for their constant support during writing this thesis.

TABLE OF CONTENTS

LIST OF TABLES

LIST OF FIGURES

LIST OF ABBREVIATIONS

AF	Amplify-and-Forward
AM	Active Mode
AWGN	Additive White Gaussian Noise
BB	Branch and Bound
BLP	Binary Linear Programming
BPSO	Binary Particle Swarm Optimization
BS	Base Station
CR	Cognitive Radio
CSI	Channel State Information
CU	Cognitive User
DBS	Drone Base Station
DF	Decode-and-Forward
D2D	Device-to-Device
EH	Energy Harvesting
GA	Genetic Algorithm
GG	Green Grid
QoS	Quality of Service
GP	Geometric Programming
GWO	Grey Wolf Optimizer
i.i.d	Independent and identical distribution
KKT	Karush-Kuhn-Tucker
LoS	Line of Sight
MBS	Micro Base Station
MIMO	Multi-Input Multi-Output

NLoS	Non-Line of Sight
OWR	One-Way Relaying
PSO	Particle Swarm Optimization
PL	Path Loss
PS	Power Splitting
PU	Primary User
RE	Renewable Energy
RF	Radio Frequency
SBS	Small Base Station
SCA	Successive Convex Approximation
SM	Sleep Mode
SNR	Signal-to-Noise Ratio
SVD	Singular Value Decomposition
TG	Traditional Grid
TS	Time Switching
TWR	Two-Way Relaying
UAV	Unmanned Aerial Vehicle

LIST OF SYMBOLS

$\in$	Set membership operator
f_c	carrier frequency
λ_0	Wavelength
$\mathbb{E}[.]$	Expectation function
$(.)^T$	Transpose operator
$(.)^H$	Hermitian operator
$Tr(.)$	Trace function
$(x)^+$	Maximum between x and zero
$\log(.)$	Logarithm function
$\Gamma(.)$	Gamma function
$\varrho(.)$	Monomial function
$\min(x, y)$	Minimum between x and y
$\max(x, y)$	Maximum between x and y
$\underset{a}{\text{minimum}}(.)$	Minimum of a set or function with respect to a
$\underset{a}{\text{maximum}}(.)$	Maximum of a set or function with respect to a
argmin(.)	The argument of minimum
argmax(.)	The argument of maximum
$\lvert.\rvert$	Absolute value of a function or cardinality of a set
$\mathbb{C}$	Complex number
$\mathbb{R}$	Real number
N_0	Noise power density
L_R	Number of relays
L_M	Number of micro base stations
L_S	Number of small base stations

M	Number of antennas
W_x	Bandwidth allocated to node x
$\boldsymbol{V}_x$	Unitary precoder matrix at node t
$\boldsymbol{U}_x$	Unitary decoder matrix at node t
$\boldsymbol{\Lambda}_A$	diagonal matrices with square roots of the eigenvalues of matrix A
$\boldsymbol{w}$	Relay amplification gain
$\boldsymbol{h}_{xy}$	Channel gain between x and y
$\boldsymbol{h}_{xy}^{b}$	Channel gain between x and y during time b
d_{xy}	Euclidean distance between x and y
ϖ	Path loss exponent
$\mathcal{S}$	initial population set
N	Number of random particles
$\boldsymbol{\mathcal{N}}$	Particle positions
$\boldsymbol{\nu}$	Particle velocity
q	Algorithm iteration
ψ_0	Inertia weight
c_1,c_2	Particle step size
r_{rand}	Pseudo-random number
Ψ_{BPSO}	Sigmoid function for transforming the velocity to probabilities
$I_{\max}$	Maximum number of iteration
y_x	Received signal at node x
R_0	Target data rate
R_{p_x}	Data rate of primary user x
R_{c_x}	Data rate of cognitive user x
$\bar{P}_p$	Primary user power budget
$\bar{P}_c$	Cognitive user power budget
P_{p_x}	Transmit power of primary user x
P_{c_x}	Transmit power of cognitive user x

η_{rf}	RF energy conversion efficiency
η_{re}	RE energy conversion efficiency
η_x	RF energy conversion efficiency at node x
ρ	Time switching ratio
μ	Power splitting ratio
Φ	Renewable energy arrival rate
$f(\varphi)$	Probability density function of RE
ϵ_x^b	Binary variable indicates the selection of node x during time b
π_x^b	Binary variable indicates the switching ON/OFF of node x during time b
α_x	Scale power consumption of node x
β_x	Offset of site power of node x
γ_x	Sleep power consumption of node x
H_x^b	Harvested energy at node x during time b
S_x^b	Stored energy at node x at the end of time b
S_x^0	Initial stored energy at node x
E_x^b	Consumed energy at node x during time b
E_{le}	Leakage energy
Υ_x^b	Signal-to-Noise Ratio at node x during time b
R_x^b	Total data rate of node x during time b
$\bar{S}_x$	Maximum stored energy at node x
U^b	Total number of users in the network during time b
$\bar{U}_x$	Maximum number of users that can be served by x
D	Number of drones
Z_D	Number of drone's possible locations
P_{hov}	Drone's hovering power consumption
P_{har}	Drone's hardware power consumption
P_s	Drone's static power consumption
P_{full}	Drone's hardware power consumption when the drone is moving at full speed

P_f	Drone's flying power consumption
m_{tot}	Mass of the drone
r_p	Radius of the drones propellers
$v_{\max}$	Maximum drone's speed
v_d	Drone's speed
ρ_a	Air density
$T_f(j,i)$	Flying time from location i to j
$T_r(j,i)$	Remaining time from location i to j
T_c	Coherence time
T_b	Time slot period

ACKNOWLEDGEMENTS

In the name of Allah, the most merciful, the most beneficent. All praise and thanks for Allah, the Lord of the universe, for helping me to complete this thesis.

I would like to take this opportunity to express my thanks to those who helped me with various aspects of conducting research and the writing of this thesis. First and foremost my supervisor Prof. Ahmed E. Kamal for his support, patience, and guidance in almost every step throughout my thesis.

I would also like to thank my committee members for their constructive comments and suggestions to this work: Prof. Zhengdao Wang, Dr. Sang W. Kim, Dr. Daji Qiao, and Dr. Mingyi Hong.

Besides, I would like to thank Prof. Mohamed-Slim Alouini from King Abdullah University of Science and Technology (KAUST), Dr. Abdullah Kadri and Dr. Hakim Ghazzai from Qatar Mobility Innovations Center (QMIC), Qatar University, for their constant help and productive advices that contributed in making this thesis a successful one.

ABSTRACT

Prospective demands of next-generation wireless networks are ambitious and will require cellular networks to support 1000 times higher data rates and 10 times lower round-trip latency. While this data deluge is a natural outcome of the increasing number of mobile devices with data hungry applications and the internet of things (IoT), the low latency demand is required by the future interactive applications such as "tactile internet", virtual and enhanced reality, and online internet gaming, etc.

The motivation behind this thesis is to meet the increasing quality of service (QoS) demands in wireless communications and reduce the global carbon footprint at the same time. To achieve these goals, energy efficient planning and operations models for wireless cellular networks are proposed and analyzed.

Firstly, a solution based on the overlay cognitive radio (CR) along with cooperative relaying is proposed to reduce the effect of the scarcity problem of the radio spectrum. In overlay technique, the primary users (PUs) cooperate with cognitive users (CUs) for mutual benefits. The achievable cognitive rate of two-way relaying (TWR) system assisted by multiple antennas is proposed. Compared to traditional relaying where the transmission to exchange two different messages between two sources takes place in four time slots, using TWR, the required number of transmission slots reduces to two slots. In the first slot, both sources transmit their signals simultaneously to the relay. Then, during the second slot the relay broadcasts its signal to the sources. Using an overlay CR technique, the CUs are allowed to allocate part of the PUs' spectrum to perform their cognitive transmission. In return, acting as amplify-and-forward (AF) TWR, the CUs are exploited to support PUs to reach their target data rates over the remaining bandwidth. A meta-heuristic approach based on particle swarm optimization algorithm is proposed to find a near optimal resource allocation in addition to the relay amplification matrix gains. Then, we investigate a multiple relay selection scheme for energy harvesting (EH)-based

on TWR system. All the relays are considered as EH nodes that harvest energy from renewable and radio frequency sources, where the relays forward the information to the sources. The power-splitting protocol, in which the receiver splits the input radio frequency signal into two components: one for information transmission and the other for energy harvesting, is adopted at the relay side. An approximate optimization framework based on geometric programming is established in a convex form to find near optimal PS ratios, the relays transmission power, and the selected relays in order to maximize the total rate utility over multiple time slots. Different utility metrics are considered and analyzed depending on the level of fairness.

Secondly, a downlink resource and energy management approach for heterogeneous networks (HetNets) is proposed, where all base stations (BSs) are equipped to harvest energy from renewable energy (RE) sources. A hybrid power supply of green (renewable) and traditional micro-grid, such that the traditional micro-grid is not exploited as long as the BSs can meet their power demands from harvested and stored green energy. Furthermore, a dynamic BS switching ON/OFF combined with the EH model, where some BSs are turned off due to the low traffic periods and their stored energy in order to harvest more energy and help efficiently during the high traffic periods. A binary linear programming (BLP) optimization problem is formulated and solved optimally to minimize the network-wide energy consumption subject to users' certain quality of service and BSs' power consumption constraints. Moreover, green communication algorithms are implemented to solve the problem with low complexity time.

Lastly, an energy management framework for cellular HetNets supported by dynamic drone small cells is proposed. A three-tier HetNet composed of a macrocell BS, micro cell BSs (MBSs), and solar powered drone small cell BSs are deployed to serve the networks' subscribers. In addition to the RE, the drones can power their batteries via a charging station located at the macrocell BS site. Pre-planned locations are identified by the mobile operator for possible drones' placement. The objective of this framework is to jointly determine the optimal locations of the drones in addition to the MBSs that can be safely turned off in order to minimize the daily energy consumption of the network. The framework takes also into account the cells' capacities and the QoS level defined by the minimum required receiving power. A BLP problem is formulated to optimally determine the network status during a time-slotted horizon.

CHAPTER 1. INTRODUCTION

1.1 Background

Frequency spectrum is expected to become more congested in next-generation wireless communications to accommodate the increasing demand of mobile data traffic [1]. Fig. 1.1, which is based on June 2015 report by the Brattle Group, shows the current bandwidth crunch facing the United States [2]. It concludes that at least around 500 MHz of spectrum would be needed by 2019 to meet minimum bandwidth demands.

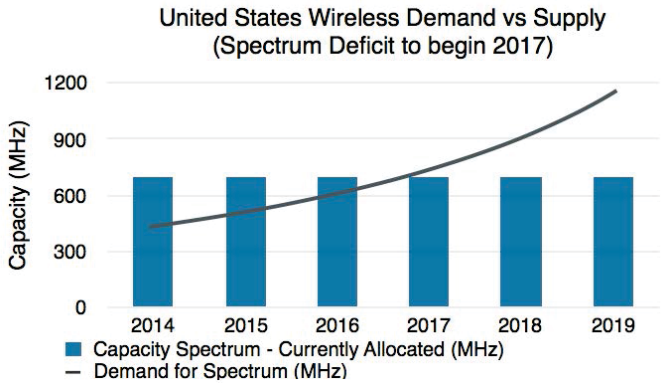

Figure 1.1: Bandwidth crunch or spectrum deficit in United States [2].

On the other hand, overall mobile data traffic is expected to grow to 49 exabytes per month by 2021, a sevenfold increase over 2016 [3]. Mobile data traffic will grow at a compound annual growth rate of 47 percent from 2016 to 2021 as shown in Fig. 1.2.

The cellular infrastructure currently contributes approximately two percent of carbon footprint and three percent of worldwide energy consumption, as a result of more than three million

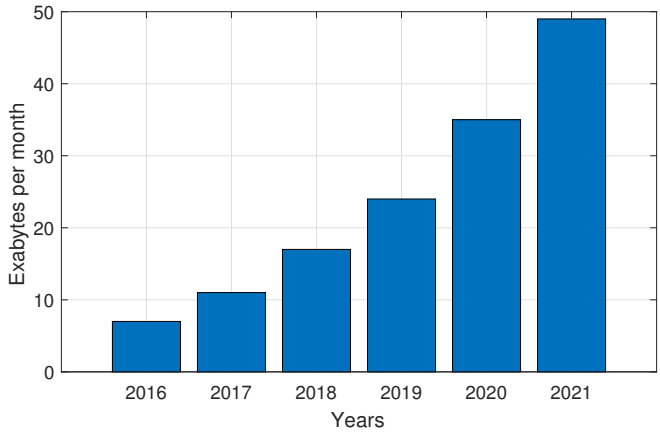

Figure 1.2: Cisco forecasts 49 exabytes per month of mobile data traffic by 2021 [3].

base stations (BSs) worldwide [4]. Also noting that the carbon emissions of information and communication technologies (ICT) is predicted to increase from 170 metric-tons in 2014 to 235 metric-tons by 2020 [5], these statistics led telecom industry, governmental institutions, and researchers to initiate green measures.

To meet these growing demands, efficient methods are required for spectrum sharing among different systems, services, and applications in a dynamic wireless access environment. Several schemes including cognitive radio (CR), cooperative communication, multi-input multi-output (MIMO) antennas, green communication, and energy harvesting (EH) have been considered as promising solutions to boost network coverage and capacity while reducing operational and capital expenditures of mobile operators.

1.1.1 Cognitive Radio (CR)

Increasing demand for wireless services such as mobile, smart devices, and many other devices is expected to lead to a deficit problem in radio spectrum. Fig. 1.3 shows measurements taken in downtown Berkeley which reveal a typical utilization in the 3 to 6 GHz frequency band. The graph shows usage over a very short period of time and represent the power spectral density of the received 6 GHz wide signal collected for a span of 50s sampled at 20 GS/s [6].

CR is proposed as an intelligent novel approach to spectrum deficit problem [7]. The basic idea of CR is that cognitive users (CUs), which are known as unlicensed users and also secondary

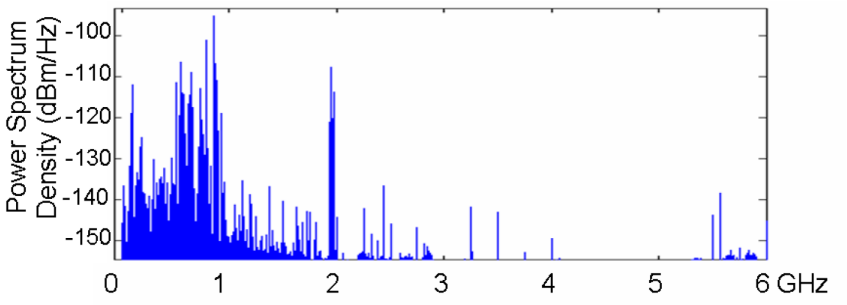

Freq (GHz)	0~1	1~2	2~3	3~4	4~5	5~6
Utilization(%)	54.4	35.1	7.6	0.25	0.128	4.6

Figure 1.3: Spectrum utilization measurement at Berkeley wireless research center [6].

users (SUs), are allowed to utilize the spectrum of primary users (PUs), which are known as licensed users, in an opportunistic manner. CR can be grouped into three main categories: interweave, underlay, and overlay [8]. The original idea of CR was proposed by Joseph Mitola III and Gerald Q. Maguire Jr in late 1990s and based on the interweave technique, in which, the CU is allowed to access the primary spectrum only when the PU is idle [9]. To protect the PUs from CUs interference, CUs are required to sense the spectrum periodically in order to utilize the spectrum holes as shown in Fig. 1.4 [10]. In the underlay technique, CUs access the spectrum simultaneously with PUs under some interference limitation constraints to maintain a certain primary quality-of-service (QoS) [11], while the CUs might be subjected to a non-limited interference caused by the PUs [12],[13]. Two different modes of underlay are reported in the literature and these are named X model and Z model. In the X model, both the interference from PU to CU and CU to PU are considered, while in the Z model, which is considered an upper limit of the Z model, only the interference from CU to PU is taken into account. In the overlay technique, CUs are allowed to use a part of their resources to enhance the primary signal. The PUs reciprocate by releasing some bandwidths for CUs data transmission [14]. This technique can be exploited together with cooperative relaying techniques i order to enhance the system performance.

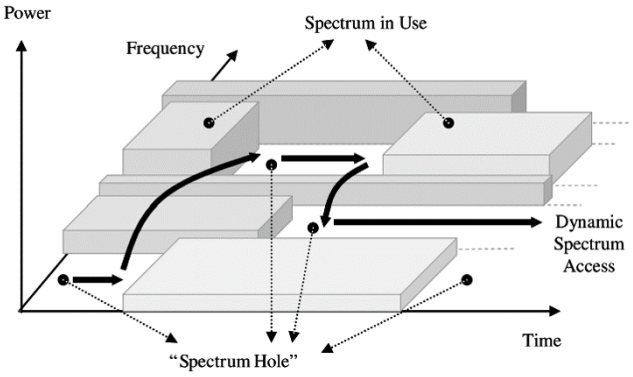

Figure 1.4: The concepts of white space and dynamic spectrum access [10].

1.1.2 Cooperative Relaying

Relay techniques were proposed to increase the overall system throughput, extend the network coverage area, and reduce the transmission powers, hence, decrease the interference power to neighboring networks. In addition to that, in some cases, absence of the direct link between terminals can be covered by relays by maintaining the communication link between the terminals [15]. Two-way relaying (TWR) has lately attracted a lot of attention in the literature. In conventional TWR, exchanging different messages between two terminals takes place in two phases only instead of four phases in the traditional one-way relaying (OWR) as shown in Fig. 1.5. In the first phase, the users transmit their signals simultaneously to the relays. Subsequently, in the second phase, the relays broadcast the signal to the users [16]. Two widely relay strategies are used in practice: namely amplify-and-forward (AF) strategy, where the relay amplifies the received signal before broadcasting it to the destination, and decode-and-forward (DF) strategy, where the relay decodes the received signal to remove the noise before transmitting a clean copy of the original signals to the destinations [17].

In this thesis, AF strategy is used due to its low computational complexity and low delay in the relay node (i.e., AF allows faster transmission without processing delay). Moreover, AF requires much less computing power compared to other strategies [18]. The performance of the network can be further improved by employing MIMO antennas that provide extra spatial dimensions [18],[19],[20].

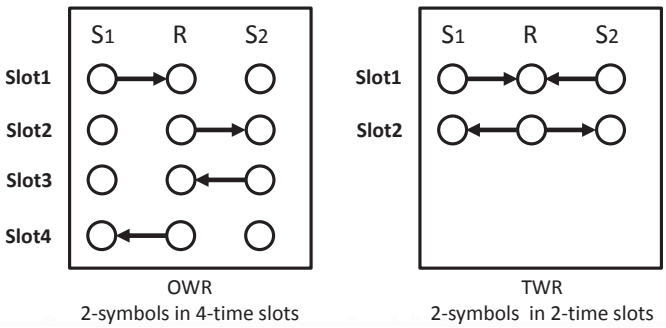

Figure 1.5: Two-way relaying versus one-way relaying.

1.1.3 Energy Harvesting (EH)

There is currently a considerable interest in the EH technique as one of the most robust methods to perpetuate the lifetime and sustainability of wireless systems [21],[22]. Many promising practical applications that can exploit this technique have been discussed recently, such as emerging ultra-dense small cell deployments, point-to-point sensor networks, far-field microwave power transfer, and dense wireless networks [23].

One of the advantages of such techniques is to cope with the issues related to the supply of wireless devices located in remote or inaccessible areas such as sensors placed in forests or mountains where replenishing a new battery or recharging it using the fact that traditional wired techniques is not always possible. In addition, EH techniques, which are also known as energy scavenging techniques, enables networks' owners to behave green towards the environment [24] as the devices will be powered by non-polluting alternative sources such as solar, wind, thermoelectric, or vibration [25]. Recently, radio frequency (RF)-based EH, which is known as wireless energy transfer (WET), has been introduced as an effective harvesting technology where energy is collected from RF signals generated by other neighbor devices. Unlike the other renewable energy (RE) sources, the radio frequency energy is widely available in the ambient atmosphere all the time [26].

There are mainly two types of RF sources. Ambient RF sources (ARFSs), where the harvested energy comes from static nearby RF transmitters such as cellular base stations and TV/radio towers or dynamic RF transmitters such as mobile devices, and dedicated RF sources (DRFSs) where the harvested energy coming from deployed and dedicated sources in order to

supply energy to network devices when needed. In the latter case, the output power of DRFSs must be permitted by FCC [26].

The RF protocols can mainly be classified into two protocols [27]. The time switching (TS) protocol where the EH node switches over time between the energy harvester equipment and the information decoder, and the power splitting (PS) protocol where a portion of the received signal is used for EH and the remaining for the information processing. Along with both protocols, three approaches can be employed for the energy and transmission management [28]. The first one consists of using the harvested energy without storing it for future use. It is known as the *harvest-and-use* approach. In the second one, known as *harvest-use-store* approach, the harvested energy is instantaneously consumed according to the system need while the remaining energy is stored for future use. The third approach, which is considered in this paper, named as *harvest-store-use*, consists of partially or totally storing the harvested energy before using it in the future.

1.1.4 Heterogenous Networks (HetNets)

With the increasing number of mobile broadband data users and bandwidth-intensive services, the demand for radio resources has increased tremendously. One of the methods used by mobile operators to meet this challenge is to deploy additional low-powered BSs (such as smallcell BSs (SBSs) and Microcell BSs (MSBs)) in areas of high demand as shown in Fig. 1.6. The resulting networks, referred to heterogeneous networks (HetNets), help in maintaining the QoS for a larger number of users by reusing the spectrum [29]. However, with the densification of these HetNets, energy consumption and the carbon footprint have significantly raised. Therefore, conserving energy while meeting the users QoS requirements has been the focus of the green communications researchers.

Most of the wireless data usage is in indoor environments such as offices, residential buildings, shopping malls, etc., where the users may face difficulties in achieving high data rates while connecting to the macrocell BSs. This is mainly due to the penetration loss incurred by the wireless signals inside the buildings. Therefore, to increase the capacity of the network in these hotspots, SBSs are deployed in close proximity to the buildings [30].

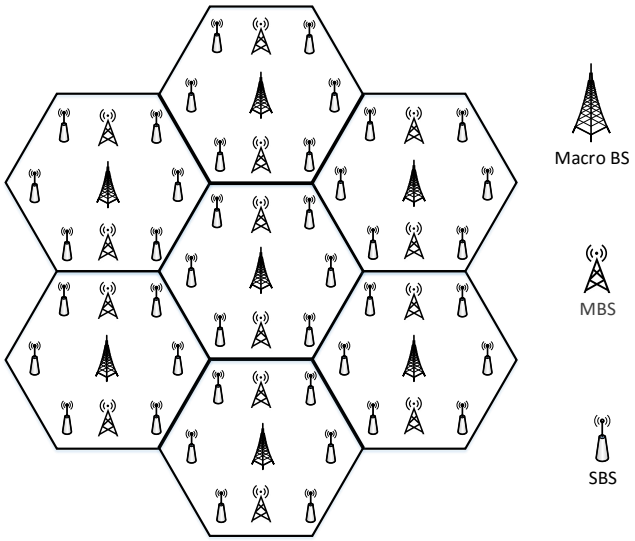

Figure 1.6: Heterogenous networks.

In general, MBSs and SBSs provide increased coverage and network capacity during peak times. However, they might not be very useful under light traffic load scenarios. Instead, they might be under-utilized or completely redundant leading to inefficient use of energy and communication resources. Hence, dynamic BS ON/OFF switching, which is known as BS sleeping strategy, is shown to be highly useful in reducing energy consumption of cellular HetNets [31]. The BSs are turned off during periods of low traffic and the small number of active users are offloaded to a nearby BS. As a result, the power consumption of lightly loaded BSs can be reduced or completely eliminated depending on the state of the turned off BSs.

1.1.5 Drone-based Communication

With the rapid growth of drones market, drone-based communication has been considered as a promising and effective solution to many of today's challenges in the area of wireless communications due to the low cost and fast deployment of drones and autonomous motion without human intervention. Recently, drones, which are also known as unmanned aerial vehicles (UAVs), are proposed to be used as SBSs to support ground cellular networks has received considerable attention [32],[33]. A drone BS (DBS) can act as an aerial BS characterized by a quick and dynamic deployment which is extremely helpful for various scenarios [34]. For

instance, in public safety communication, where ground infrastructure is damaged by natural disasters, DBSs represent an alternative solution for mobile operators to maintain coverage and connectivity. In fact, DBSs are more robust against such environmental changes thanks to their mobility. DBSs are also useful for temporary/unexpected high traffic demand situations where already deployed infrastructure becomes overloaded and requires additional communication equipment to maintain the high QoS level. For example, in big events such as football games, Olympic games, or concerts, it is infeasible from economical perspective to invest in the ground infrastructure for a relatively short time period. In this context, many companies have developed prototypes for LTE DBSs such as Nokia, AT&T, Qulacomm, Intel [35],[36]. For instance, Nokia has showcased its newly developed LTE DBS at the UAE Drones for Good (D4G) Award event in Dubai, UAE this year, as shown in Fig. 1.7 [37]. This new technology provides centralized monitoring and control of DBSs via an operators existing LTE network or dedicated LTE network.

Figure 1.7: Nokia LTE DBSs in Drones for Good (D4G) Award event [37].

The placement of DBSs is considered as one of the main challenges in drone-based communications [38],[39] particularly in the case of multiple DBSs. Optimizing the DBS movement and locations can significantly enhance the network performance either by reducing the load of other ground BSs or by covering areas with limited radio access. Another challenging issue in drone-based communications is the power management of these battery limited DBSs since traditional wired charging methods are not feasible. Therefore, EH techniques can be considered

as some of the most effective and robust solutions to protract the lifetime and sustainability of drones' batteries. In drone-based communications, EH can be an attractive technology to power DBSs by offering additional energy to charge their batteries [40].

1.2 Thesis Scope and Contributions

The thesis deals with energy efficient planning and operation of wireless communication and develops algorithms to achieve theses objectives. The main contribution of this dissertation to the insight and design of energy efficient models of wireless cellular networks are as follows

1. In Chapter 3, the problem of the resource allocation for TWR-MIMO overlay cognitive networks using multiple AF relays is investigated. The contributions of the first chapter can be summarized as follows:

    - Formulating an optimization problem that maximizes the TWR-MIMO overlay cognitive rate utility while taking into account all transceivers power budgets in addition to the PU QoS requirements. In this framework, it is assumed that each CU is allowed to share the primary bandwidth in order to perform its transmission. In return, they assist the PUs transmissions by amplifying and forwarding the PUs data over the remaining bandwidth.
    - Due to the non-convexity of the problem, we firstly derive expressions of the transmit powers allocated to primary and cognitive users for a fixed user bandwidth and relay amplification gain. Then, we employ a meta-heuristic approach based on particle swarm optimization (PSO) algorithm to find a near optimal CU bandwidth allocation in addition to the relay amplification matrix gains.
    - Considering different cognitive objective functions depending on the level of fairness among CUs.
    - Finally, analyzing the scheme's performance under different system parameters and comparing the proposed algorithm in terms of convergence speed and computational complexity with a recently proposed heuristic approach entitled the grey wolf optimizer (GWO) [41].

2. In Chapter 4, the idea of EH with TWR system are combined. Unlike the model of Chapter 3, all relays are equipped with EH devices and only a subset of the relays can be selected to maintain communication. The contributions of this chapter can be summarized as follows:

   - Formulating an optimization problem that maximizes the rate utility of the EH TWR system over a certain number of time slots while respecting the power budget and the storage capacity constraints at each relay. This is performed by determining, for each relay, its active or idle status, the fraction of signals to be harvested, and the amplification gain to be allocated for the second phase. In this context, some of the relays can be switched to the idle mode such that they do not participate in the broadcasting process but continue harvesting energy from other transmitting (i.e., active) relays.
   - Due to the non-convexity of the problem, we propose to employ a joint-optimization approach to optimize the system parameters. A binary particle swarm optimization (BPSO) algorithm is adopted to find the set of active relays selected for data transmission.
   - To optimize the other decision variables, we implement a geometric programming (GP) technique allowing us to achieve an approximate solution to the problem [42].
   - The performance of the proposed EH TWR approach is compared to that of the branch-and-bound (BB) solution in addition to the dual problem-based solution.

3. In Chapter 5, EH for downlink communication in HetNets is considered where each BS is equipped to harvest from RE. Moreover ON/OFF switching strategy is used to reduce the total energy consumption. The contribution of this chapter can be summarized as follows

   - Considering a hybrid power supply consisting of green (renewable) and traditional micro-grid, such that traditional micro-grid is not exploited as long as the BSs can meet their power demands from harvested and stored green energy.

- Formulating an optimization problem with the objective of minimizing the network-wide energy consumption over a given time horizon. The goal is to optimize the BS sleeping and user-cell association variables under BS's maximum power constraint, maximum BS's storing energy constraint, and user's QoS constraint.
- Two cases depending on the knowledge level about future RE generation are investigated:
  (a) The zero knowledge case: in this case, future RE generation statistics are unknown for the mobile operator. A binary linear programming (BLP) problem is formulated to optimize the BS sleeping status and user-cell association.
  (b) The perfect knowledge case: this case assumes that the all future statistics of the network are perfectly known and estimated.
- Proposing a low complexity green optimization approach based on BPSO algorithm to find a near optimal solution and comparing its performance with the well known evolutionary genetic algorithm (GA) [43].

4. Finally, in Chapter 6, a drone-based communication problem is addressed from a new perspective by investigating the placement of multiple EH DBSs in order to support typical HetNets composed of a single macrocell BS and multiple ground MBSs. The proposed method can be generalized to the context of large-scale HetNets. It is assumed that each drone can charge its battery either using traditional electric energy when it is placed in a charging station located at the macrocell BS site or using RE harvested through solar panels placed on top of the drones [44],[45]. The objective of the framework is to exploit the mobility and quick deployment of these solar-powered drones to support the ground cells whenever it is needed and whenever the drones' batteries permit it. Inactive drones, which are originally placed at the charging station, will be directed to fly to particular locations to serve users and support the overloaded HetNet or replace lightly loaded MBSs during a short period of time. In the latter case, the MBSs can be safely turned off to reduce fossil fuel consumption. For realistic deployment of the drones, a finite set of pre-planned possible locations known by the mobile operator is considered.

At these locations, the drones can land and serve the users under their coverage. We aim to optimize the spatial and temporal management of these multiple drones under different traffic and situations. Moreover, since the RE is random in nature, we develop a stochastic programming solution to deal with this source of uncertainty. The main contributions of this chapter can be summarized as follows:

- Formulating an optimization problem that aims to minimize the total fossil fuel consumption of the drones-assisted HetNet. The objective is to support the network operation by employing multiple drones as flying BSs to be placed at specific potential pre-planned locations.
- The green operation of the HetNet is investigated while taking into account several factors including a QoS metric, the cells' capacity, drones' battery limit, photovoltaic generation at the drone levels, and the power consumption related to drones' mobility.
- This green framework involves the application of the ON/OFF switching strategy to the MBSs whenever it is possible. A joint optimization solution is proposed for drones' placement and MBSs deactivation during a long period of time.
- Three cases depending on the knowledge level about future RE generation are investigated:
  (a) The zero knowledge case: in this case, future RE generation statistics are unknown for the mobile operator. A BLP problem is formulated to determine the HetNet and drone statuses based on past and present realizations.
  (b) The perfect knowledge case: this case assumes that all future statistics of the network are perfectly known and estimated. A non-linear programming problem is formulated to determine the future deployment strategies for the drones. To reduce its complexity, a linearization approach is employed to transform the problem into a BLP optimization problem.
  (c) The partial knowledge case: in this case, only partial statistics of the future RE generation are known, i.e., probability density function. To deal with the

uncertainty effect, a stochastic programming problem is formulated and solved using the two-stage recourse method. In this case, the uncertainty effect is also considered.

1.3 Thesis Organization

The rest of the thesis is organized as follows:

Chapter 2 includes most recent related works.

Chapter 3 investigates the problem of bandwidth and power allocation for TWR-MIMO overlay cognitive networks using multiple AF relays.

Chapter 4 studies the multiple relay selection of TWR-AF scheme with PS protocol over a certain number of time horizon while respecting the power budget and the storage capacity constraints at each relay.

Chapter 5 studies the problem of the resource management using BS sleeping strategies in EH-based downlink transmission over a certain time horizon.

Chapter 6 proposes a mobility and quick deployment of solar-powered drones to support the ground cells whenever it is needed and whenever the drones' batteries permit it.

Chapter 7 concludes the thesis and outline its main contributions in Section 7.1. Some potential open problems and possible future works are then presented in Section 7.2.

CHAPTER 2. RELATED WORKS

Before going into the details of our proposed energy efficient planning and operation models, some recent related works are stated in this chapter.

2.1 Overlay Cognitive Radio with Cooperative Communications

The leasing model, which is also called property rights model, can be categorized into two categories: spectrum leasing and time leasing. Under spectrum leasing, PUs who own the spectrum can possibly lease part of the spectrum to CUs for appropriate remuneration and can exploit the existence of CUs to enhance their performance and QoS. In return, CUs can use the leased spectrum for their own transmission by performing decentralized power control [46],[47]. On the other hand, for time leasing, PUs can lease a portion of their time for CUs' transmission. In return, in the remaining time, CUs help the PUs to enhance their performance. Indeed, under time leasing, data transmission takes place in three time slots, in the first time slot PUs transmit their signals to CUs, while in the second time slot CUs broadcast the primary signal to the primary destination, and finally the CUs use the remaining time slot for their own transmission [48],[49]. In this thesis, the "*overlay*" model term is used to indicate the spectrum leasing model.

The overlay CR technique has been introduced in the literature as a solution to enhance the spectral efficiency of primary transmissions while exploiting the existence of CUs [50]. Most of the studies model CUs as OWR that decode the primary signals, then broadcast it to the destination in order to improve the system reliability. This operation requires the knowledge of the primary user's data sequence and/or codebook [50]. Furthermore, in overlay CR, CUs need to know the primary channel gains in addition to encoding techniques if they

will decode the primary signal. However, compared to interweave and underlay CR, overlay offers the possibility to freely transmit their signals without any constraints in terms of time and transmitted power. It just requires that PUs know the existence of overlaying cognitive relays in order to coordinate their transmissions. Note here that the priority is given to PUs in contrast with the non-cognition case where relays have the unique role of forwarding the primary signals.

Few papers have employed TWR systems with overlay CR technique [51],[52],[53],[54],[55]. These studies assume that the PUs are not within the communication range of each other and utilize CU relays to forward their signals simultaneously. This scenario overcomes the hidden terminal problem which happens when the PUs are shadowed or are in severe multipath fading. In return, CUs are allowed to share a part of the primary bandwidth to perform their communication. This spectrum sharing scenario might involve some form of coordination and cooperation between the two types of users (i.e., PUs and CUs), mainly when this cooperation is optimized. For instance, this can be implemented when all users belong to the same network as suggested in [51]. The authors have considered a device-to-device (D2D) communication scenario overlaying a cellular network where D2D users, playing the role of CUs, communicate bi-directionally with each other while assisting the two-way communications between a cellular user and its BS. The work in [52] and [53] proposed a typical model comprising a pair of PUs and a pair of CUs. The objective was to find an optimal power allocation at the single relaying cognitive node that minimizes the outage probability at the cognitive receiver for given outage constraints on the primary system. A joint relay selection and resource allocation algorithm for TWR overlay CR networks is also proposed in [54], where the best relays (i.e., CUs) with higher channel gain are selected to act as relays to help for primary transmission.

2.2 Cooperative Communications Assisted with Energy Harvesting

Most of the studies proposed in the literature utilize the RF-based EH technique and the RE-based EH one separately. In cooperative relaying network, the RF-based EH techniques are mainly designed for the traditional OWR technique [56],[57]. In [56], the authors proposed AF delay-limited and delay-tolerant transmission modes and investigated the outage probability

and the ergodic capacity for each mode. In [58], a single relay selection scenario is discussed. The work presented in [59] proposed a continuous time and discrete time EH scheme based on TS protocol. The buffer-aided throughput maximization problem is proposed in [60] where both the source and the relay are considered as harvesting nodes and equipped with finite energy and data buffers. A low complexity suboptimal algorithm was proposed to maximize the delivered data to the destination. In [61], the authors considered a hybrid model that combines TS and PS. They aim to optimize the TS and PS ratios in order to maximize the throughput. OWR single relay selection with outage probability derivations has been discussed in [62] under the causal energy arrivals scenario. Furthermore, approximated solution based on Markov chain has been used to make the relay selection decision. However, few studies dealt with RF-based EH with TWR scheme and they mainly focus on the special case of using one relay only. For instance, in [63], the authors studied the achievable EH TS throughput using AF relay without optimizing the total EH output for TWR system. The authors of [64] focused on RE EH scheme considering that all nodes harvest energy only from RE sources where the power allocation of all nodes for different relaying strategies are discussed. These works mainly focused on the special case using one relay only. The RE-based EH techniques are mainly dealing with the uncertainty effect due to the randomness of RE generation and generally designed for point-to-point or cellular network scenarios [65].

Recently, few studies advocating the combination of RF and RE EH solutions have been presented in the literature. They are essentially focusing on their combined implementation in practice for small wireless communication devices, e.g., internet-of-things-enabled (IoT-enabled) devices and standalone sensor platforms [66],[67],[68]. The potential of employing these combined energy sources with low power wireless devices has shown an important gain in perpetuating the lifetime of these devices [69]. A cooperative communication network involving hybrid EH sources has been investigated in [70] where a joint relay selection and power allocation scheme is proposed for OWR DF with multiple-relay system. The PS protocol is employed at only one selected relay to support the source transmission.

2.3 Heterogeneous Networks Assisted with Energy Harvesting

Downlink communication in cellular networks accounts for around 70% of the total energy consumption in the network [71]. Therefore, many of the proposed researches in the literature tried to reduce the downlink power consumption by switching off BSs during their off-peak hours when data traffic is low [72]. The work presented by Koudouridis *et. al* in [73] proposed a simulated annealing-based algorithm to turn on-off BSs in HetNets. In [74], the authors presented a complete framework for a smart-grid powered LTE system based on evolutionary algorithms such as GA and BPSO algorithm, these heuristic switching ON/OFF approaches were proposed under equal power distribution scenario. In [75], the impact of turning off macrocell BSs on the energy efficiency of the HetNet is studied while keeping the SBSs active. Several robust and efficient schemes for BS ON/OFF switching have been proposed in the literature [76],[77]. For instance, in [76], three different approaches for SBS switching in HetNets are discussed. The ON/OFF status of the SBSs is controlled by either the detection of active users by the SBSs, wake-up signals by the core network, or wake-up signals by the users. In [77], the authors have introduced two switching modes which operate on intermediate and fast time scales in order to cater for the short and long idle periods of the users. It is shown that dense HetNets can be used to achieve higher capacity and performance while simultaneously reducing energy consumption.

Most of promising solutions of energy efficient in HetNets are based on RE-based EH technique to power cellular networks [78],[79],[80],[81],[82],[83]. The benefit of using RE-based EH technique in HetNets has been recently discussed in literature [84],[85],[86]. RE-based EH technique has shown to yield a significant carbon dioxide (CO2) reduction by reducing the reliance on traditional electricity supplies [87]. One of the limitation of the RE-based EH is the discontinuity of the power generation which affects reliability of service. In [88], the authors develop a tractable model based on discrete-time Markov chain to analyze the performance of downlink heterogeneous cellular networks with both power-grid-connected BS and energy harvesting SBSs. Each SBS forms a personal cell that is active only when its own priority user requests service and its battery contains sufficient energy to transmit. In [89], the authors

consider hybrid powering BSs connected to different micro-grids that cooperate to minimize the total power cost by optimizing their resources allocation. The authors assume that each micro-grid can purchase back-up power from the main grid when needed, in order to ensure a reliable service to users. A hybrid energy sharing framework is presented in [90], where the BSs are powered by smart grid and have RE generation capabilities. In addition to that, physical power lines infrastructure between BSs is proposed to share energy between BSs when needed.

2.4 Drone-based Communication Assisted with Energy Harvesting

Few works in the literature investigated the deployment of the DBSs and its challenges. In [91], a placement technique that uses the drones as relays for cell overloading and outage compensation is proposed. Although an analytical model is provided for evaluating system performance in the downlink direction, the paper did not discuss the DBSs' coverage performance and did not suggest any deployment method. The authors in [92] discussed the optimal deployment position for drones that maximizes the average data rate while keeping the symbol error rate under a certain level. However, their work is limited to only one relaying drone. In [93], the authors proposed a computational method to find the optimal and fast drone deployment in order to enhance the coverage performance in the case of public safety communications.

On the other hand, some works discussed the connectivity and safe path planing management for drone-based communication scenarios. For instance, improving the connectivity of ad-hoc networks using drones has been discussed in [94],[95]. The authors in [94] developed a simple heuristic suboptimal algorithm to optimize the drones movement by tracking changes in the network. Safe path planning algorithms with multiple drones are proposed in [96],[97] with the objective to ensure that the drones can return to the charging station before their energies are depleted.

Channel modeling in drone-based communications also remains an important research direction that has extensively been discussed [98],[99],[100]. Indeed, one of the advantages of using flying DBSs is their ability to establish line of sight (LoS) link with ground users which helps in enhancing the signal quality. In [98], the authors analyzed the optimal altitude of one DBS for a certain coverage area that minimizes the DBS's transmit power. Moreover, they

investigated the coverage of two DBSs positioned at a fixed altitude and interfering with each other over a certain coverage area. The probability of air-to-ground LoS link is determined in [99] for a dense urban area. It depends on the altitude, elevation angle, and the distance between the drone and the user or ground node. On the other hand, the air-ground path loss (PL) model for urban environment has been discussed in [100]. In [101], the authors provided both closed-form expressions for predicted probability of LoS and PL model for air-to-ground environment using low altitude platform. In [102], the authors studied the coexistence between the drones and underlaid D2D communication in the downlink scenario. More specifically, they derived the average downlink coverage probabilities for the users and analyzed the impact of the drones' altitudes and density on the overall performance for static and moving drones.

CHAPTER 3. TWO WAY RELAYS-ASSISTED OVERLAY COGNITIVE RADIO NETWORK

In this chapter, the problem of resource allocation for TWR-MIMO overlay cognitive networks using multiple AF relays is investigated. The goal is to maximize the TWR-MIMO overlay cognitive rate while taking into account all transceiver power budgets in addition to the PU QoS requirements. In this framework, it is assumed that each CU is allowed to share the primary bandwidth in order to perform its transmission. In return, they are engaged to complete the primary transmission by amplifying and forwarding the PU data over the remaining bandwidth.

3.1 System Model

We consider an overlay half duplex CR network with two primary users PU_1 and PU_2 in addition to a cognitive network consisting of L_R CUs and one cognitive BS. All nodes are equipped with M antennas as illustrated in Fig. 3.1. PU_1 and PU_2 are assumed out of communication range. The L_R CUs act as TWR for the PUs over the primary bandwidth. In exchange, the PUs may release some of their bandwidths to the CUs to accomplish their own data transmission as long as the PUs maintain their QoS.

Let T denote the time duration that a PU is allowed to transmit data over the bandwidth W_{tot}. In our overlay MIMO-CR scheme, we assume that the total bandwidth is divided into $L_R + 1$ fractions denoted W_0, W_1,...,W_{L_R}, where the primary transmission is held over W_0 while for each l^{th} CU, we allocate the bandwidth fraction W_l such that there is no inter-user interference between all the primary and secondary nodes $\left(\sum_{l=0}^{L_R} W_l = W_{\mathrm{tot}}\right)$, as shown in Fig. 3.2.

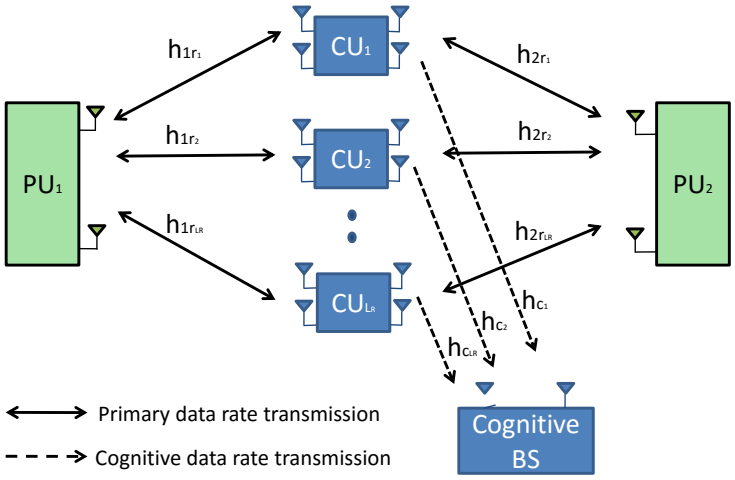

Figure 3.1: Overlay TWR-MIMO system model.

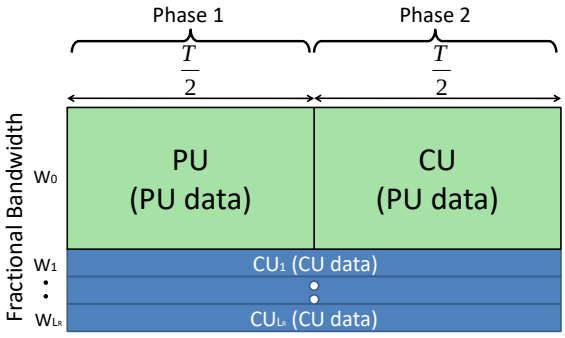

Figure 3.2: Time-bandwidth allocation.

Assuming independent and identically distributed (i.i.d) complex Gaussian signals, PUs exchange their messages via L_R CUs as follows: In the first phase, both PU_1 and PU_2 transmit their messages $\boldsymbol{x}_1$ and $\boldsymbol{x}_2$ simultaneously to the L_R CUs with a covariance power matrix of vector $\boldsymbol{x}_t$ denoted $\boldsymbol{P}_t = \mathbb{E}[\boldsymbol{x}_t \boldsymbol{x}_t^H]$ Watt/Hz (power per unit frequency), where $t = \{1, 2\}$. Perfect synchronization between PU_1 and PU_2 is assumed [103]. In the second phase, the CUs play the role of relays by transmitting the amplified signal to the PUs with a covariance power matrix denoted $\boldsymbol{P}_{r_l}$ Watt/Hz, where $l = 1, ..., L_R$. During PUs transmission and reception, the CUs transmit their data $\boldsymbol{x}_{c_l}$ to the cognitive BS over the remaining bandwidth (i.e., W_1,...,W_{L_R}) with a covariance power matrix denoted $\boldsymbol{P}_{c_l} = \mathbb{E}(\boldsymbol{x}_{c_l} \boldsymbol{x}_{c_l}^H)$ Watt/Hz, where $l = 1, ..., L_R$.

Let us define $\bar{E}_p$ and $\bar{E}_c$ as the peak energy at each PU and the peak energy at each CU,

respectively. $\boldsymbol{h}_{1r_l} \in \mathbb{C}^{M\times M}, \boldsymbol{h}_{2r_l} \in \mathbb{C}^{M\times M}$, and $\boldsymbol{h}_{c_l} \in \mathbb{C}^{M\times M}$ are the MIMO channel gains in the first time slot between PU_1 and the l^{th} CU, PU_2 and the l^{th} CU, and the l^{th} CU and the cognitive BS, respectively. Where in the second time slot the MIMO channel gains are denoted by $\hat{\boldsymbol{h}}_{1r_l} \in \mathbb{C}^{M\times M}, \hat{\boldsymbol{h}}_{2r_l} \in \mathbb{C}^{M\times M}$, and $\hat{\boldsymbol{h}}_{c_l} \in \mathbb{C}^{M\times M}$. All the channel gains are assumed to be i.i.d fading channel gains and constant during the coherence time. If the channels are highly correlated during two consecutive time slots, then channel reciprocity is assumed i.e., $\boldsymbol{h}_{1r_l} = \hat{\boldsymbol{h}}_{1r_l}, \boldsymbol{h}_{2r_l} = \hat{\boldsymbol{h}}_{2r_l}, \boldsymbol{h}_{c_l} = \hat{\boldsymbol{h}}_{c_l}$ In addition to that, perfect channel state information (CSI) at transmitters and receivers are considered. Without loss of generality, all the noise variances are assumed to be equal to N_0.

Let $\boldsymbol{V}_t$ and $\boldsymbol{U}_t$, where $t \in \{1, 2\}$ be two unitary precoder and decoder matrices, respectively, employed by PUs. In the first phase, PU_t employs the precoder matrix $\boldsymbol{V}_t$ such as: $\boldsymbol{x}_t = \boldsymbol{V}_t\tilde{\boldsymbol{x}}_t$ where $\boldsymbol{x}_t$ is the transmitted signal after being precoded by PU_t. Subsequently, during the second phase, PU_t employs the decoder matrix $\boldsymbol{U}_t$ such as: $\boldsymbol{r}_t = \boldsymbol{U}_t^H\boldsymbol{y}_t$, where $\boldsymbol{y}_t$ and $\boldsymbol{r}_t$ are the received signals at PU_t before and after decoding, respectively. The choice of $\boldsymbol{V}_t$ and $\boldsymbol{U}_t$ will be defined later.

This approach was initially designed to a scenario where PUs and CUs belong to the same legacy system; e.g. LTE with LTE D2D communications. In the case where it must be extended to deal with different legacy scenario, then the following rules apply:

- Each CU needs to support both standards.
- Each CU needs to have two separate RF chains: one to be used for the secondary transmissions over the secondary system (e.g., 802.11ac standard) and one to be used over the primary system (e.g., LTE standard) to relay PUs' data.
- This requires doubling the number of antennas since transmission over both systems will be simultaneous: If M is the current number of antennas, i.e., each CU would need "$2M$" antennas: M to be used over the primary system (LTE) and another M to be used over the secondary system.
- This will lead to increase the costs of the CU devices, but they would still be able to use the spectrum for free.

- It should be noted that the different legacy scenario assumes that the two standards use overlapping spectrum bands. Otherwise, PUs cannot share a portion of their bandwidth with CUs, since the technology used by CUs would be operational on different frequency bands.

3.2 Problem Formulation

In this section, we formulate an optimization problem that maximizes the cognitive objective function for multiple MIMO TWR-CR networks while satisfying the required QoS of the PUs. Different utility metrics leading to different bandwidth and power allocation are presented and discussed depending on the cognitive objective. Without loss of generality, channel reciprocity is assumed.

3.2.1 Primary Data Rate

In the first phase, the baseband received signal at the l^{th} CU over W_0 is given as follows

$$\boldsymbol{y}_{r_l} = \boldsymbol{h}_{1r_l}\boldsymbol{x}_1 + \boldsymbol{h}_{2r_l}\boldsymbol{x}_2 + \boldsymbol{n}_{r_l}, \tag{3.1}$$

where $\boldsymbol{n}_{\boldsymbol{r_i}}$ is the additive Gaussian noise at the l^{th} relay and $\boldsymbol{x}_t$ is the transmitted signal after precoding by PU_t, where $t \in \{1, 2\}$. During the second phase, each relay CU amplifies $\boldsymbol{y}_{r_l}$ by multiplying it by a full matrix $\boldsymbol{w}_l \in \mathbb{C}^{M\times M}$ and broadcasting it to the PUs. Finally, the received signals at PU_1 and PU_2 are respectively given as

$$\boldsymbol{y}_1 = \underbrace{\hat{\boldsymbol{\Theta}}\boldsymbol{x}_1}_{\text{Self Interference}} + \boldsymbol{\Theta}\boldsymbol{x}_2 + \boldsymbol{z}_1, \tag{3.2}$$

$$\boldsymbol{y}_2 = \boldsymbol{\Psi}\boldsymbol{x}_1 + \underbrace{\hat{\boldsymbol{\Psi}}\boldsymbol{x}_2}_{\text{Self Interference}} + \boldsymbol{z}_2, \tag{3.3}$$

where $\boldsymbol{\Theta} = \sum_{l=1}^{L_R} \boldsymbol{h}_{1r_l}^T \boldsymbol{w}_l \boldsymbol{h}_{2r_l}, \hat{\boldsymbol{\Theta}} = \sum_{l=1}^{L_R} \boldsymbol{h}_{1r_l}^T \boldsymbol{w}_l \boldsymbol{h}_{1r_l}, \boldsymbol{\Psi} = \sum_{l=1}^{L_R} \boldsymbol{h}_{2r_l}^T \boldsymbol{w}_l \boldsymbol{h}_{1r_l}$, and $\hat{\boldsymbol{\Psi}} = \sum_{l=1}^{L_R} \boldsymbol{h}_{2r_l}^T \boldsymbol{w}_l \boldsymbol{h}_{2r_l}$, are the equivalent MIMO channels obtained at PU_1 and PU_2, respectively before decoding. $\boldsymbol{z}_t = \sum_{l=1}^{L_R} \left(\boldsymbol{h}_{tr_l}^T \boldsymbol{w}_l \boldsymbol{n}_{r_l}\right) + \boldsymbol{n}_t$ and $\boldsymbol{n}_t$ are the equivalent amplified noise at $\mathrm{PU_t}$ before decoding and the additive Gaussian noise vectors at $\mathrm{PU_t}$, respectively, where $t \in \{1, 2\}$. Using the knowledge

of the channel information and channel reciprocity, the PUs can remove the self interference by eliminating their own signals (i.e., $\boldsymbol{x}_1$ for PU_1 and $\boldsymbol{x}_2$ for PU_2). Thus, the received signal $\boldsymbol{r}_1$ and $\boldsymbol{r}_2$ after employing the decoders $\boldsymbol{U}_t$ are given, respectively, by

$$\boldsymbol{r}_1 = \boldsymbol{U}_1^H \boldsymbol{\Theta} \boldsymbol{x}_2 + \tilde{\boldsymbol{z}}_1 = \boldsymbol{U}_1^H \boldsymbol{\Theta} \boldsymbol{V}_2 \tilde{\boldsymbol{x}}_2 + \tilde{\boldsymbol{z}}_1 \tag{3.4}$$

$$\boldsymbol{r}_2 = \boldsymbol{U}_2^H \boldsymbol{\Psi} \boldsymbol{x}_1 + \tilde{\boldsymbol{z}}_2 = \boldsymbol{U}_2^H \boldsymbol{\Psi} \boldsymbol{V}_1 \tilde{\boldsymbol{x}}_1 + \tilde{\boldsymbol{z}}_2 \tag{3.5}$$

where $\tilde{\boldsymbol{z}}_t = \boldsymbol{U}_t^H \boldsymbol{z}_t$ is the equivalent amplified noise at $\mathrm{PU_t}$ after decoding. The covariance matrix of the noise $\tilde{\boldsymbol{z}}_t$ can be given as

$$\boldsymbol{C}_{\tilde{\boldsymbol{z}}_t} = \mathbb{E}[\tilde{\boldsymbol{z}}_t \tilde{\boldsymbol{z}}_t^H] = N_0 \sum_{l=1}^{L_R} \boldsymbol{U}_t^H \boldsymbol{h}_{tr_l}^T \boldsymbol{w}_l (\boldsymbol{U}_t^H \boldsymbol{h}_{tr_l}^T \boldsymbol{w}_l)^H + N_0 \mathrm{I}_M, \tag{3.6}$$

where I_M denotes the identity matrix of size M.

Let us now define the unitary precoding and decoding matrices using the singular value decomposition (SVD) which converts the MIMO channel into parallel channels characterized by their associated eigenmodes. Thus, we perform SVDs for the matrices $\boldsymbol{\Theta}$ and $\boldsymbol{\Psi}$ as follows: $\boldsymbol{\Theta} = \boldsymbol{U}_1 \boldsymbol{\Lambda}_\Theta \boldsymbol{V}_2^H$ and $\boldsymbol{\Psi} = \boldsymbol{U}_2 \boldsymbol{\Lambda}_\Psi \boldsymbol{V}_1^H$, where $\boldsymbol{\Lambda}_\Theta$ and $\boldsymbol{\Lambda}_\Psi$ are diagonal matrices with square roots of the eigenvalues of matrix $\boldsymbol{\Theta}$ and $\boldsymbol{\Psi}$, respectively. As such, the primary rates of the PU_1 and PU_2 after SVD can be respectively given as

$$R_{p_1} = \frac{W_0}{2} \sum_{m=1}^{M} \log_2 \left(1 + \frac{\boldsymbol{\Lambda}_\Theta^2(m,m) \boldsymbol{P}_2(m,m)}{\boldsymbol{C}_{\tilde{\boldsymbol{z}}_1}(m,m)} \right), \tag{3.7}$$

$$R_{p_2} = \frac{W_0}{2} \sum_{m=1}^{M} \log_2 \left(1 + \frac{\boldsymbol{\Lambda}_\Psi^2(m,m) \boldsymbol{P}_1(m,m)}{\boldsymbol{C}_{\tilde{\boldsymbol{z}}_2}(m,m)} \right). \tag{3.8}$$

The factor $\frac{1}{2}$ is added as primary transmission is held over two time slots. In order to meet the target transmission rate for the primary network, R_{p_1} [bits/s] and R_{p_2} [bits/s] should be no less than the primary target transmission rate R_0[bits/s], i.e.,

$$R_{p_1} \geq R_0 \quad \text{and} \quad R_{p_2} \geq R_0, \tag{3.9}$$

From (3.9), we can show that the fractional bandwidth needed for the primary network W_0 should satisfy the following bandwidth condition(i.e., the PUs may release the remaining fractional bandwidth $(W_{\mathrm{tot}} - W_0)$ to CUs)

$$W_0 \geq \max \left(\frac{2R_0}{\sum_{m=1}^{M} \log_2 \left(1 + \frac{\boldsymbol{\Lambda}_\Theta^2(m,m) \boldsymbol{P}_2(m,m)}{\boldsymbol{C}_{\tilde{\boldsymbol{z}}_1}(m,m)} \right)}, \frac{2R_0}{\sum_{m=1}^{M} \log_2 \left(1 + \frac{\boldsymbol{\Lambda}_\Psi^2(m,m) \boldsymbol{P}_1(m,m)}{\boldsymbol{C}_{\tilde{\boldsymbol{z}}_2}(m,m)} \right)} \right). \tag{3.10}$$

3.2.2 Secondary Data Rate

On other hand, the received signal at the cognitive BS from the l^{th} CU over bandwidth W_l can be given as

$$\boldsymbol{y}_{c_l} = \boldsymbol{h}_{c_l}\boldsymbol{x}_{c_l} + \boldsymbol{n}_{c_l}, \tag{3.11}$$

where $\boldsymbol{n}_{c_l}$ is the additive Gaussian noise at the cognitive BS. Thus, the received signal $\boldsymbol{r}_{c_l}$ after decoding is given by

$$\boldsymbol{r}_{c_l} = \boldsymbol{U}_{c_l}^H\boldsymbol{h}_{c_l}\boldsymbol{x}_{c_l} + \boldsymbol{U}_{c_l}^H\boldsymbol{n}_{c_l} = \boldsymbol{U}_{c_l}^H\boldsymbol{h}_{c_l}\boldsymbol{V}_{c_l}\tilde{\boldsymbol{x}}_{c_l} + \boldsymbol{U}_{c_l}^H\boldsymbol{n}_{c_l}. \tag{3.12}$$

Define $\boldsymbol{h}_{c_l} = \boldsymbol{U}_{c_l}\boldsymbol{\Lambda}_{c_l}\boldsymbol{V}_{c_l}^H$, where $\boldsymbol{\Lambda}_{c_l}$ is a diagonal matrix with square roots of the eigenvalues of matrix $\boldsymbol{h}_{c_l}$.

Therefore, the cognitive rate of l^{th} CU at the cognitive BS can be expressed in [bits/s] as

$$R_{c_l} = W_l \sum_{m=1}^{M} \log_2\left(1 + \frac{\boldsymbol{\Lambda}_{c_l}^2(m,m)\boldsymbol{P}_{c_l}(m,m)}{N_0}\right). \tag{3.13}$$

3.2.3 Optimization Problem

Recall that the PUs and CUs have as energy budgets $\bar{E}_p$ and $\bar{E}_c$ expressed in Joules, respectively, and that the power budgets of PU and CU equal to $\bar{P}_p$ and $\bar{P}_c$ Watt, respectively. Thus, the energy budget constraints at the t^{th} PU and l^{th} CU are over time duration T given respectively as

$$\begin{aligned} &\frac{T}{2}W_0\mathrm{Tr}(\boldsymbol{P}_t) \le \bar{E}_p, \\ &TW_l\mathrm{Tr}(\boldsymbol{P}_{c_l}) + \frac{T}{2}W_0\mathrm{Tr}\Big(\boldsymbol{\Omega}_{1r_l}\boldsymbol{P}_1\boldsymbol{\Omega}_{1r_l}^H + \boldsymbol{\Omega}_{2r_l}\boldsymbol{P}_2\boldsymbol{\Omega}_{2r_l}^H + N_0\boldsymbol{w}_l\boldsymbol{w}_l^H\Big) \le \bar{E}_c. \end{aligned} \tag{3.14}$$

or equivalently

$$\begin{aligned} &\frac{W_0}{2}\mathrm{Tr}(\boldsymbol{P}_t) \le \bar{P}_p, \\ &W_l\mathrm{Tr}(\boldsymbol{P}_{c_l}) + \frac{W_0}{2}\mathrm{Tr}\Big(\boldsymbol{\Omega}_{1r_l}\boldsymbol{P}_1\boldsymbol{\Omega}_{1r_l}^H + \boldsymbol{\Omega}_{2r_l}\boldsymbol{P}_2\boldsymbol{\Omega}_{2r_l}^H + N_0\boldsymbol{w}_l\boldsymbol{w}_l^H\Big) \le \bar{P}_c. \end{aligned} \tag{3.15}$$

where $\boldsymbol{\Omega}_{1r_l} = \boldsymbol{w}_l\boldsymbol{h}_{1r_l}$ and $\boldsymbol{\Omega}_{2r_l} = \boldsymbol{w}_l\boldsymbol{h}_{2r_l}$ are the MIMO equivalent channel gains. Let $U(R_{c_l})$ denote the rate utility of the cognitive system. Thus, the optimization problem of MIMO

TWR-CR with multiple relays that maximizes the rate utility while satisfying specific power budgets and target primary rate constraints can be formulated as

$$\underset{\boldsymbol{W},\boldsymbol{P}_1,\boldsymbol{P}_2,\boldsymbol{P}_{c_l},\boldsymbol{w}_l\geq 0}{\text{maximize}} \quad U(R_{c_l}) \tag{3.16}$$

subject to:

$$0 \leq \frac{W_0}{2}\text{Tr}(\boldsymbol{P}_t) \leq \bar{P}_p, \quad \forall t = 1, 2, \tag{3.17}$$

$$W_l\text{Tr}(\boldsymbol{P}_{c_l}) + \frac{W_0}{2}\text{Tr}\Big(\boldsymbol{\Omega}_{1r_l}\boldsymbol{P}_1\boldsymbol{\Omega}_{1r_l}^H + \boldsymbol{\Omega}_{2r_l}\boldsymbol{P}_2\boldsymbol{\Omega}_{2r_l}^H + N_0\boldsymbol{w}_l\boldsymbol{w}_l^H\Big) \leq \bar{P}_c, \quad \forall l = 1, ..., L_R, , \tag{3.18}$$

$$R_{p_t} \geq R_0, \quad \forall t = 1, 2, \tag{3.19}$$

$$\sum_{l=0}^{L_R} W_l = W_{\text{tot}}, \tag{3.20}$$

where $\boldsymbol{W} = [W_0, W_1, ..., W_{L_R}]$ is the vector that contains the fractions of bandwidth assigned to primary and cognitive transmissions. Constraints (3.17) and (3.18) represent the peak power constraints at PUs and CUs, respectively. The term $\text{Tr}\Big(\boldsymbol{\Omega}_{1r_l}\boldsymbol{P}_1\boldsymbol{\Omega}_{1r_l}^H + \boldsymbol{\Omega}_{2r_l}\boldsymbol{P}_2\boldsymbol{\Omega}_{2r_l}^H + N_0\boldsymbol{w}_l\boldsymbol{w}_l^H\Big)$ in constraint (3.18) is equivalent to the relay amplified power of the l^{th} CU. Constraint (3.19) represent the QoS constraint defined by the target data rate. Finally, constraint (3.20) represent the total bandwidth constraint.

3.3 Utility Selection

We characterize three different utility metrics that will be employed in the optimization problem (3.16).

3.3.1 Max Sum Utility

The utility of this metric is equivalent to the sum data rate of the cognitive network $U(R_{c_l}) = \sum_{l=1}^{L_R} R_{c_l}$. This approach is known in the literature as max C/I [104] as it promotes users with favorable channel and interference conditions by allocating to them most of the resources, whereas users suffering from higher propagation losses and/or interference levels will be deprived from the bandwidth as well as the power and will have very low data rates. Note that, thanks to the employed overlay scheme, and thus, the elimination of user interference, the max sum utility promotes users with favorable channels conditions only.

3.3.2 Max Min Utility

Due to the unfairness of max sum resource allocation, the need for more fair utility metrics arises. Max min utilities are a family of utility functions attempting to maximize the minimum data rate in the network $U(R_{c_l}) = \min_l(R_{c_l})$ [105]. By increasing the priority of users having lower rates, max min utilities lead to more fairness in the network. In order to simplify the problem for this approach, we define a new decision variable $R_{\min} = \min_l(R_{c_l})$. Therefore, our optimization problem becomes

$$\underset{\boldsymbol{W},\boldsymbol{P}_1,\boldsymbol{P}_2,\boldsymbol{P}_c,\boldsymbol{w}_l,R_{\min}\geq 0}{\text{maximize}} \quad R_{\min} \tag{3.21}$$

subject to:

$$R_{c_l} \geq R_{\min} \quad \forall l = 1, ..., L_R, \tag{3.22}$$

$$0 \leq \frac{W_0}{2}\text{Tr}(\boldsymbol{P}_t) \leq \bar{P}_p, \quad \forall t = 1, 2, \tag{3.23}$$

$$W_l\text{Tr}(\boldsymbol{P}_{c_l}) + \frac{W_0}{2}\text{Tr}\Big(\boldsymbol{\Omega}_{1r_l}\boldsymbol{P}_1\boldsymbol{\Omega}_{1r_l}^H + \boldsymbol{\Omega}_{2r_l}\boldsymbol{P}_2\boldsymbol{\Omega}_{2r_l}^H + N_0\boldsymbol{w}_l\boldsymbol{w}_l^H\Big) \leq \bar{P}_c, \quad \forall l = 1, ..., L_R, , \tag{3.24}$$

$$R_{p_t} \geq R_0, \quad \forall t = 1, 2, \tag{3.25}$$

$$\sum_{l=0}^{L_R} W_l = W_{\text{tot}}, \tag{3.26}$$

Constraints (3.23)-(3.26) are the same as constraints (3.17)-(3.20), but they have been repeated for completeness.

3.3.3 Proportional Fair Utility

A tradeoff between the maximization of the sum rate and the maximization of the minimum rate could be the maximization of the geometric mean data rate $U(R_{c_l}) = (\prod_{l=1}^{L_R} R_{c_l})$ [106]. The proportional fair (PF) metric is fair, since a user with a data rate close to zero will make the whole product go to zero. Hence, any algorithm maximizing the geometric means would avoid having any user with very low data rate. In addition to this, the metric will reasonably promote users with good wireless channels (capable of achieving high data rates), since a high data rate will contribute in increasing the product.

3.4 Optimal Power Allocation and Particle Swarm Optimization Algorithm

The formulated optimization problem is a non-convex problem and its optimal solution remains unsolved. For this reason, two steps are proposed to solve this problem. In the first step, we derive power expressions at each iteration for the optimal transmit primary powers (i.e., $\boldsymbol{P}_1$ and $\boldsymbol{P}_2$) and cognitive transmit powers (i.e., $\boldsymbol{P}_{c_l}$) by assuming fixed bandwidths of both primary and cognitive users and fixed amplification matrix gains (equivalent to fixed relay power), at all CUs. As a result, we convert our formulated problem to a convex one. The primal-dual method is used due to its simplicity and to the fact that it provides an expression of the power allocation per each antenna for the different utility functions. This can help in interpreting the behavior of each terminal in the network thanks to the water-filling expressions that will be derived next. Then, we propose to employ the subgradient method in order to optimize the Lagrangian multipliers. Note that the interior-point method could be also employed to solve the problem by finding numerically the optimal solution using the Newton method. Although the convergence of the subgradient method is slower than the interior-point method, the subgradient method remains competitive mainly for large scale problems as it requires little storage [107]. In the second step, we employ swarm intelligence to jointly optimize the system bandwidths with the CU amplification gain matrices.

3.4.1 Optimal Transmit Power Allocation

We can solve our convex optimization problem for fixed $\boldsymbol{W}$ and $\boldsymbol{w}_l, \forall l = 1, ..., L_R$, by exploiting its strong duality as follows [107]:

$$\underset{\boldsymbol{\lambda}\geq 0}{\text{minimum}} \quad \underset{\boldsymbol{P}_1,\boldsymbol{P}_2,\boldsymbol{P}_{c_l}\geq 0}{\text{maximum}} \quad \mathcal{L}(\boldsymbol{\lambda}, \boldsymbol{P}_1, \boldsymbol{P}_2, \boldsymbol{P}_{c_l}), \tag{3.27}$$

$$\mathcal{L}(\boldsymbol{\lambda}, \boldsymbol{P}_1, \boldsymbol{P}_2, \boldsymbol{P}_c) = U(R_{c_l}) - \sum_{t=1}^{2} \lambda_{p_t} \left(\frac{W_0}{2} \mathrm{Tr}(\boldsymbol{P}_t) - \bar{P}_p \right) - \sum_{l=1}^{L_R} \lambda_{c_l} \Big(W_l \mathrm{Tr}(\boldsymbol{P}_{c_l}) + \frac{W_0}{2} \mathrm{Tr}\Big(\boldsymbol{\Omega}_{1r_l} \boldsymbol{P}_1 \boldsymbol{\Omega}_{1r_l}^H + \boldsymbol{\Omega}_{2r_l} \boldsymbol{P}_2 \boldsymbol{\Omega}_{2r_l}^H + N_0 \boldsymbol{w}_l \boldsymbol{w}_l^H \Big) - \bar{P}_c \Big) + \lambda_{th_1} \left(R_{p_1} - R_0 \right) + \lambda_{th_2} \left(R_{p_2} - R_0 \right) - \lambda_W \left(\sum_{l=0}^{L_R} W_l - W_{\mathrm{tot}} \right) + \sum_{l=1}^{L_R} \lambda_{R_l} \left(R_{c_l} - R_{\min} \right). \tag{3.28}$$

where $\mathcal{L}$ is the Lagrangian function [107]. $\boldsymbol{\lambda}$ is a vector that contains all the Lagrangian multipliers of the system, where λ_{p_t}, $\lambda_{c_l}, \lambda_{th_t}$ and λ_W, represent the Lagrangian multipliers related to the peak power budget constraint at the t^{th} PU, peak power budget constraint at the l^{th} CU, the primary target rate constraint for the t^{th} PU, and the bandwidth constraint, respectively. It includes also $\lambda_{R_l}, l = 1, \cdots, L_R$ related to constraint (3.22) if the max min utility is used.

By taking the derivative of the Lagrangian with respect to the $P_t(m,m)$, and $P_{c_l}(m,m)$ where $t \in \{1,2\}, m = 1, ..., M$ and $l = 1, ..., L_R$, we can find the optimal primary power allocated to the m^{th} antenna at PU_t as well as the optimal transmit powers allocated to the m^{th} antenna at CU_l that maximize the Lagrangian function and, consequently, the cognitive utility rate. Since the primary powers are independent of the cognitive utility expression, we can derive the closed-form expressions of $P_1(m,m)$ and $P_2(m,m)$ at each iteration for fixed bandwidth and relay amplification factors as given respectively as follows

$$P_1(m,m) = \left(\frac{\lambda_{th_2}}{\ln(2)\left(\lambda_{p_1} + \sum_{l=1}^{L_R} \lambda_{c_l} |\boldsymbol{\Omega}_{1r_l}(m,m)|^2\right)} - \frac{\boldsymbol{C}_{\tilde{\boldsymbol{z}}_2}(m,m)}{\boldsymbol{\Lambda}^2_{\Psi}(m,m)} \right)^+, \tag{3.29}$$

$$P_2(m,m) = \left(\frac{\lambda_{th_1}}{\ln(2)\left(\lambda_{p_2} + \sum_{l=1}^{L_R} \lambda_{c_l} |\boldsymbol{\Omega}_{2r_l}(m,m)|^2\right)} - \frac{\boldsymbol{C}_{\tilde{\boldsymbol{z}}_1}(m,m)}{\boldsymbol{\Lambda}^2_{\Theta}(m,m)} \right)^+, \tag{3.30}$$

where $\ln(2)$ is the natural logarithm of 2. However, the expression of the l^{th} CU transmit power depends on the utility approach as follows:

Max Sum Utility: For max sum utility, the l^{th} CU transmit power over the m^{th} antenna can be expressed as

$$P_{c_l}(m,m) = \left(\frac{1}{\lambda_{c_l} \ln(2)} - \frac{N_0}{\boldsymbol{\Lambda}^2_{c_l}(m,m)} \right)^+. \tag{3.31}$$

One can see from (3.31) that the value of the $P_{c_l}(m,m)$ depends on λ_{c_l} related to constraint (3.18) (i.e., corresponding to the primary powers and primary bandwidth). Also, it depends on the channel values between the CUs and cognitive BS. In this approach it is clear that, all resources are allocated to the CUs with favorable channel conditions.

Max Min Utility: By taking the derivative of the Lagrangian of (3.21)-(3.26) with respect to $P_{c_l}(m,m)$ and equating it to zero, the l^{th} CU transmit power over the m^{th} antenna can be derived as

$$P_{c_l}(m,m) = \left(\frac{\lambda_{R_l}}{\lambda_{c_l} \ln(2)} - \frac{N_0}{\mathbf{\Lambda}^2_{c_l}(m,m)} \right)^+ . \tag{3.32}$$

By taking the derivative of the Lagrangian with respect to $R_{\min}$, we can deduce that $\sum_l^{L_R} \lambda_{R_l} = 1$, which means that $\lambda_{R_l} \in [0,1]$. By comparing (3.32) with (3.31), we can see that λ_{R_l} values control the priority of the resource allocation. However, enhancing the worst channel condition (i.e., corresponding to the minimum rate achieved) could come at the expense of users with good channel conditions which leads to more fairness between the CUs.

Proportional Fair Utility: For PF utility, the l^{th} CU transmit power over the m^{th} antenna can be derived as

$$P_{c_l}(m,m) = \left(\frac{1}{\lambda_{c_l} \ln(2)} \prod_{\substack{k=1 \\ k \neq l}}^{L_R} W_k . \sum_{m=1}^{M} \log_2 \left(1 + \frac{P_{c_k}(m,m) \mathbf{\Lambda}^2_{c_k}(m,m)}{N_0} \right) - \frac{N_0}{\mathbf{\Lambda}^2_{c_l}(m,m)} \right)^+ . \tag{3.33}$$

In this approach, a tradeoff between the maximization of the sum rate and the maximization of the minimum rate can be clearly deduced in (3.33). The l^{th} CU transmit power over the m^{th} antenna $P_{c_l}(m,m)$ depends directly on the sum rate of other antennas at the same CU and the product of the other CUs rates. This approach tries to avoid having any user with very low data rate and maximize the product of the CUs rates simultaneously.

For all utilities, we can employ the subgradient method to find the optimal Lagrangian multipliers of this problem [108]. Hence, to obtain the solution, we can start with any initial values for the different Lagrangian multipliers and evaluate the optimal powers. We then update the Lagrangian multipliers at the next iteration $(i+1)$ as follows

$$\lambda_{p_t}^{(i+1)} = \lambda_{p_t}^{(i)} - \delta_{p_t}^{(i)} \left(\bar{P}_p - \frac{W_0}{2} \mathrm{Tr}(\boldsymbol{P}_t) \right), \forall t = 1, 2, \tag{3.34}$$

$$\lambda_{c_l}^{(i+1)} = \lambda_{c_l}^{(i)} - \delta_{c_l}^{(i)} \left(\bar{P}_c - \left(W_l \mathrm{Tr}(\boldsymbol{P}_{c_l}) + \frac{W_0}{2} \mathrm{Tr}\left(\boldsymbol{\Omega}_{1r_l} \boldsymbol{P}_1 \boldsymbol{\Omega}_{1r_l}^H + \boldsymbol{\Omega}_{2r_l} \boldsymbol{P}_2 \boldsymbol{\Omega}_{2r_l}^H + N_0 \boldsymbol{w}_l \boldsymbol{w}_l^H \right) \right) \right)$$

$$\forall l = 1, ..., L_R, \tag{3.35}$$

$$\lambda_{th_1}^{(i+1)} = \lambda_{th_1}^{(i)} - \delta_{th_1}^{(i)} \left(R_{p_1} - R_0 \right) \tag{3.36}$$

$$\lambda_{th_2}^{(i+1)} = \lambda_{th_2}^{(i)} - \delta_{th_2}^{(i)} \left(R_{p_2} - R_0 \right), \tag{3.37}$$

$$\lambda_{W}^{(i+1)} = \lambda_{W}^{(i)} - \delta_{W}^{(i)} \left(W_{\mathrm{tot}} - \left(\sum_{l=0}^{L_R} W_l \right) \right), \tag{3.38}$$

$$\lambda_{R_l}^{(i+1)} = \lambda_{R_l}^{(i)} - \delta_{R_l}^{(i)} \left(R_{c_l} - R_{\min} \right), \forall l = 1, ..., L_R. \tag{3.39}$$

where $\delta_{p_t}^{(i)}, \delta_{c_l}^{(i)}, \delta_{th_1}^{(i)}, \delta_{th_2}^{(i)}, \delta_{W}^{(i)}$ and $\delta_{R_l}^{(i)}$ are the updated step size according to the nonsummable diminishing step length policy (see [108] for more details). The updated values of the optimal powers and the Lagrangian multipliers are repeated until convergence.

3.4.2 Particle Swarm Optimization Algorithm

In the second step, the PSO algorithm is employed to optimize $\boldsymbol{W}$ and $\boldsymbol{w}_l, \forall l = 1, ..., L_R$. Details of PSO algorithm is given in Appendix A.

First, the PSO generates N random particles (i.e., a vector contains random $\boldsymbol{W}$ and $\boldsymbol{w}_l, \forall l = 1, ..., L_R$) $\boldsymbol{\mathcal{N}}^{(n)}$, $n = 1, \cdots, N$, of length $1 \times (L_R(2M)^2 + (L_R + 1))$ to form an initial population set $\mathcal{S}$, where $(2M)$ corresponds to the fact that during the PSO algorithm we optimize complex amplification gain matrices of multiple antenna relays. Note that when $M = 1$, we focus on optimizing a single real entry per relay: the amplification gain. The algorithm computes the achieved utility (3.16) of all particles by computing the optimal terminal powers derived in Section 3.4.1 for this $\boldsymbol{\mathcal{N}}^{(n)}$. Then, it finds the particle that provides the global optimal utility for this iteration, denoted $\boldsymbol{\mathcal{N}}^{(\mathrm{global})}$. In addition, for each particle n, it memorizes the position of its previous best performance, denoted $\boldsymbol{\mathcal{N}}^{(\mathrm{n,local})}$. After finding these two best values, PSO updates its velocity $\boldsymbol{\nu}_j^{(n)}$ and its particle positions $\boldsymbol{\mathcal{N}}_j^{(n)}$, respectively at each iteration q as

Algorithm 3.1 Proposed Algorithm for Overlay TWR-CR Networks

1: Generate an initial population $\mathcal{S}$ composed of N random particles $\boldsymbol{\mathcal{N}}^{(n)}$, $n = 1 \cdots N$.
2: **while** Not converged **do**
3: **for** $n = 1, \cdots, N$ **do**
4: Find the optimal primary and cognitive powers by computing (3.29)-(3.33) corresponding to the particle $\boldsymbol{\mathcal{N}}^{(n)} \in \mathcal{S}$.
5: Compute the utility U_n depending on the used metric as given in Section 3.3.
6: **end for**
7: Find $(n_g, q_g) = \arg\max_{n,q} U_n(q)$ (i.e., n_g and q_g indicate the index and the position of the particle that results in the highest utility).
8: Set $U_{(\text{global})} = U_{n_g}(q_g)$ and $\boldsymbol{\mathcal{N}}^{(\text{global})} = \boldsymbol{\mathcal{N}}^{n_g}(q_g)$.
9: Find $q_n = \arg\max_{q} U_n(q)$ for each particle n (i.e., q_n indicates the position of the particle n that results in the highest local utility).
10: Set $U_{(\text{n,local})} = U_n(q_n)$ and $\boldsymbol{\mathcal{N}}^{(\text{n,local})} = \boldsymbol{\mathcal{N}}^{n}(q_n)$.
11: Adjust the velocities and positions of all particles using equations (A.1) and (A.2) in Appendix A, respectively.
12: Move to the new iteration $q = q + 1$.
13: **end while**

follows:

$$\begin{aligned}\boldsymbol{\nu}_j^{(n)}(q+1) = \psi_0 \boldsymbol{\nu}_j^{(n)}(q) + c_1\psi_1(q)\left(\boldsymbol{\mathcal{N}}_j^{(\text{n,local})}(q) - \boldsymbol{W}_j^{(n)}(q)\right) \\ + c_2\psi_2(q)\left(\boldsymbol{\mathcal{N}}_j^{(\text{global})}(q) - \boldsymbol{\mathcal{N}}_j^{(n)}(q)\right),\end{aligned} \tag{3.40}$$

$$\boldsymbol{\mathcal{N}}_j^{(n)}(q+1) = \left(\boldsymbol{\mathcal{N}}_j^{(n)}(q) + \boldsymbol{\nu}_j^{(n)}(q+1)\right)^{+}, \tag{3.41}$$

where ψ_0 is the inertia weight used to control the convergence speed ($0.8 \leq \psi_0 \leq 1.2$). ψ_1 and ψ_2 are two random positive numbers generated for iteration q ($\psi_1, \psi_2 \in [0, 2]$) [109]. Finally, c_1 and c_2 are the step size that a particle takes towards the best individual candidate solution $\boldsymbol{\mathcal{N}}^{(\text{n,local})}$ and the global best solution $\boldsymbol{\mathcal{N}}^{(\text{global})}$. This procedure is repeated until convergence (i.e., the utility remains constant for a certain number of iterations or reaching maximum number of iterations). Details of the proposed algorithm as it is applied to our optimization problem are given in Algorithm 3.1.

3.5 Simulation Results

In this section, we provide selected simulation results for i.i.d Rayleigh fading channels to study the performance of the proposed scheme given in Fig. 3.1. The total bandwidth and average noise power per unit frequency are assumed to be equal to $W_{\text{tot}} = 5$ MHz and

$N_0 = 1$ Watt/Hz, respectively. The PSO algorithm is executed using these parameters: the initial number of particles is set to $N = 30$ and the maximum number of iterations is equal to 200. It is assumed that the PSO algorithm converges when the utility remains constant for 10 consecutive iterations or reaching maximum number of iterations.

3.5.1 System Performance

Table 3.1: Strategy of cognitive users corresponding to each utility with $L_R = 4$, $R_0 = 10$ Mbits/s, and $\bar{P}_p = \bar{P}_c = 20$ dBm.

	M=1			M=2		
	Max Sum	PF	Max Min	Max Sum	PF	Max Min
$\sum_{l=1}^{L_R} R_{c_l}$[Mbits/s]	6.51	4.83	3.64	9.87	8.05	7.06
R_{c_1}[Mbits/s]	~ 0	0.87	0.91	~ 0	2.01	1.77
R_{c_2}[Mbits/s]	~ 0	1.39	0.91	9.87	2.35	1.77
R_{c_3}[Mbits/s]	6.51	1.37	0.91	~ 0	1.95	1.77
R_{c_4}[Mbits/s]	~ 0	1.19	0.91	~ 0	1.74	1.77
W_0 [%]	41.90	44.96	44.91	31.85	33.24	33.44
W_1 [%]	~ 0	13.76	17.16	~ 0	16.69	19.56
W_2 [%]	~ 0	13.76	12.51	67.59	16.69	12.78
W_3 [%]	58.10	13.76	10.61	~ 0	16.69	19.01
W_4 [%]	~ 0	13.76	14.81	~ 0	16.69	15.21

All simulations show that max sum utility leads to the highest sum rate in the network. However, this comes at the expense of fairness as it is shown in Table 3.1. Indeed, the table compares between the different utilities for the same channel realization with fixed $L_R = 4$, $R_0 = 10$ Mbits/s, and $\bar{P}_p = \bar{P}_c = 20$ dBm. By using one realization, it can be shown that max sum enhances the cognitive sum rate, by allocating most of the resources to a unique user having the best channel conditions (i.e., CU_3 for $M = 1$ and CU_2 for $M = 2$). On the other hand, the PF approach maximizes the geometric mean for all the users by allocating almost the same amount of bandwidths to CUs, while max min approach maximizes the minimum cognitive rate and provides the same rate for all cognitive users, hence, leads to fairness performance. The choice of the utility is related to the service used by the CUs. For instance, if the application requires same uplink rates max min utility can be used. However, if it consists in a pure cognitive transmission without priorities, then max sum could be employed.

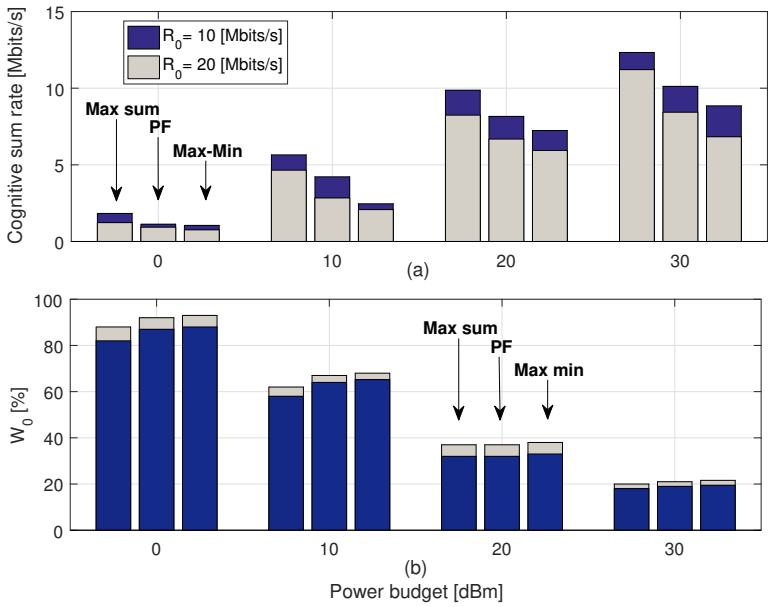

Figure 3.3: (a) Cognitive sum rate, (b) primary bandwidth fraction (W_0 [%]) versus power budget constraint ($\bar{P}_p = \bar{P}_c$), for $L_R = 4, M = 2$.

In Fig. 3.3, we aim to investigate the impact of the power budget constraint on the system performance. In this figure, we plot the cognitive sum rate for all the utilities versus the power budget ($\bar{P}_p = \bar{P}_c$) with $L_R = 4$, $M = 2$, and different values of $R_0 = \{10, 20\}$ Mbits/s. It is shown that increasing the target rate R_0 for the same power budget reduces the cognitive sum rate, since satisfying constraint (3.19) requires more bandwidth (i.e., higher W_0) as Fig. 3.3(b) shows, as well as higher $\boldsymbol{P}_1$ and $\boldsymbol{P}_2$ values. As a result, CUs are forced to reduce their transmitted power $\boldsymbol{P}_{c_l}, \forall 1, ..., L_R$, to support primary transmission and respect constraint (3.18). For instance, for $\bar{P} = 10$ dBm with max sum approach, the total cognitive sum rate is reduced by around 20% by going from around 6.00 Mbits/s to around 4.80 Mbits/s using $R_0 = 20$ Mbits/s instead of $R_0 = 10$ Mbits/s. On the other hand, we can see that increasing the power budget will provide more bandwidth to secondary users to accomplish their transmission. For instance, with 10 dBm, primary transmission needs 60% of the total bandwidth whereas with 30 dBm only 20% of the bandwidth is needed using max sum utility. Thus, the secondary sum rate is multiplied by 2.

Fig. 3.4 illustrates the cognitive sum rate as a function of M for $L_R = 4$, $R_0 = 10$ Mbits/s, and $\bar{P}_p = \bar{P}_c = 20$ dBm. From this figure, we can deduce that the achievable rate is improving

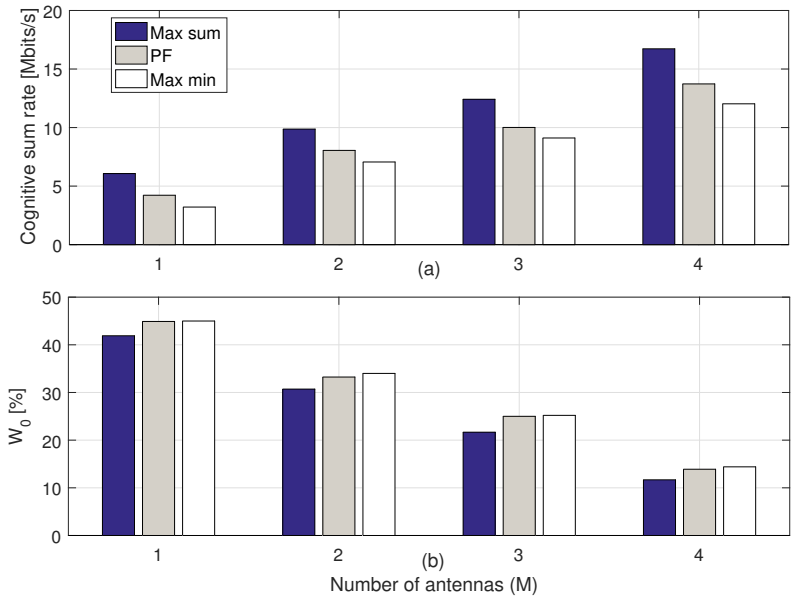

Figure 3.4: (a) Cognitive sum rate, (b) primary bandwidth fraction (W_0 [%]), versus number of antennas for $L_R = 4$, $R_0 = 10$ Mbits/s, and $\bar{P}_p = \bar{P}_c = 20$ dBm.

when M increases, in other words, MIMO antennas provide more degrees of freedom to the system which enhances the cognitive sum rate. Similar to the power budget effect, increasing the number of antennas offers more bandwidth to secondary transmissions. Indeed, with MIMO antennas, primary transmission is enhanced as it demands less relay power and thus more power can be allocated to secondary transmissions.

3.5.2 Convergence Speed

In Fig. 3.5, we compare between the performance of PSO and a recently proposed meta-heuristic approach entitled GWO, which are both employed with the primal-dual method, by investigating their convergence speed defined by the number of iterations needed to reach convergence. Note that an iteration in Fig. 3.5 corresponds to one iteration of the "while loop" given in Algorithm 1 line 2-13. GWO is inspired by grey wolf hunt. It mimics the leadership hierarchy and hunting mechanism of grey wolves in nature. During an iteration, the algorithm categorizes the candidates (i.e., grey wolves) into four groups for simulating the leadership hierarchy: Group 1 corresponds to the fittest solution, Group 2 and 3 are the second and third best solutions. Finally, Group 4 contains the remaining candidates of the population. Also, the

algorithm simulates the hunting, searching for prey, encircling prey, and attacking prey of grey wolves. For example, the hunting corresponds to the position update of each candidate from an iteration to another (see [41] for more details). We plot the cognitive sum rate versus the number of iterations for PSO and GWO. It can be clearly seen that PSO achieves its suboptimal solution faster than GWO. For instance, it requires around 10-20 iterations to converge with the max sum utility while GWO needs 30-40 iterations. Moreover, we can notice that PSO reaches a better suboptimal solution than GWO.

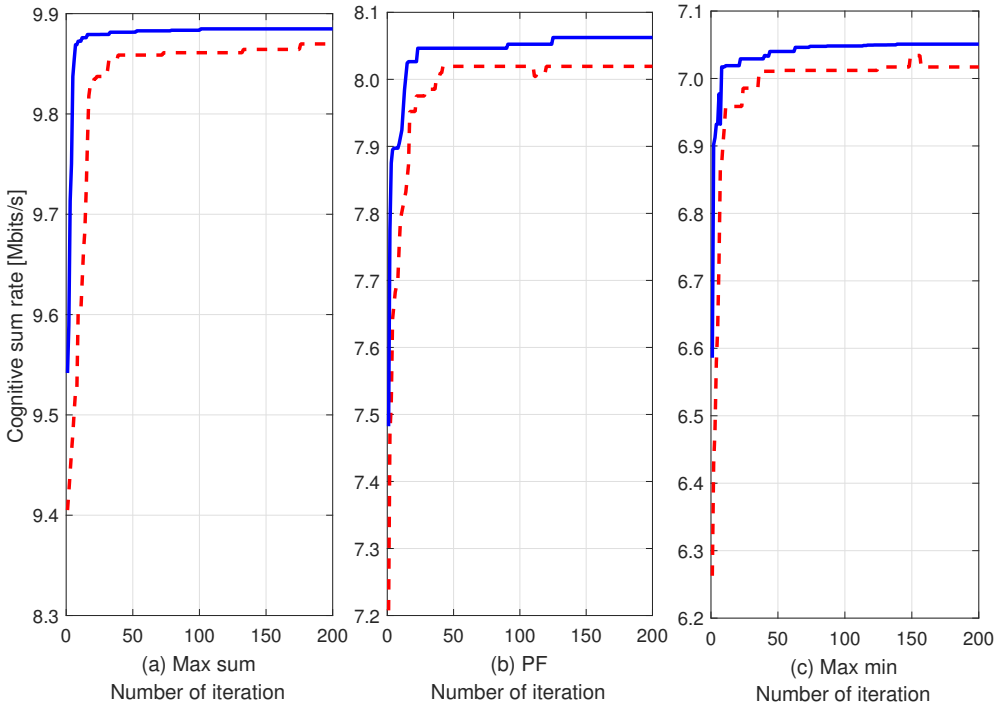

Figure 3.5: Algorithms convergence speed for $L_R = 4, M = 2, R_0 = 10$ Mbits/s, and $\bar{P}_p = \bar{P}_c =$ 20 dBm.

For a given maximum number of iterations of the subgradient method $I_{\max}$, the complexity is given by $\min(I_{\max}, 1/\varepsilon^2)$, where ε represents the accuracy-guarantee which is defined by the difference between the best value and the iterate value [107]. According to (3.34)-(3.39), subgradient needs to calculate $12ML_R + 8M + 16L_R + 15$ multiplications and $6ML_R + 8M + 9L_R + 12$ additions at each iteration. These operations are computed for each particle of the meta-heuristic approach. On the other hand, PSO and GWO are two meta-heuristic algorithms

where the exact number of iterations needed to reach the solution is arbitrary and depends on the studied scenario. However, the computational complexity per iteration can be determined. According to Appendix A, PSO needs to calculate 5 multiplications and 5 additions for every element of $\boldsymbol{W}^{(n)}$. Hence, $5(L_R(2M)^2+(L_R+1))N$ multiplications and $5(L_R(2M)^2+(L_R+1))N$ additions are calculated every iteration for the total N particles whereas GWO calculates $13(L_R(2M)^2+(L_R+1))N$ multiplications and $11(L_R(2M)^2+(L_R+1))N$ additions according to [41]. In our simulation results, we set $\varepsilon = 0.1$ and $I_{\max} = 200$ iterations for subgradient algorithm. While PSO and GWO algorithms are executed for at most 200 iterations (i.e., the utilities are computed at most $200 \times N$ times), they are stopped if the achieved utility remains constant for a certain number of consecutive iterations.

Table 3.2: CPU times (sec) and number of iterations for the proposed joint-optimization method.

	Max Sum		PF		Max Min	
	PSO	**GWO**	**PSO**	**GWO**	**PSO**	**GWO**
Total CPU time	39	59	57	86	76	121
I^*	15	32	22	48	16	39

For 200 realizations, $N = 30$, $L_R = 4$ and $M = 2$, results show that on average PSO is faster than GWO and requires less time to converge as shown in Table 3.2. In Table 3.2, we compute the CPU times in seconds of both algorithms and record the iteration number (denoted by I^*) needed to reach the near optimal solution of the joint optimization (i.e., optimizing the power, bandwidth, and relay amplification matrices), which exactly marks the instant when the algorithm achieves its steady state utility. Increasing the number of particles N would enhance the convergence speed of the algorithms. In fact, PSO and GWO are able to achieve their solutions with a lower number of iterations but they require more CPU times as they need to perform more additions and multiplications during each iteration. Note that all tests were performed on a laptop machine featuring an Intel(R) Core(TM) i7 CPU and running Windows 8.1. The clock of the machine is set to 2.66 GHz with a 8 GB memory.

3.6 Chapter Summary

In this chapter, MIMO TWR scheme for overlay CR networks where CUs are engaged to support primary transmission over a fraction of the bandwidth is investigated. More specifically, we considered multiple AF relays where the primary and cognitive terminal powers were optimized adaptively with the bandwidth and amplification gains. The objective was based on maximizing the cognitive utility while satisfying a certain primary target data rate. Starting with expressions of primary and cognitive powers for fixed bandwidths and amplification gains, the heuristic PSO algorithm was employed to reach a near-optimal solution. Moreover, in addition to the sum rate objective function, other utilities were investigated to introduce more fairness among CUs.

CHAPTER 4. TWO WAY RELAYING WITH ENERGY HARVESTED RELAYS

In this chapter, the TWR-AF scheme with PS protocol for multiple relays scenario is proposed and analyzed. The PS protocol is adopted in this chapter as it outperforms the TS protocol mainly at high SNR levels as shown in [110]. We consider that relays are simultaneously powered through RF signals and RE. The objective of the framework is to maximize the total throughput of the EH TWR system over a certain number of time slots while respecting the power budget and the storage capacity constraints at each relay. This is performed by determining, for each relay, its active or idle status, the fraction of signals to be harvested, and the transmitted power (i.e., amplification gain to be allocated in the second phase). In this context, some of the relays can be turned to the idle mode such that they do not participate in the broadcasting process but continue harvesting energy from other transmitting (i.e., active) relays.

4.1 Comparison between Time switching and Power Splitting

4.1.1 Single Relay System Model

We consider a half-duplex TWR system where two battery-powered sources, denoted by S_1 and S_2, exchange information through the help of an intermediate EH relay node, denoted by R as shown in Fig. 4.1. It is assumed that relay R is equipped with two components: an EH components, where the task is to convert the RF signal to direct current, and information processing components responsible in forwarding the received signal to the sources S_1 and S_2 using the harvested energy [111]. It is assumed that each node is equipped with a single antenna and that S_1 and S_2 are not within the communication range of each other.

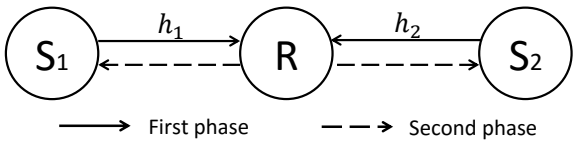

Figure 4.1: System model of two-way relaying.

In the phase of TWR, both S_1 and S_2 transmit their messages x_1 and x_2 simultaneously to R with a power denoted by P_1 and P_2, respectively. In the second phase, the relay R transmits the broadcast signal to the sources with a harvested power denoted by P_h. Let us define T as the total time slot or epoch length to exchange messages between S_1 and S_2, and η as the energy conversion efficiency ratio when converting the RF signal to current ($0 \leq \eta \leq 1$). Let us define $\bar{P}_s, \bar{P}_r, h_1$, and h_2 as the peak power at each source, the peak power at R, the channel gain between S_1 and R, and the channel gain between S_2 and R, respectively. Without loss of generality, all channel gains are assumed to be constant during the two transmission phases. Also, all noise variances are assumed to be equal to N_0, and $\mathbb{E}\left[|x_1|^2\right] = \mathbb{E}\left[|x_2|^2\right] = 1$.

4.1.2 Energy Harvesting Protocols

In the first phase, the received signal at the relay is given by

$$y_r = \sqrt{P_1} h_1 x_1 + \sqrt{P_2} h_2 x_2 + n_r. \tag{4.1}$$

Based on the relay receiver architecture, two practical protocols, named as TS relaying protocol and PS relaying protocol, can be adopted in the cooperative EH context.

4.1.2.1 Time Switching Relaying Protocol

In TS protocol, the relay spends a portion of time for EH and the remaining time for information processing. Let us assume ρ as the TS ratio where during ρT time, the relay can harvest energy from the received signal ($0 < \rho < 1$), as shown in Fig. 4.2.

The remaining time $(1-\rho)T$ is used for communications such that the first $(1-\rho)T/2$ is used for information transmission from S_1 and S_2 to the relay R (i.e., first phase), while the second $(1-\rho)T/2$ is used to broadcast the received signal from the relay to S_1 and S_2 (i.e., the second phase). Later, it will be shown that the choice of the TS ratio affects the achievable

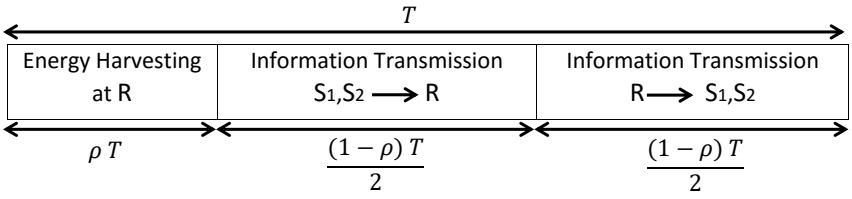

Figure 4.2: Block diagram of the TS protocol.

sum rate. In fact, increasing ρ allows the relay to harvest more energy that will be employed in forwarding the received signals to the destination. However, this will reduce the allocated time to perform the whole transmission and vice versa. Therefore, an optimal choice of ρ is required in order to enhance the TS sum rate.

The harvested energy and power (energy normalized) at the relay R using *harvest-and-use* approach, denoted by H_{TS} and P_{TS}, are given, respectively, by

$$H_{\mathrm{TS}} = \eta \left(P_1|h_1|^2 + P_2|h_2|^2\right) \rho T, \tag{4.2}$$

$$P_{\mathrm{TS}} = \frac{H_{\mathrm{TS}}}{(1-\rho)T/2} = \frac{2\eta\rho \left(P_1|h_1|^2 + P_2|h_2|^2\right)}{(1-\rho)}. \tag{4.3}$$

During the second phase, R amplifies y_r by multiplying it by the relay amplification gain, denoted by w_{TS}, and broadcasts it to S_1 and S_2. Hence, the received signals at S_1 and S_2 are given, respectively, as

$$\begin{aligned} y_1 &= h_1 w_{\mathrm{TS}}(h_1\sqrt{P_1}x_1 + h_2\sqrt{P_2}x_2 + n_r) + n_1, \\ y_2 &= h_2 w_{\mathrm{TS}}(h_1\sqrt{P_1}x_1 + h_2\sqrt{P_2}x_2 + n_r) + n_2, \end{aligned} \tag{4.4}$$

where the amplification gain at the relay R using TS protocol can be expressed as [112]

$$w_{\mathrm{TS}} = \sqrt{\frac{P_{\mathrm{TS}}}{P_1|h_1|^2 + P_2|h_2|^2 + N_0}} \approx \sqrt{\frac{P_{\mathrm{TS}}}{P_1|h_1|^2 + P_2|h_2|^2}}. \tag{4.5}$$

In (4.5), the noise effect in the denominator is ignored [113],[114]. Without loss of generality, this approximation simplifies the subsequent derivations without having a significant impact on the achieved results. Since the channels are known perfectly at S_t, $t = \{1, 2\}$, S_i can remove the self interference. Note that in the case when imperfect channel estimation is considered, self interference can still be applied, however, it will introduce an error related to the channel

estimation that can be included in the noise. The investigation of the impact of the imperfect channel estimation on the system performance is left for a future extension of this work. Therefore, signal-to-noise ratios (SNRs) at S_1 and S_2 can be, respectively, given as follows

$$\Upsilon_{1,\mathrm{TS}}(\rho) = \frac{P_2 w_{\mathrm{TS}}^2 |h_1|^2 |h_2|^2}{N_0 \left(1 + w_{\mathrm{TS}}^2 |h_1|^2\right)}, \Upsilon_{2,\mathrm{TS}}(\rho) = \frac{P_1 w_{\mathrm{TS}}^2 |h_1|^2 |h_2|^2}{N_0 \left(1 + w_{\mathrm{TS}}^2 |h_2|^2\right)}. \tag{4.6}$$

By substituting (4.5) into (4.6), and after some simplifications, the SNRs can be re-written as

$$\Upsilon_{1,\mathrm{TS}}(\rho) = \frac{2\eta P_2 |h_1|^2 |h_2|^2}{N_0 \left(\frac{1}{\rho} + 2\eta |h_1|^2 - 1\right)}, \quad \Upsilon_{2,\mathrm{TS}}(\rho) = \frac{2\eta P_1 |h_1|^2 |h_2|^2}{N_0 \left(\frac{1}{\rho} + 2\eta |h_2|^2 - 1\right)}, \tag{4.7}$$

Thus, the TWR sum rate can be expressed

$$R_{\mathrm{TS}}(\rho) = \frac{1-\rho}{2} \left[\log 2 \left(1 + \Upsilon_{1,\mathrm{TS}}(\rho)\right) + \log 2 \left(1 + \Upsilon_{2,\mathrm{TS}}(\rho)\right)\right], \tag{4.8}$$

Hence, the optimization problem that maximizes the sum rate for TS protocol while satisfying relay power limitation constraint can now be formulated as

$$\underset{0<\rho<1}{\text{maximize}} \quad R_{\mathrm{TS}}(\rho) \tag{4.9}$$

subject to:

$$\rho \left(2\eta \left(P_1 |h_1|^2 + P_2 |h_2|^2\right) + \bar{P}_r\right) \leq \bar{P}_r. \tag{4.10}$$

Constraint (4.10) is equivalent to the relay harvested power constraint given in (4.3) (i.e., $P_{\mathrm{TS}} = \eta\rho \left(P_1 |h_1|^2 + P_2 |h_2|^2\right) / (1-\rho) \leq \bar{P}_r$) and indicates that the harvested power has to be less than the relay power limitation. Indeed, exceeding $\bar{P}_r$ will affect the relay performance or affect the relay circuit. This can be applied in the case where energy storage is not available at the relay. In this case, if the harvested power is higher than $\bar{P}_r$, the system will decide to reduce ρ in order to avoid the loss of energy (i.e., the extra harvested energy that will not be used by the relay).

4.1.2.2 Power Splitting Relaying Protocol

In PS protocol, the relay uses a part of the received signal for EH and the remaining part for information transmission. Let us assume that $1-\mu$ is the relay PS ratio, where $0 < \mu < 1$. At the relay, $\sqrt{1-\mu} y_r = \sqrt{1-\mu}(\sqrt{P_1} h_1 x_1 + \sqrt{P_2} h_2 x_2 + n_r)$ corresponds to the

part of RF signal that will be converted to a current, while the remaining part of the signal $\sqrt{\mu}y_r = \sqrt{\mu}(\sqrt{P_1}h_1x_1 + \sqrt{P_2}h_2x_2 + n_r)$ is used for information processing as shown in Fig. 4.3. In this protocol, the transmission in each phase is performed during $T/2$.

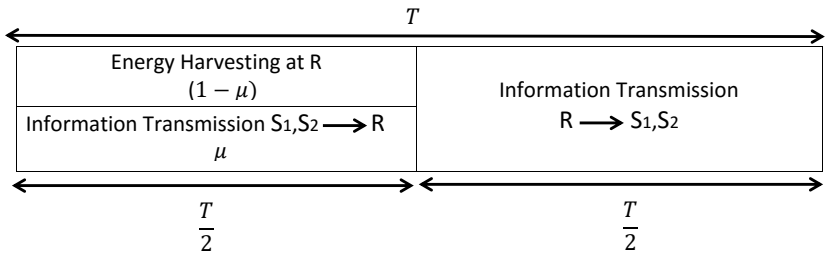

Figure 4.3: Block diagram of the PS protocol.

As will be shown in the sequel, the choice of the PS ratio affects the achievable sum rate. Indeed, high values of $(1-\mu)$ will provide more input RF signal to the energy harvester receiver. However, this will reduce the quality of the signal that will be forwarded by the relay and vice versa. Therefore, an optimized choice of μ will enhance the achievable sum rate. The harvested energy and power (energy normalized) at the relay R using *harvest-and-use* approach, denoted by E_h and P_h, are given, respectively, by

$$H_{\mathrm{PS}} = \eta(1-\mu)\left(P_1|h_1|^2 + P_2|h_2|^2\right)\frac{T}{2}, \tag{4.11}$$

$$P_{\mathrm{PS}} = \frac{H_{\mathrm{PS}}}{T/2} = \eta(1-\mu)\left(P_1|h_1|^2 + P_2|h_2|^2\right). \tag{4.12}$$

During the second phase, the relay amplifies the received signal y_r by the relay amplification gain denoted as w_{PS} and broadcasts it to S_1 and S_2. Finally, the received signals at S_1 and S_2 are given respectively as

$$\begin{aligned} y_1 &= h_1 w_{\mathrm{PS}}\sqrt{\mu}(h_1\sqrt{P_1}x_1 + h_2\sqrt{P_2}x_2 + n_r) + n_1, \\ y_2 &= h_2 w_{\mathrm{PS}}\sqrt{\mu}(h_1\sqrt{P_1}x_1 + h_2\sqrt{P_2}x_2 + n_r) + n_2, \end{aligned} \tag{4.13}$$

where the amplification gain at the relay using PS protocol can be expressed as

$$w_{\mathrm{PS}} = \sqrt{\frac{P_{\mathrm{PS}}}{\mu\left(P_1|h_1|^2 + P_2|h_2|^2 + N_0\right)}} \approx \sqrt{\frac{P_{\mathrm{PS}}}{\mu\left(P_1|h_1|^2 + P_2|h_2|^2\right)}} \tag{4.14}$$

After removing the self interference, the SNRs at S_1 and S_2 can be given, respectively, as follows

$$\Upsilon_1^{\mathrm{PS}}(\mu) = \frac{\mu P_2 w_{\mathrm{PS}}^2|h_1|^2|h_2|^2}{\sigma^2(1+\mu w_{\mathrm{PS}}^2|h_1|^2)}, \quad \Upsilon_2^{\mathrm{PS}}(\mu) = \frac{\mu P_1 w_{\mathrm{PS}}^2|h_1|^2|h_2|^2}{\sigma^2(1+\mu w_{\mathrm{PS}}^2|h_2|^2)}. \tag{4.15}$$

By substituting (4.14) into (4.15) and after some simple manipulations, the SNRs at S_1 and S_2 can be written as

$$\Upsilon_1^{\mathrm{PS}}(\mu) = \frac{\mu\eta P_2|h_1|^2|h_2|^2}{N_0(\frac{1}{1-\mu}+\eta|h_1|^2)}, \quad \Upsilon_2^{\mathrm{PS}}(\mu) = \frac{\mu\eta P_1|h_1|^2|h_2|^2}{N_0(\frac{1}{1-\mu}+\eta|h_2|^2)}, \tag{4.16}$$

Therefore, the TWR sum rate can be expressed as

$$R_{\mathrm{PS}}(\mu) = \frac{1}{2}\left[\log 2\left(1+\Upsilon_1^{\mathrm{PS}}(\mu)\right) + \log 2\left(1+\Upsilon_2^{\mathrm{PS}}(\mu)\right)\right]. \tag{4.17}$$

Hence, the optimization problem that maximizes the sum rate for PS protocol while satisfying relay power limitation constraint can be now formulated as

$$\underset{0<\mu<1}{\text{maximize}} \quad R_{\mathrm{PS}}(\mu) \tag{4.18}$$

subject to:

$$\eta\mu\left(P_1|h_1|^2 + P_2|h_2|^2\right) \leq \bar{P}_r, \tag{4.19}$$

where constraint (4.19) corresponds to the relay harvested power imitation constraint.

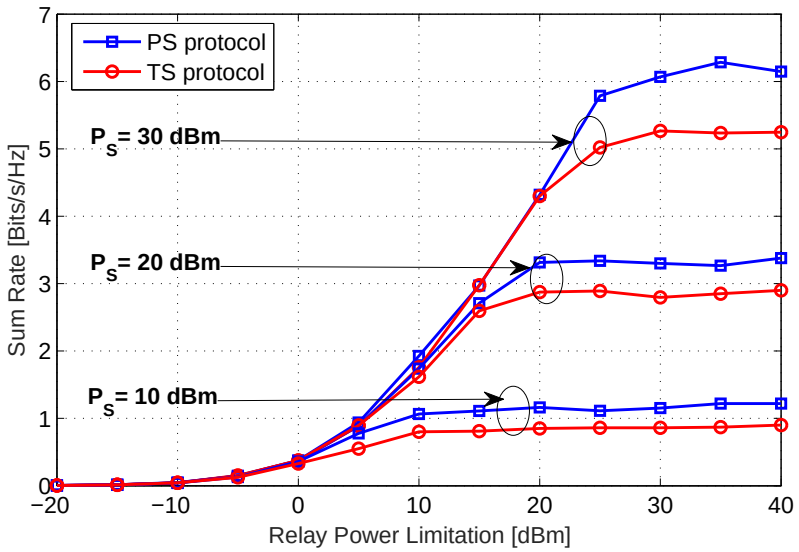

Figure 4.4: The harvest-and-use achieved rate and for PS and TS protocols versus $\bar{P}_r$.

Fig. 4.4 plots the achievable throughput versus the power relay limitation $\bar{P}_r$ for different values of source power $P_s = \{10, 20, 30\}$ dBm for *harvest-and-use* approach. It is noticed that by increasing the relay power budget, the relay is allowed to harvest more RF power and hence

increase the total sum rate till a certain maximum value where the sum rate achieves a steady-state region limited by P_s. Indeed, if P_s is low, the relay cannot harvest energy greater than a certain level.

Comparing the two protocols: PS and TS, it is shown that PS protocol achieves greater sum-rates with both relaying strategies mainly at high $\bar{P}_r$ values. This can be explained by the fact that the PS protocol performs its transmission over the total interval T, while TS transmits the signals during $(1-\rho)T$. Indeed, at high SNR regime, the transmission time duration is more influential than the SNR effect in the $\log_2$ function due to the availability of harvested power for both protocols.

4.2 Multiple Relay Selection of Energy Harvested Relays

4.2.1 System and Channel Models

We consider a half-duplex TWR system consists of two terminals, separated by a distance $\mathcal{D}$ and denoted by S_1 and S_2, aiming to exchange information between each other through the help of multiple self-powered EH relays, denoted by $r_l, l = 1, .., L$, placed within the communication range of both terminals.

The relays are placed within a circle centered in the middle of S_1 and S_2 with a radius equals to $\frac{\mathcal{D}}{2}$ as shown in Fig. 4.5. Each node is equipped with a single antenna and S_1 and S_2 are not within the communication range of each other. In the TWR first phase, both S_1 and S_2 send their messages x_1 and x_2 simultaneously to r_l, $\forall l = 1, .., L_R$, with a power denoted by P_1 and P_2, respectively. In the second phase, a set of relays are selected to broadcast the signal to the sources with a power denoted by $P_{r_l,b}$, $\forall l = 1, .., L$. We assume that the transmission will be performed in a finite period of time divided into B blocks of equal size T_c, where T_c is the time slot or epoch length to exchange messages between S_1 and S_2.

We denote by $h^b_{1r_l}$ and $h^b_{2r_l}$ the channel gains during the b^{th} time slot between S_1 and R_l and between S_2 and r_l, respectively, where $b = 1, \cdots, B$. The communication channel between two nodes x and y of the TWR system at time slot b is given as follows:

$$h^b_{xy} = \frac{\tilde{h}^b_{xy}}{\sqrt{\mathrm{PL}_{xy}}}, \tag{4.20}$$

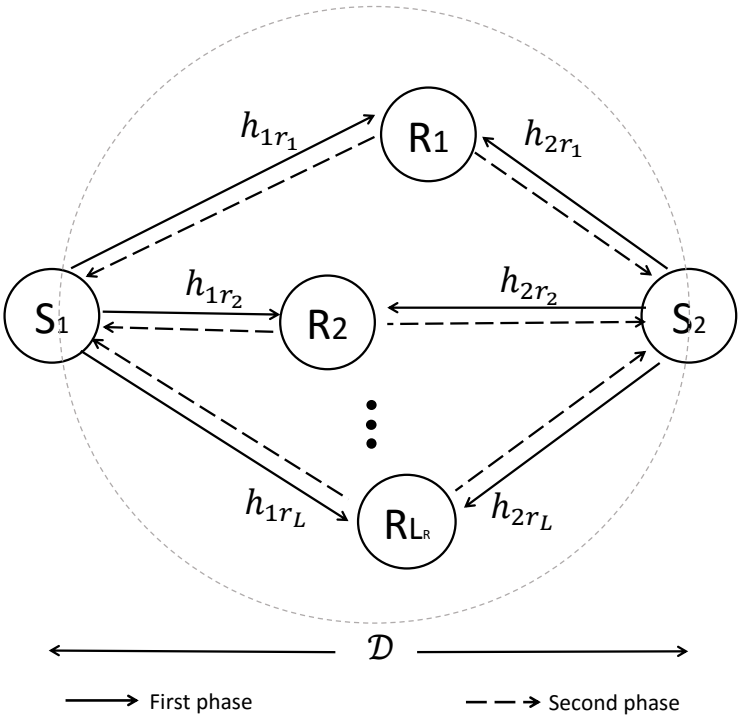

Figure 4.5: System model of multiple two-way relays.

where PL_{xy} represents the path loss effect and $\tilde{h}^b_{xy}$ is a fading coefficient with a coherence time T_c sec. Line-of-sight (LoS) link between the sources and the relays is considered. Hence, we adopt the following free-space path loss expression:

$$\mathrm{PL}_{xy} = 10\varpi \log_{10}\left(\frac{4\pi d_{xy} f_c}{C_{\text{light}}}\right) + \mathrm{PL}^{\text{LoS}}, \tag{4.21}$$

where d_{xy} is the Euclidean distance between the nodes x and y, ϖ is a pathloss exponent, f_c is the carrier frequency, C_{light} is the speed of light, and PL^{LoS} represents additional losses which depends on the environment. The fast-fading effect, $\tilde{h}^b_{xy}$, can be modeled using fading distributions considering the existence of LoS link such as the Rician model. Without loss of generality, all channel gains are assumed to be constant during the two transmission phases of TWR (i.e., one time slot).

Although it is more important to investigate scenarios with causal channel state (i.e., the current and future channels are imperfectly known), in this study, we consider a simpler scenario assuming non-causal channel state known through prediction [58]. The results obtained in this chapter constitute an upper bound for realistic scenarios and they provide a good insight on the behavior of the system over the time. The analysis of imperfect channel state information

scenarios are more elaborate and will be investigated in the future extension of this work. The transmitted signal power levels during each slot b are given as $\mathbb{E}\left[|x_{1,b}|^2\right] = \mathbb{E}\left[|x_{2,b}|^2\right] = 1$.

4.2.2 Energy Harvesting Model

In this chapter, two EH models are combined, i.e., the RE and RF models. We model the RE stochastic energy arrival rate as a random variable Φ Watt defined by a probability density function (pdf) $f(\varphi)$. For example, for photovoltaic energy, Φ can be interpreted as the received amount of energy per time unit with respect to the received luminous intensity in a particular direction per unit solid angle. By respecting the half-duplex RF EH constraint, each node cannot harvest from RF and transmit simultaneously. On the other hand, each relay can harvest from RE during the whole period T_c. Note that, the non-selected relays remain silent and harvest energy during the whole period T_c including the RF signal coming from the selected relays in the second information processing slot. The harvested energy is partially or totally stored to be used in future time blocks.

In this chapter, $\varphi_{l,b}$ represents the instantaneous amount of RE produced during slot b at relay l, and $\mathcal{J}_b$ is the set of selected relays during slot b. η_{rf} and η_{re} denote the energy conversion efficiency coefficient of the RF and RE where $0 \leq \eta_{\text{rf}}, \eta_{\text{re}} \leq 1$. A binary variable, denoted by ϵ_l^b, is introduced to indicate the status of each relay where $\epsilon_l^b = 1$ if the relay is selected to amplify the signals, and $\epsilon_l^b = 0$, otherwise.

4.2.3 Relay Power Model

Since the energy arrivals and energy consumption are random and the energy storage capacities are finite, some relays might not have enough energy to serve users at a particular time. Under such scenario, it is preferred that some of the relays are kept OFF and allowed to recharge. Hence, each relay can be selected for transmission or not at each time slot b. The decision of relays selection is made centrally, i.e., the decision is taken by a central entity based on the amounts of stored and consumed energy at each relay. The total power consumption of a relay, denoted by $P_{r_l,b}^{\text{tot}}$, can be computed as follows:

$$P_{r_l,b}^{\text{tot}} = \alpha P_{r_l,b} + \beta \tag{4.22}$$

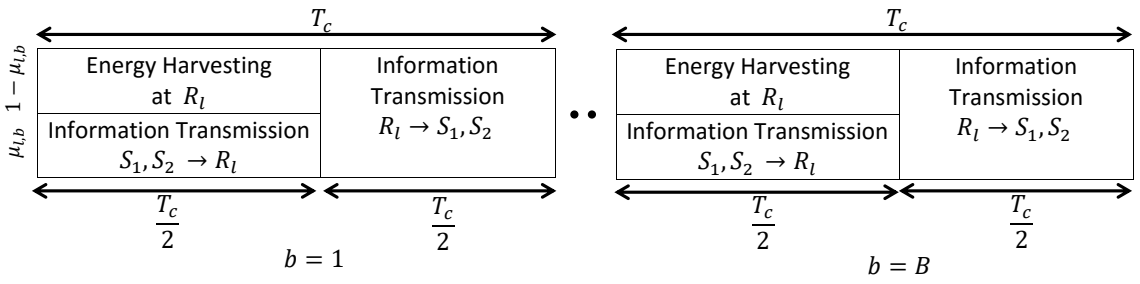

Figure 4.6: Block diagram of the PS protocol during B blocks for one relay.

where α and β correspond to the power consumption that scales with the radiated power due to amplifier and feeder losses and the offset of site power which is consumed independently of the transmit power and is due to signal processing, battery backup, and cooling, respectively. $P_{r_l,b}$ denotes the radiated power by relay l at a given time slot b.

4.3 Problem Formulation

In the first phase, the received signal at the l^{th} relay during each T_c is given by

$$y_{r_l,b} = \sqrt{P_1} h^b_{1r_l} x_{1,b} + \sqrt{P_2} h^b_{2r_l} x_{2,b} + n_{r,b}. \tag{4.23}$$

where $n_{r,b}$ is the sum of two noises. An AWGN at the l^{th} relay during slot b with variance N_r and a noise introduced by the signal processing circuit from passband to baseband also assumed to be AWGN with zero mean and variance N_0. In practice, the antenna noise has a negligible effect on the information signal and the average power of the received signal as well [115]. Hence, we ignore its impact in (4.23) (i.e., $N_r \ll N_0$).

In the PS protocol, before transforming the received signal from passband to baseband, the relay uses part of it for EH and the remaining part for information transmission. Let us assume that $\sqrt{1-\mu_{l,b}}$ is the relay l PS ratio during the b^{th} slot, where $0 \leq \mu_{l,b} \leq 1$, such that $\sqrt{1-\mu_{l,b}}(\sqrt{P_1} h^b_{1r_l} x_{1,b} + \sqrt{P_2} h^b_{2r_l} x_{2,b})$ corresponds to the part of RF signal that will be converted to a current, while the remaining part of the signal $\sqrt{\mu_{l,b}}(\sqrt{P_1} h^b_{1r_l} x_{1,b} + \sqrt{P_2} h^b_{2r_l} x_{2,b})$ is used for information processing as shown in Fig. 4.6. In this protocol, the transmission in each phase is performed during $T_c/2$.

The total harvested energy of the l^{th} relay during slot b for selected and non-selected relay, denoted by H^b_l, is given as follows

$$H_l^b = \underbrace{[\eta_{\text{re}}\varphi_{l,b}]\,T_c}_{\text{RE EH}} + \epsilon_l^b \Bigg(\underbrace{(1-\mu_{l,b})\left[\eta_{\text{rf}}\left(P_1|h_{1r_l}^b|^2 + P_2|h_{2r_l}^b|^2\right)\right]\frac{T_c}{2}}_{\text{RF EH from sources}} \Bigg)$$
$$+ (1-\epsilon_l^b)\Bigg(\underbrace{\left[\eta_{\text{rf}}\left(P_1|h_{1r_l}^b|^2 + P_2|h_{2r_l}^b|^2\right)\right]\frac{T_c}{2}}_{\text{RF EH from sources}} + \underbrace{\left[\eta_{\text{rf}}\sum_{j\in\mathcal{J}_b} P_{r_l,b}|h_{r_l r_j}^b|^2\right]\frac{T_c}{2}}_{\text{RF EH from selected relays}} \Bigg). \tag{4.24}$$

The stored energy at the end of slot b at relay l, denoted by S_l^b, is given as follows:

$$S_l^b = S_l^{b-1} + H_l^b - E_l^b - E_{le}, \tag{4.25}$$

where E_l^b corresponds to the consumed energy by relay l during slot b due to information processing and is given as:

$$E_l^b = \beta T_c + \epsilon_l^b \left[(\alpha P_{r_l,b})\frac{T_c}{2}\right]. \tag{4.26}$$

Note that, initially, we assume that the battery of relay l may already have a certain amount of charge denoted by $S_{r_l,0}$. During the second phase, the selected relays amplify the received signal by multiplying it by the relay amplification gain denoted by $w_{l,b}$. Then, they broadcast it to S_1 and S_2. Hence, the received signals at S_1 and S_2 at slot b are given, respectively, as

$$y_{1,b} = \sum_{l=1}^{L} \epsilon_l^b h_{1r_l}^b w_{l,b}(\sqrt{\mu_{l,b}}(\underbrace{h_{1r_l}^b\sqrt{P_1}x_{1,b}}_{\text{Self Interference}} + h_{2r_l}^b\sqrt{P_2}x_{2,b}) + n_{r_l,b}) + n_{1,b},$$
$$y_{2,b} = \sum_{l=1}^{L} \epsilon_l^b h_{2r_l}^b w_{l,b}(\sqrt{\mu_{l,b}}(h_{1r_l}^b\sqrt{P_1}x_{1,b} + \underbrace{h_{2r_l}^b\sqrt{P_2}x_{2,b}}_{\text{Self Interference}}) + n_{r_l,b}) + n_{2,b}, \tag{4.27}$$

where $n_{1,b}$ and $n_{2,b}$ are the AWGN noise at the receivers S_1 and S_2, respectively. The amplification gain at the relay l and during time slot b can be expressed as:

$$w_{l,b} = \sqrt{\frac{P_{r_l,b}}{\mu_{l,b}(P_1|h_{1r_l}^b|^2 + P_2|h_{2r_l}^b|^2) + N_0}} \approx \sqrt{\frac{P_{r_l,b}}{\mu_{l,b}(P_1|h_{1r_l}^b|^2 + P_2|h_{2r_l}^b|^2)}}. \tag{4.28}$$

In (4.28), we ignore the noise effect in the denominator [113]. Without loss of generality, this approximation simplifies the subsequent derivations without having a significant impact on the achieved results. Therefore, the SNRs at S_q, $q \in \{1,2\}$ during the slot b can be expressed as as follows:

$$\Upsilon_t^b = \frac{P_{\bar{t}} \left(\sum_{l=1}^{L} \epsilon_l^b w_{l,b} \sqrt{\mu_{l,b}} |h_{tr_l,b} h_{\bar{t}r_l,b}| \right)^2}{N_0 \left(1 + \sum_{l=1}^{L} \epsilon_l^b w_{l,b}^2 |h_{tr_l,b}|^2 \right)}, \tag{4.29}$$

where $\bar{t} = 1$ if $t = 2$ and vice versa. Hence, the TWR sum rate during the time slot b can be expressed:

$$R^b = \frac{T_c}{2} \sum_{q=1}^{2} \log_2(1 + \Upsilon_t^b). \tag{4.30}$$

Consequently, the optimization problem maximizing the TWR sum rate, denoted by R, while satisfying the energy consumed and stored constraints for EH with PS protocol using AF is given as:

$$\underset{\boldsymbol{\epsilon},\boldsymbol{\mu},\boldsymbol{P_r} \geq 0}{\text{maximize}} \qquad R = \sum_{b=1}^{B} R^b \tag{4.31}$$

subject to:

$$E_l^b + E_{le} \leq S_l^{b-1}, \quad \forall l = 1, .., L, \forall b = 1, .., B, \tag{4.32}$$

$$S_l^{b-1} + H_l^b \leq \bar{S}, \quad \forall l = 1, .., L, \forall b = 1, .., B, \tag{4.33}$$

$$0 \leq P_{r_l,b} \leq \bar{P}_r, \quad \forall l = 1, .., L, \forall b = 1, .., B, \tag{4.34}$$

$$0 \leq \mu_{l,b} \leq 1, \quad \forall l = 1, .., L, \forall b = 1, .., B, \tag{4.35}$$

$$\epsilon_l^b \in \{0, 1\}, \quad \forall l = 1, .., L, \forall b = 1, .., B, \tag{4.36}$$

where $\boldsymbol{\epsilon} = [\epsilon_l^b]_{L \times B}$, $\boldsymbol{\mu} = [\mu_{l,b}]_{L \times B}$, and $\boldsymbol{P_r} = [P_{r_l,b}]_{L \times B}$ are matrices containing the relay status, the PS ratios, and the relay transmit power levels of each relay l at each slot b, respectively. Constraint (4.32) ensures that the consumed energy during slot b for any relay is always less than or equal to the stored energy at slot $b-1$. Constraint (4.33) indicates that the energy stored at a relay cannot exceed the capacity of its super-capacitor at any time. Constraints (4.34) and (4.35) indicate the transmit power and PS ratio limits. Finally, constraint (4.36) represent the relay selection constraint.

4.4 Joint-Optimization Solution

Due to the non-convexity of the optimization problem formulated in (4.31)-(4.36), we propose to proceed with a joint-optimization approach where we optimize the binary matrix $\boldsymbol{\epsilon}$ using the PSO algorithm and the other continuous decision variables ($\boldsymbol{\mu}$ and $\boldsymbol{P_r}$) using GP.

For a fixed and known $\boldsymbol{\epsilon}$, a successive convex approximation (SCA) approach is applied to transform the non-convex problem into a sequence of relaxed convex subproblems to approximated solution [116],[42].

4.4.1 Approximations

In order to convert the optimization problem formulated in (4.31)-(4.36) to a GP standard form, we propose to apply approximations for the objective and constraint functions. The single condensation method is employed to convert these functions to posynomials as described below:

Definition 1. The single condensation method for GP involves upper bounds on the ratio of a posynomial over a posynomial. It is applied to approximate a denominator posynomial $g(z)$ to a monomial function, denoted by $\tilde{g}(z)$ and leaving the numerator as a posynomial, using the arithmetic-geometric mean inequality as a lower bound [42]. Given the value of z at the iteration $i-1$ of the SCA $z^{(i-1)}$, the posynomial g that, by definition, has the form $g(z) \triangleq \sum_{k=1}^{K} \varrho_k(z)$, where $\varrho_k(z)$ are monomials, can be approximated as:

$$g(z) \geq \tilde{g}(z) = \prod_{k=1}^{K} \left(\frac{\varrho_k(z)}{\vartheta_k(z^{(i-1)})} \right)^{\vartheta_k(z^{(i-1)})}, \tag{4.37}$$

where $\vartheta_k(z^{(i-1)}) = \frac{\varrho_k(z^{(i-1)})}{g(z^{(i-1)})}$. K corresponds to the total number of monomials in $g(z)$.

4.4.2 Utility Selection

4.4.2.1 Max Sum Utility

For a given $\boldsymbol{\epsilon}$, we transform the sum-rate objective function as follows:

$$\begin{aligned}\underset{\boldsymbol{z}\geq 0}{\text{maximize}} \sum_{b=1}^{B} R^b &= \underset{\boldsymbol{z}\geq 0}{\text{maximize}} \frac{T_c}{2} \sum_{b=1}^{B}\sum_{q=1}^{2} \log_2(1+\Upsilon_t^b) \\ &\equiv \underset{\boldsymbol{z}\geq 0}{\text{minimize}} \prod_{b=1}^{B}\prod_{t=1}^{2} \frac{1}{1+\Upsilon_t^b},\end{aligned} \tag{4.38}$$

where $\boldsymbol{z} \triangleq [\boldsymbol{\mu}, \boldsymbol{P_r}]$. For notational convenience, let us define the following:

$$\begin{aligned}\frac{f_{r_l,b,t}(z)}{g_{r_l,b,t}(z)} &\triangleq \frac{1}{1+\Upsilon_t^b}, \\ \delta^{(1)}_{r_l,b,t} &\triangleq \frac{\epsilon_{r_l,b}|h_{tr_l,b}|^2}{P_1|h^b_{1r_l}|^2 + P_2|h^b_{2r_l}|^2}, \\ \delta^{(2)}_{r_l,b,t} &\triangleq \frac{\epsilon_{r_l,b}|h_{tr_l,b}h_{\bar{t}r_l,b}|}{\sqrt{P_1|h^b_{1r_l}|^2 + P_2|h^b_{2r_l}|^2}}.\end{aligned} \tag{4.39}$$

Hence, after some manipulations, (4.38) can be re-expressed as:

$$\underset{\boldsymbol{z}\geq 0}{\text{minimize}} \prod_{b=1}^{B}\prod_{q=1}^{2} \frac{1}{1+\Upsilon_t^b} \equiv \underset{\boldsymbol{z}\geq 0}{\text{minimize}} \prod_{b=1}^{B}\prod_{q=1}^{2} \frac{\left(1+\sum_{l=1}^{L}\delta^{(1)}_{r_l,b,t}P_{r_l,b}\mu^{-1}_{l,b}\right)}{1+\sum_{l=1}^{L}\delta^{(1)}_{r_l,b,t}P_{r_l,b}\mu^{-1}_{l,b} + \frac{P_{\bar{q}}}{N_0}\left(\sum_{l=1}^{L}\delta^{(2)}_{r_l,b,t}\sqrt{P_{r_l,b}}\right)^2}. \tag{4.40}$$

It can be noticed from (4.39) and (4.40) that $f_{r_l,b,t}(z)$ and $g_{r_l,b,t}(z)$ are posynomials, however, the ratio is not necessary a posynomial. Therefore, in order to convert the objective function to a posynomial, we propose to apply the single condensation method given in Definition 1 to approximate the denominator posynomial $g_{r_l,b,t}(z)$ to a monomial function, denoted by $\tilde{g}_{r_l,b,t}(z)$. The upper limit of the product K is equal to $(L_R+1)(L_R+2)/2$ and corresponds to the total number of monomials in $g_{r_l,b,t}(z)$ given in (4.40). It can be seen that the objective function is now a posynomial because a posynomial over a monomial is a posynomial and the product of posynomials remains a posynomial.

4.4.2.2 Max Min Utility

Since the log function is a monotonically increasing function then, for a given $\boldsymbol{\epsilon}$, we can simplify the problem by defining a new decision variable $\Upsilon_{\min} = \min_{t,b} \Upsilon_t^b$, $\forall b, \forall t$. The objective function with this utility can be expressed as:

$$\begin{aligned} &\underset{\boldsymbol{z}\geq 0}{\text{maximize}} \quad \min_{t,b} \quad \frac{T_c}{2}\log_2(1+\Upsilon_t^b) \equiv \\ &\underset{\boldsymbol{z}\geq 0}{\text{maximize}} \quad \min_{t,b} \quad \Upsilon_t^b \equiv \\ &\underset{\boldsymbol{z},\Upsilon_{\min}\geq 0}{\text{minimize}} \quad \frac{1}{\Upsilon_{\min}}, \quad \text{s.t} \quad \Upsilon_{\min} \leq \Upsilon_t^b. \end{aligned} \tag{4.41}$$

It can be shown that the objective function $\frac{1}{\Upsilon_{\min}}$ is a posynomial and we just need to approximate the corresponding constraints $\Upsilon_{\min} \leq \Upsilon_t^b$.

4.4.3 Problem Constraints

Next, we apply the same approximations given in Definition 1 to the inequality constraints to obtain posynomials that fit into the GP standard form. Let us define the following expressions associated to the different energy expressions defined in (4.24) and (4.26), respectively:

$$\zeta_{l,b}^{(1)} \triangleq \epsilon_{r_l,b}\left[\eta_{\text{rf}}\left(P_1|h_{1r_l}^b|^2 + P_2|h_{2r_l}^b|^2\right)\right]\frac{T_c}{2}, \tag{4.42}$$

$$\zeta_{l,b}^{(2)} \triangleq (1-\epsilon_{r_l,b})\eta_{\text{rf}}\frac{T_c}{2}, \tag{4.43}$$

$$\begin{aligned} \zeta_{l,b}^{(3)} \triangleq\ & \epsilon_{r_l,b}\left[\eta_{\text{rf}}\left(P_1|h_{1r_l}^b|^2 + P_2|h_{2r_l}^b|^2\right)\right]\frac{T_c}{2} + \\ & (1-\epsilon_l^b)\left[\eta_{\text{rf}}\left(P_1|h_{1r_l}^b|^2 + P_2|h_{2r_l}^b|^2\right)\right]\frac{T_c}{2} + \left[\eta_{\text{re}}\varphi_{r_l,b}\right]T_c, \end{aligned} \tag{4.44}$$

$$\theta_{l,b}^{(1)} \triangleq \epsilon_{r_l,b}\alpha\frac{T_c}{2}, \tag{4.45}$$

$$\theta_{l,b}^{(2)} \triangleq \beta T_c. \tag{4.46}$$

Hence, $H_{r_l,b}$ and $E_{r_l,b}$ given in (4.24) and (4.26) can be, respectively, expressed as:

$$H_{r_l,b} = -\zeta_{r_l,b}^{(1)}\mu_{l,b} + \zeta_{r_l,b}^{(2)}\sum_{j\in\mathcal{J}_b} P_{r_l,b}|h_{r_l r_j}^b|^2 + \zeta_{r_l,b}^{(3)}, \tag{4.47}$$

$$E_{r_l,b} = \theta_{r_l,b}^{(1)}P_{r_l,b} + \theta_{r_l,b}^{(2)}. \tag{4.48}$$

By expanding $E^s_{l,b-1}$, constraint (4.32) can be re-written as:

$$\frac{\sum_{x=1}^{b}(\theta^{(1)}_{l,x}P_{r_l,x}+\theta^{(2)}_{l,x}+E_{le}+\zeta^{(1)}_{l,x}\mu_{l,x})}{\sum_{x=1}^{b}\left(\zeta^{(2)}_{l,x}\sum_{j\in\mathcal{J}_x}P_{r_l,x}|h_{r_lr_j,x}|^2+\zeta^{(3)}_{l,x}\right)}\leq 1,\quad \forall l,\forall b. \tag{4.49}$$

The equivalent constraint given in (4.49) is a posynomial over a posynomial. Therefore, we can use the same approximation used in (4.37) to lower bound the denominator in (4.49) by $\tilde{u}_{r_l,b}(z)$ with a total number of monomials $K=(\sum_{x=1}^{b}|\mathcal{J}_x|)+1$. Similarly, we can rewrite constraint (4.33) as follows:

$$\frac{\sum_{x=1}^{b}\left(\zeta^{(2)}_{l,x}\sum_{j\in\mathcal{J}_x}P_{r_l,x}|h_{r_lr_j,x}|^2+\zeta^{(3)}_{l,x}\right)}{\bar{S}+\sum_{x=1}^{b-1}(\theta^{(1)}_{l,x}P_{r_l,x}+\theta^{(2)}_{l,x}+E_{le})+\sum_{x=1}^{b}(\zeta^{(1)}_{l,x}\mu_{l,x})}\leq 1,\ \forall l,\forall b. \tag{4.50}$$

The same approximation used in (4.37) to lower bound the numerator can be used in (4.50) by $\tilde{v}_{r_l,b}(z)$ and $K=2b$.

4.4.3.1 GP Standard Form

By considering the approximations of (4.40), (4.49), and (4.50) and given a fixed value of $\boldsymbol{\epsilon}$, we can formulate the GP approximated subproblem at the i^{th} iteration of the SCA for the max sum utility as follows:

$$\underset{\boldsymbol{z}\geq 0}{\text{minimize}}\quad \prod_{b=1}^{B}\prod_{t=1}^{2}\frac{f_{l,b,t}(z)}{\tilde{g}_{l,b,t}(z)} \tag{4.51}$$

subject to:

$$\frac{\sum_{x=1}^{b}(\theta^{(1)}_{l,x}P_{r_l,x}+\theta^{(2)}_{l,x}+E_{le}+\zeta^{(1)}_{l,x}\mu_{l,x})}{\tilde{u}_{r_l,b}(z)}\leq 1,\quad \forall l,\forall b, \tag{4.52}$$

$$\frac{\sum_{x=1}^{b}\left(\zeta^{(2)}_{l,x}\sum_{j\in\mathcal{J}_x}P_{r_l,x}|h_{r_lr_j,x}|^2+\zeta^{(3)}_{l,x}\right)}{\tilde{v}_{r_l,b}(z)}\leq 1,\quad \forall l,\forall b, \tag{4.53}$$

$$\frac{P_{r_l,b}}{\bar{P}_r}\leq 1,\quad \forall l,\forall b, \tag{4.54}$$

$$0\leq\mu_{l,b}\leq 1,\quad \forall l=1,..,L,\forall b=1,..,B, \tag{4.55}$$

$$\epsilon^b_l\in\{0,1\},\quad \forall l=1,..,L,\forall b=1,..,B, \tag{4.56}$$

Constraints (4.55) and (4.56) are the same as constraints (4.35) and (4.36), but they have been repeated for completeness.

For max-min utility, in addition to the above constraints, we need to approximate the following constraint $\Upsilon_{\min} \leq \Upsilon_t^b$. Using Definition 1, the approximated subproblem at the i^{th} iteration for the max min utility optimization problem is given as follows:

$$\underset{\boldsymbol{z}, \Upsilon_{\min} \geq 0}{\text{minimize}} \quad \frac{1}{\Upsilon_{\min}} \tag{4.57}$$

subject to:

$$\frac{N_0 \Upsilon_{\min} \left(1 + \sum_{l=1}^{L_R} \delta_{l,b,q}^{(1)} P_{r_l,b} \mu_{l,b}^{-1}\right)}{\tilde{s}_{l,b,q}(z)} \leq 1, \quad \forall b, \forall q, \tag{4.58}$$

$$\frac{\sum_{x=1}^{b} (\theta_{l,x}^{(1)} P_{r_l,x} + \theta_{l,x}^{(2)} + E_{le} + \zeta_{l,x}^{(1)} \mu_{l,x})}{\tilde{u}_{r_l,b}(z)} \leq 1, \quad \forall l, \forall b, \tag{4.59}$$

$$\frac{\sum_{x=1}^{b} \left(\zeta_{l,x}^{(2)} \sum_{j \in \mathcal{J}_x} P_{r_l,x} |h_{r_l r_j,x}|^2 + \zeta_{l,x}^{(3)}\right)}{\tilde{v}_{r_l,b}(z)} \leq 1, \quad \forall l, \forall b, \tag{4.60}$$

$$\frac{P_{r_l,b}}{\bar{P}_r} \leq 1, \quad \forall l, \forall b, \tag{4.61}$$

$$0 \leq \mu_{l,b} \leq 1, \quad \forall l = 1, .., L, \forall b = 1, .., B, \tag{4.62}$$

$$\epsilon_l^b \in \{0, 1\}, \quad \forall l = 1, .., L, \forall b = 1, .., B, \tag{4.63}$$

where $\tilde{s}_{l,b,t}(z)$ is the approximate monomial of $P_{\bar{t}} \left(\sum_{l=1}^{L_R} \delta_{l,b,t}^{(2)} \sqrt{P_{r_l,b}}\right)^2$ with $K = L(L+1)/2$. Constraints (4.59) and (4.63) are the same as constraints (4.52) and (4.56), but they have been repeated for completeness.

Hence, these optimization problems can be solved at each iteration of the SCA as given in Algorithm 4.1. In Algorithm 4.1, each GP in the iteration loop (line 3-7) tries to improve the accuracy of the approximations to a particular minimum in the original feasible region until no improvement can be made.

Algorithm 4.1 SCA Algorithm

1: i=1.
2: Select a feasible initial value of $\boldsymbol{z}^{(i)} = [\boldsymbol{\mu}^{(i)}, \boldsymbol{P_r}^{(i)}]$.
3: **repeat**
4: i=i+1.
5: Approximate the denominators using the arithmetic-geometric mean as indicated in (4.37) using $\boldsymbol{z}^{(i-1)}$.
6: Solve the optimization problem using the interior-point method to determine the new approximated solution $\boldsymbol{z}^{(i)} = [\boldsymbol{\mu}^{(i)}, \boldsymbol{P_r}^{(i)}]$.
7: **until** No improvement in the objective function.

4.4.4 Selected Relays Optimization

In this section, we focus on the optimization of the relays' selection parameters represented in the binary matrix $\boldsymbol{\epsilon}$. First, we propose to employ a meta-heuristic algorithm, namely BPSO, to reach a near-optimal solution of the problem. Then, we propose to compare its performance to that of the optimal BB algorithm that will be described in Section 4.4.4.2.

4.4.4.1 Binary Particle Swarm Optimization

The BPSO starts by generating N particles $\boldsymbol{\epsilon}^{(n)},\ n = 1 \cdots N$ of size $L_R \times B$ to form an initial population $\mathcal{S}$. Then, it determines the sum rate achieved by each particle by solving the optimization problem using GP approach developed in Appendix B (or the dual-method for comparison purpose in the simulation results section). Then, it finds the particle that provides the highest solution for this iteration, denoted by $\boldsymbol{\epsilon}^{\max}$. In addition, for each particle n, it saves a record of the position of its previous best performance, denoted by $\boldsymbol{\epsilon}^{(\text{n,local})}$. Then, at each iteration q, BPSO computes a velocity term $\boldsymbol{\nu}_{l,b}^{(n)}$ as follows:

$$\begin{aligned}\boldsymbol{\nu}_{l,b}^{(n)}(q+1) =& \psi_0 \boldsymbol{\nu}_{l,b}^{(n)}(q) + \psi_1(q)\left(\epsilon_{l,b}^{(\text{n,local})}(q) - \epsilon_{l,b}^{(n)}(q)\right) \\ &+ \psi_2(q)\left(\epsilon_{l,b}^{\max}(q) - \epsilon_{l,b}^{(n)}(q)\right),\end{aligned} \tag{4.64}$$

where ψ_0 is the inertia weight used to control the convergence speed ($0.8 \leq \psi_0 \leq 1.2$). ψ_1 and ψ_2 are two random positive numbers generated for iteration q ($\psi_1, \psi_2 \in [0, 2]$) [109]. Then, it updates each element q of a particle $\boldsymbol{\epsilon}^{(n)}$ as follows:

$$\epsilon_{l,b}^{(n)}(q+1) = \begin{cases} 1 \text{ if } r_{\text{rand}} < \Psi_{\text{BPSO}}\left(\boldsymbol{\nu}_{l,b}^{(n)}(q+1)\right), \\ 0 \text{ otherwise.} \end{cases} \tag{4.65}$$

Algorithm 4.2 BPSO with GP for PS-based EH TWR using AF

$q = 1$.
Generate an initial population $\mathcal{S}$ composed of N random particles $\boldsymbol{\epsilon}^{(n)}$, $n = 1 \cdots N$.
while Not converged **do**
  for $n = 1 \cdots N$ **do**
    Find $\boldsymbol{z}^{(n)}$ by solving the optimization problem for particle n using Algorithm 4.1.
    Compute the corresponding rate $R^{(n)}(q)$.
  end for
  Find $(n_m, q_m) = \arg\max_{n,q} R^{(n)}(q)$ (i.e., n_m and q_m indicate the index and the position of the particle that results in the highest rate). Then, set $R_{\max} = U^{(n_m)}(q_m)$ and $\boldsymbol{\epsilon}^{\max} = \boldsymbol{\epsilon}^{(n_m)}(q_m)$.
  Find $q_n = \arg\max_{q} R^{(n)}(q)$ for each particle n (i.e., q_n indicates the position of the particle n that results in the highest local utility). Then, set $U_{(\text{n,local})} = R^{(n)}(q_n)$ and $\boldsymbol{\epsilon}^{(\text{n,local})} = \boldsymbol{\epsilon}^{(n)}(q_n)$.
  Adjust velocities and positions of all particles using (A.3)-(A.4).
  $q = q + 1$.
end while

where r_{rand} is a pseudo-random number selected from a uniform distribution in $[0, 1]$ and Ψ_{BPSO} is a sigmoid function for transforming the velocity to probabilities and is given as:

$$\Psi_{\text{BPSO}}(x) = \frac{1}{1 + e^{-x}}. \tag{4.66}$$

More details about BPSO is given in Appendix A. Details of the joint-optimization approach are given in Algorithm 4.2.

4.4.4.2 Branch-and-Bound Method

The performance of the proposed BPSO method jointly applied with GP will be compared to that of the well-know BB algorithm, that will be also jointly applied with GP. BB was first introduced by A. H. Land and A. G. Doig in 1960 [117]. It is an optimal algorithm for solving combinatorial problems, but it requires a very high computational complexity compared to BPSO [118]. At each iteration of the BB, Algorithm 4.1 is executed to find the corresponding solution using GP. The BB is a search tree-based algorithm that iteratively solves the optimization problems given in (4.51) and (4.57) using their relaxed forms. In other words, the problems are solved for continuous solutions of $\boldsymbol{\epsilon}$ in $[0, 1]$ where the GP is executed to determine the optimum solution with non-binary values of $\boldsymbol{\epsilon}$. We denote the optimum continuous solution and the corresponding utility by $\boldsymbol{\epsilon}_0^*$ and $U(\boldsymbol{\epsilon}_0^*)$, respectively. If the obtained solution satisfies the binary constraints for all elements of $\boldsymbol{\epsilon}$ then, the optimal solution is reached. Otherwise,

further steps are needed. The algorithm solves the problem assuming that the first element of $\boldsymbol{\epsilon}$ is fixed to 0 or 1. Hence, the problem is split into two subproblems named the children nodes of the original problem called the parent node. If the solutions of these subproblems do not satisfy the binary constraints, they will be also split into two more subproblems. This process is called branching and will be executed until the optimal binary solution is obtained. In order to reduce the complexity compared to the exhaustive search method where all the possibilities are tested, the BB can stop searching in one of the directions of the tree if at any node, the cost function value is greater than a previously defined upper-bound solution. More details about the BB algorithm can be found in [119].

4.5 Simulation Results

In this section, selected numerical results are provided to evaluate the performance of the PS protocol with multiple EH relays in TWR systems.

4.5.1 Simulation Parameters

Two sources S_1 and S_2 are considered aiming at exchanging their messages during $B = 8$ time slots unless otherwise stated where each time slot length is equal to $T_c = 175$ milliseconds (ms). In the following simulations, we consider the scenario of small wireless devices employing the ZigBee protocol [120]. Hence, the frequency carrier is set to $f = 2.45$ GHz and the system bandwidth is selected to be $W = 2$ MHz [120]. All the fading channel gains adopted in the framework are assumed to be independent and identically distributed (i.i.d) Rician fading gains with a K-factor equals to 7.78 dB unless otherwise stated. The path loss parameters are selected as follows: $\varpi = 2$ and $\mathrm{PL}^{\mathrm{LoS}} = 0$ dB. The relays are randomly placed inside a circle centered in the middle of S_1 and S_2 with a distance $\mathcal{D} = 50$ meters unless otherwise stated. The noise variance and the efficiency conversion ratios are set to $N_0 = -141$ dBm, $\eta_{\mathrm{rf}} = 0.4$ [121], and $\eta_{\mathrm{re}} = 0.3$ [122]. For simplicity and without loss of generality, we assume that $P_1 = P_2 = P_s$. The relay power parameters are given as: $\alpha = 4$ mW and $\beta = 1.2$ mW [123]. At each relay, RE is assumed to be generated following a truncated normal distribution with mean 2 W and variance 0.25 in the interval $[0, 2.4]$ [124],[125]. RE is generated such that the constant

power consumption of the relays, i.e., namely β, is frequently handled. In other words, the transmit power consumption is covered by the harvested RF energy in addition to the available extra RE. The total stored energy cannot exceed $\bar{E}^s = 5$ J and the battery leakage is set to be $E_{le} = 10\,\text{mJ}$ over every time slot b. A Monte Carlo simulation with 5000 iterations is performed to determine the average performance of the investigated TWR system using the BPSO-based solution given in Algorithm 4.2.

The BPSO is executed with the following parameters: $N = 20$ and $\psi_0 \in [0, 1]$ is a linear decreasing function of the BPSO iterations expressed as follows: $\psi_0 = 0.9 - \frac{n(0.9-0.2)}{I_{\max}}$, where $I_{\max} = 200$ is the maximum number of iterations. The joint-optimization approach solution using BPSO is compared to three other approaches: a BB-based solution with GP, a BPSO-based solution with the dual method, and a BB-based solution with the dual method. Note that, for a given $\boldsymbol{\epsilon}$, the dual solution corresponds to the solution obtained by solving the dual problem of the primal problem given in (4.31)-(4.35). The corresponding solution represents a lower-bound of the optimal one due to the non-convexity of the problem (i.e., weak duality). On the other hand, the BB method achieves an optimal solution with respect to $\boldsymbol{\epsilon}$ but it requires a very high computational complexity [118].

4.5.2 System Performance

Table 4.1 studies the behavior of the TWR system for a given channel realization, a relay power budget $\bar{P}_r = 0$ dBm, and a terminal transmit power $P_s = 0$ dBm. The objective is to study in details the advantages and disadvantages of the max sum and max min utilities and the differences in the corresponding decision variables. It can be noticed that the use of max min utility helps in avoiding low rates achieved in certain slots with the sum utility such as the rates in slots 4, 5, and 8: $R_4 = 2.12$, $R_5 = 1.32$, and $R_8 = 1.72$ Mbps, respectively. However, this advantage is compensated by a lower total sum rate over the slots. With sum utility, the system prefers to harvest more RF energy in order to exploit it during next time slots to achieve higher rates. For instance, it achieves $R_3 = 8.88$ and $R_4 = 7.96$ Mbps with the sum utility instead of $R_3 = 3.36$ and $R_4 = 2.88$ Mbps with the max min one.

In Fig. 4.7, we compare between the performances of the two utilities by plotting the cor-

Table 4.1: Behavior of the relay selection scheme for $P_s = \bar{P}_r = 0$ dBm, $L_R = 3$, and $B = 8$.

	Max Sum	Max Min
$\boldsymbol{\epsilon}$	$\begin{bmatrix} 1\,0\,1\,0\,1\,0\,1\,1 \\ 0\,0\,1\,1\,0\,1\,0\,0 \\ 1\,1\,0\,1\,0\,0\,1\,1 \end{bmatrix}$	$\begin{bmatrix} 0\,1\,0\,1\,0\,1\,1\,0 \\ 1\,0\,1\,0\,1\,0\,0\,1 \\ 0\,0\,1\,0\,1\,0\,1\,0 \end{bmatrix}$
$\boldsymbol{R}$	[4.28, 4.12, 8.88, 7.96, 2.12, 1.32, 5.52, 1.72]	[2.44, 2.84, 3.36, 2.88, 3.44, 2.60, 3.20, 2.88]
$\sum_{b=1}^{B} R^b$	37.72	23.63

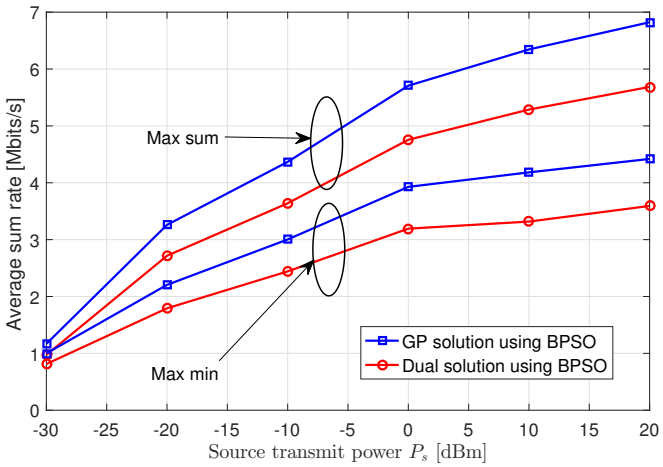

Figure 4.7: Achievable average sum rate per slot as a function of P_s For $\bar{P}_r = 0$ dBm, $L_R = 3, D = 50$ m.

responding sum-rate versus the terminals' power levels P_s for a TWR system transmitting messages over $B = 8$ time slots and equipped with $L_R = 3$ relays. The relays have a maximum power budget $\bar{P}_r = 0$ dBm. The proposed joint-optimization approach is employed for a distance $\mathcal{D} = 50$ m and is compared to the dual solution employed jointly with BPSO. Obviously, as P_s increases, the total sum-rate increases up to a certain value. In fact, increasing P_s allows the relays to harvest more RF energy and, at the same time, contributes to the rate improvement. The results in Fig. 4.7 corroborate those of Table 4.1 as, on average, the max sum utility reaches higher performance than the max min one. On the other hand, we notice a notable gap achieved by using the GP method instead of the dual method.

In Fig. 4.8, we investigate the path loss effect on the system performance by varying the distance separating the terminals $\mathcal{D}$ from 25 to 200 meters with system parameters similar to those of Fig. 4.7 and $P_s = [0, 10]$ dBm. We notice that the achieved throughput is decreasing

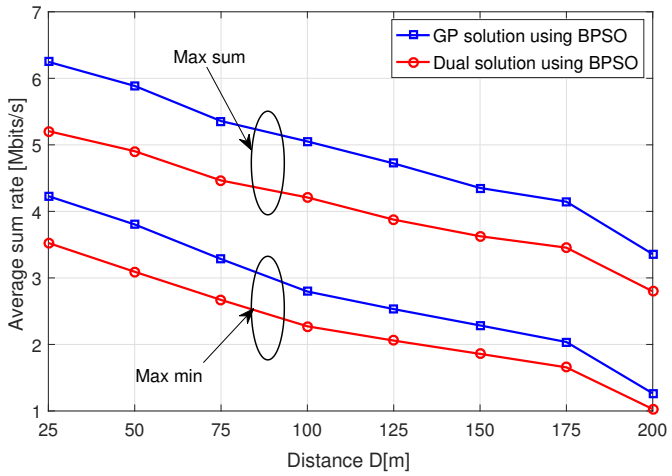

Figure 4.8: Achievable average sum rate per slot versus $\mathcal{D}$ for $\bar{P}_r = P_s = 0$ dBm and $L_R = 3$.

with the increase of distance $\mathcal{D}$. This is due to the path loss effect on both the SINR and the amount of harvested RF. Notice that, for large distances, the achieved sum-rate is relatively high. This is mainly due to the extra RE generated. Indeed, as it is shown in Fig. 4.9, the amount of harvested power using RF EH is no more available for data transmission as the harvested power is almost zero. This confirms that RF EH is only applicable within ultra-dense wireless networks and the importance of employing hybrid RE/FR EH technique with energy autonomous devices. Fig. 4.9 also shows that high values of terminals' transmission power P_s help in producing more RF energy.

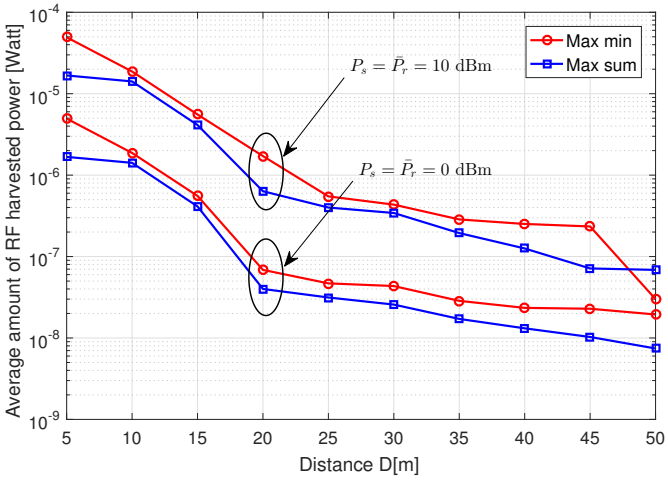

Figure 4.9: Average RF harvested energy versus $\mathcal{D}$ for $L_R = 3$ and different values of $\bar{P}_r = P_s$.

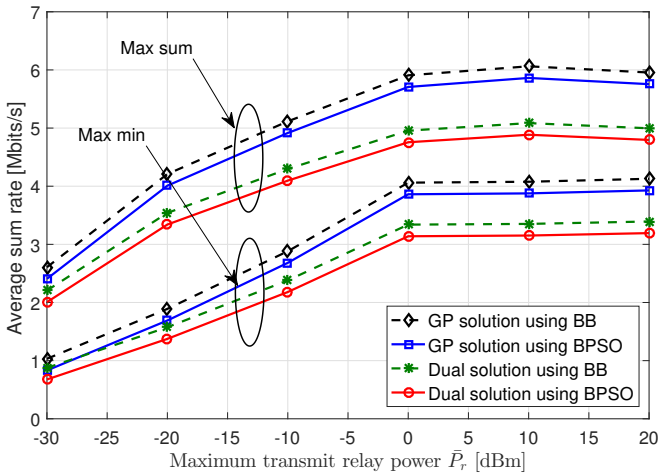

Figure 4.10: Achievable average sum rate versus $\bar{P}_r$ for $P_s = 0$ dBm, $L_R = 3$, and $\mathcal{D} = 50$ m.

In Fig. 4.10, we investigate the impact of the relay power budget $\bar{P}_r$ on the achieved sum-rate. Similar to Fig. 4.7, as $\bar{P}_r$ increases, the sum-rate increases up to a certain level where the TWR system becomes limited by the power budget of the terminals S_1 and S_2. We also compare between the performance of the proposed joint-optimization approach (GP with BPSO) with those of GP with BB, dual solution with BPSO, and dual-solution with BB. We can clearly deduce that BPSO is able to achieve close performances to those of the solutions obtained with BB while presenting a much lower complexity compared to that of BB. Furthermore, GP enables the achievement of better solutions than the dual problem-based optimization ones.

In Fig. 4.11, we compare the performances of the proposed approach with those of another suboptimal scenario where all $P_{r_l,b}$ are chosen to be fixed and constant ($P_{r_l,b} = \bar{P}_r$). This is performed to show the importance of the optimization of the relay transmit power levels simultaneously with the PS ratios and its impact on the reached sum-rate. We adopt the GP-based solution to optimize the PS ratios $\boldsymbol{\beta}$. For instance, for low $\bar{P}_r$ level, it can be noticed that optimizing both $\boldsymbol{P_r}$ and $\boldsymbol{\beta}$ outperforms the fixed $\boldsymbol{P_r}$ case by more than 1.5 Mbps when using the max sum utility. However, for high $\bar{P}_r$ level, the sum-rate drops significantly with the fixed $\boldsymbol{P_r}$ optimization, while with the optimized $\boldsymbol{P_r}$ case, the achieved sum-rate remains constant. Indeed, for fixed $\boldsymbol{P_r}$, some of the relays are non-selected in order to respect their storage constraints and hence, the energy is consumed in an un-optimized manner which results

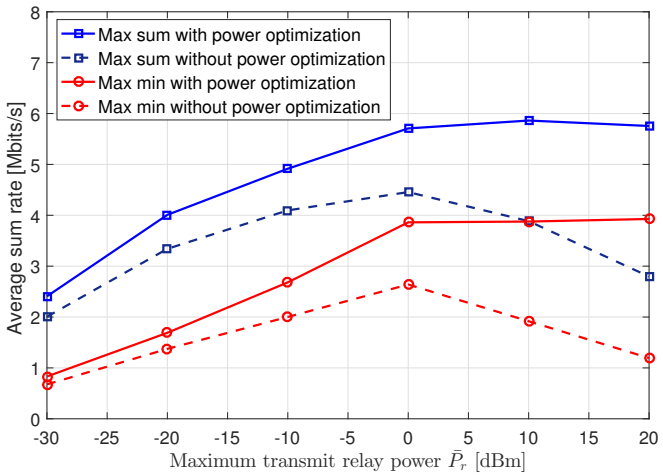

Figure 4.11: The effect of the relay power budget $\bar{P}_r$ on the average sum rate for $P_s = 0$ dBm, $L_R = 3$, and $\mathcal{D} = 50$ m.

in performance degradation.

In order to show the benefits of employing the RF EH technique jointly with the RE to power the energy autonomous relays, we investigate, in Fig. 4.12, the impact of optimizing the PS ratios $\boldsymbol{\beta}$ by comparing it to two other cases: i) assuming the absence of RF EH (i.e., $\beta_{r_l,b} = 1, \forall r_l, \forall b$) so that the relay are using the RE only and ii) assuming fixed PS ratios for all the relays, $\beta_{r_l,b} = 0.5$. The results are illustrated for two different distances separating the sources $\mathcal{D} = 10$ and $\mathcal{D} = 100$ meters for two power budgets values 0 dBm and 10 dBm. We notice that at high distance ($\mathcal{D} = 100$ m), the RF energy signal has no effect on the achieved data rate (i.e., sum-rate). Indeed, optimizing $\boldsymbol{\beta}$ or setting it to 1 provides the same results. This shows that the system is only depending on the RE energy. Using constant $\boldsymbol{\beta}$ leads to very bad results mainly for mobile sources as this setting forces the input signal at the relay level to be splitted into two components. Hence, adaptive and optimized PS ratios is mandatory for such scenarios. For short distances ($\mathcal{D} = 10$ m), we notice that the RF energy, when available, plays a role in enhancing the achievable rates which is increased by around 1 Mbits/s compared to the one of the case using RE only. This confirms that RF EH is applicable for short range communication only. As discussed earlier, higher transmit power budget levels of the sources enhance the achievable rate in general as it increases the resulting SNRs.

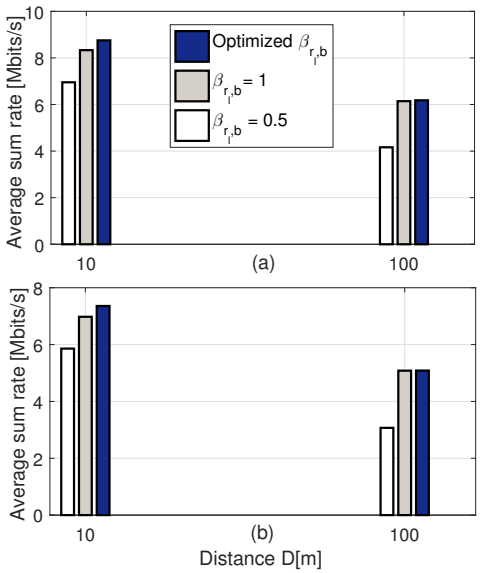

Figure 4.12: The effect of optimized the PS ratios $\boldsymbol{\beta}$ on the system performance with $L_R = 3$ for different values of $\mathcal{D}$ (a) $P_s = \bar{P}_r = 10$ dBm, (b) $P_s = \bar{P}_r = 0$ dBm.

4.5.3 Convergence Speed

The analysis of convergence speed of the proposed solution is studied in Fig. 4.13 and Fig. 4.14. In Fig. 4.13, we compare between the performances of BPSO using max sum utility and those of the BPSO with the max min utility by investigating their convergence speed defined by the number of iterations needed to reach convergence. Note that an iteration in Fig. 4.13 corresponds to one iteration of the "while loop" given in Algorithm 2 (i.e., line 3-12). In other words, it corresponds to one iteration of BPSO but it includes the execution of the SCA. The figure shows that BPSO achieves its near optimal solution with few iterations only (i.e., 10-20 iterations). In BPSO, we executed it for at most 100 iterations and we stop it if the achieved utility remains constant for a certain number of consecutive iterations.

In Fig 4.14, we plot number of GP iterations needed to find the best approximation solution given in Algorithm 1 (line 3-7) for each BPSO iteration. In other words, each dot in Fig 4.14 represents the required GP number of iterations for a specific BPSO iteration. It can be shown that GP requires a very small number of iterations to converge for a best approximation solution. Feasibility and sensitivity of GP are given in details in [107].

In Table 4.2, we compute the average CPU times in seconds for all algorithms (BPSO

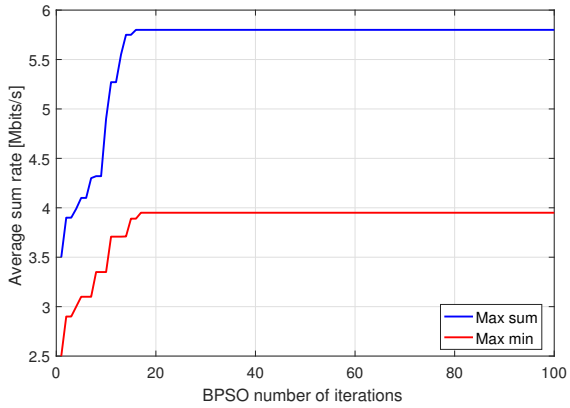

Figure 4.13: Convergence speed using BPSO for $P_s = \bar{P}_r = 0$ dBm, $L_R = 3$, and $\mathcal{D} = 50$ m.

Table 4.2: CPU times (sec) and number of iterations for the proposed joint-optimization solution for $P_s = \bar{P}_r = 0$ dBm, $L_R = 3$, and $\mathcal{D} = 50$ m.

		Max Sum		Max Min	
		PSO	**BB**	**PSO**	**BB**
GP approach	CPU time	6.11	260.02	9.12	313.01
	I^*	15	22	16	34
	$\sum_{b=1}^{B} R_b/B$	5.81	5.95	3.93	4.08
Dual approach	CPU time	4.10	155.11	7.03	188.10
	I^*	13	19	15	25
	$\sum_{b=1}^{B} R_b/B$	4.80	4.95	3.15	3.27

or BB using GP or dual problem based approach at each iteration) and record the iteration number (denoted by I^*) needed to reach the near optimal solution of the joint optimization (i.e., optimizing $\boldsymbol{\epsilon}$, $\boldsymbol{\beta}$, and $\boldsymbol{P_r}$), which exactly marks the instant when the algorithm achieves its steady state utility. The simulation is run for 100 realizations and $L_R = 3$ and $B = 8$. On average, BPSO is much faster than BB (optimal with respect to $\boldsymbol{\epsilon}$). It requires less time to converge, and achieves close performance to those of BB as shown in Fig. 4.8. By increasing the number of particles, BPSO may enhance the convergence efficiency of the algorithm to reach very close performance to BB. However, it requires more CPU times as they need to perform more additions and multiplications during each iteration.

Note that all tests were performed on a desktop machine featuring an Intel(R) Core(TM)

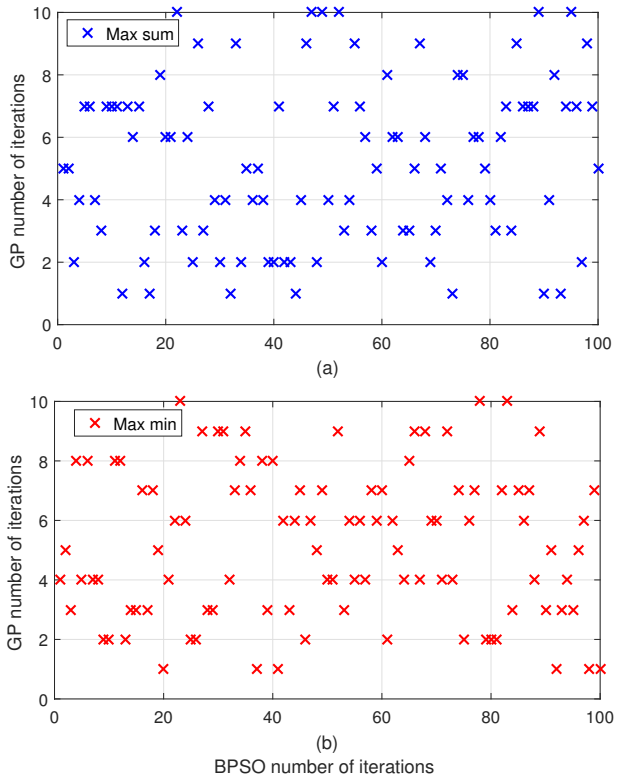

Figure 4.14: Number of GP iterations for each BPSO iteration for $P_s = \bar{P}_r = 0$ dBm, $L_R = 3$, and $\mathcal{D} = 50$ m.

i7-4790 CPU and running Windows 7. The clock of the machine is set to 3.6 GHz with a 16 GB memory.

4.6 Chapter Summary

In this chapter, the multiple relay selection scheme for PS protocol-based EH TWR is proposed. The relays harvest energy from RE and RF sources. We formulated an optimization problem aiming to maximize the total sum rate over multiple time blocks. Due to the non-convexity of the optimization problem, a joint-optimization approach based on BSOP algorithm and geometric programming was adopted. The proposed solution enables the system to achieve near optimal solutions with a significant gain compared to dual problem-based solution. The behavior of the TWR system was studied via multiple numerical simulations.

CHAPTER 5. ENERGY EFFICIENCY IN HETEROGENOUS NETWORKS

In this chapter, the downlink EH HetNets system where each BS is equipped to harvest from renewable source is proposed. A hybrid energy model is considered where the energy supply sources consisting of green (renewable) and traditional micro-grid, such that traditional micro-grid is not exploited as long as the BSs can meet their power demands from harvested and stored green energy. The goal is to minimize the network-wide energy consumption over a certain time slots. The is performed by optimizing the BS sleeping and user-cell association variables under BS's maximum power constraint, maximum BS's storing energy constraint, and user's QoS constraint. Two cases depending on the knowledge level about future RE generation are investigated: (1) The zeros knowledge case: in this case, future RE generation statistics are unknown. a BLP problem is formulated to optimize the BS sleeping status and user-cell association. (2)The perfect knowledge case: this case assumes that the future statistics of the network are perfectly and estimated.

5.1 System Model

In this chapter,a time-slotted system of a finite period of time divided into $b = 1, .., B$, time slots of equal duration T_b is investigated.

5.1.1 Network Model

We consider a half duplex downlink transmission of three-tiers HetNets consisting of a macrocell tier, microcell tier, and smallcell tier with a total of $L+1$ BSs (i.e., a single macrocell BS and L_M MBSs, and L_S SBSs, where $L = L_M + L_S$). The locations of all BSs are modeled by

an independent homogeneous Poisson Point Process (PPP). The hybrid power supply micro-grid sources consisting of a green grid (GG) and a traditional grid (TG) is considered. The former uses renewable sources to generate the electric power, while the latter uses classical sources to generate the electric power. Each BS is connected to the GG so that can provide help in energy when needed.

The GG has the ability to purchase a back-up power from the TG that is controlled by a control unit when needed as shown in Fig. 5.1.

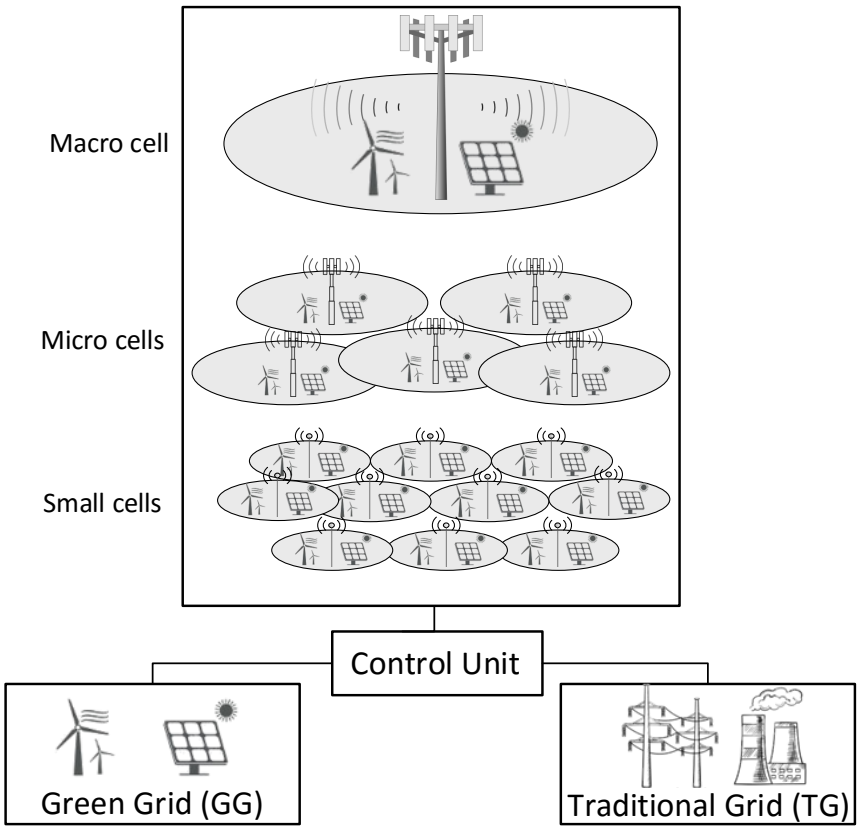

Figure 5.1: System model of hybrid EH.

Denoted U^b as the total number of users in the network during time slot b. We denote by $\bar{U}_l$, the maximum number of users that can be served by a BS l, where index $l = 0$ for macrocell BS and $l \geq 1$ for other BS tiers, such that $\bar{U}_l \ll \bar{U}_0$. These numbers reflect the BSs' capacities due to available number of frequency carriers and/or hardware and transmit power limitations. In order to avoid the co-channel interference, all the channels are assumed to share

the spectrum orthogonally between the BS. Finally, it is assumed that each user is served by at most one BS (either macrocell BS, MBS, or SBS).

In general, we assume that the communication channel between two nodes x and y at time slot b is given as follows

$$h_{xy}^{b} = \sqrt{d_{xy}^{-\varpi}}\tilde{h}_{xy}^{b}, \tag{5.1}$$

where d_{xy} is the Euclidean distance between the nodes x and y, ϖ is a pathloss exponent, and $\tilde{h}_{xy}^{b}$ is a fading coefficient with a coherence time slot T_b sec. Without loss of generality, all channel gains are assumed to be constat during T_b.

5.1.2 Base Station Power Model

Since the energy arrivals and energy consumption of the BSs are random and their energy storage capacities are finite, some BSs might not have enough energy to serve users at a particular time. Under such scenario, it is preferred that some of the BSs are kept OFF and allowed to recharge while their load is handled by the neighboring BSs that are ON. On the other hand, dynamic BS switching-ON/OFF can help in ensuring power saving of HetNets by reducing the traditional (non-renewable) power consumption of BSs that have a heavy energy usage mainly during low traffic period.

Each BS can be set in either of two operational modes: active mode (AM) or sleep mode (SM). The decision to toggle the operational state from one to another is taken centrally (i.e., the decision is taken by some central entity based on the current load offered to the network). In the AM, the BS is serving a certain number of users, thus, the BS radiated power can be expressed as

$$P_{l}^{\mathrm{BS}} = \sum_{u=1}^{U_l} P_{l,u}, \tag{5.2}$$

that corresponds to the sum of the radiated power over all users U_l connected to a certain BS l.

In the SM, the BS l consumes power equal to γ_l. The sleep mode is a reduced power consumption state in which the BS in not completely turned off and can be readily activated. Although the BS is not radiating power in this mode, elements such as power supply, baseband digital signal processing, and cooling are still active. Therefore, the BS keeps consuming power

unless it is in a state of complete shutdown. For simplicity, the total power consumption of BS l can be approximated by a linear model as follows [123]

$$P_l = \begin{cases} \alpha_l P_l^{\text{BS}} + \beta_l, & \text{for AM,} \\ \gamma_l, & \text{for SM,} \end{cases} \tag{5.3}$$

where α_l corresponds to the power consumption that scales with the radiated power due to amplifier and feeder losses and β_l models an offset of site power which is consumed independently of the average transmit power.

Let $\boldsymbol{\epsilon}^b$ denotes a binary matrix of size $(L+1) \times U$. Its entries $\epsilon_{l,u}^b$ is given by

$$\epsilon_{l,u}^b = \begin{cases} 1, & \text{if user } u \text{ is allocated to BS } l \text{ during time slot } b, \\ 0, & \text{otherwise.} \end{cases} \tag{5.4}$$

On the other hand, a dynamic ON/OFF switching mechanism is considered to turn off redundant MBSs and SBSs whenever it is possible. More specifically, BS l can be turned off during low traffic periods and the small number of active users are offloaded to nearby BSs A binary vector $\boldsymbol{\pi}^b$ of size $L \times 1$ is introduced to indicate the status of each BS l. Its entries π_l^b is given by and is given as

$$\pi_l^b = \begin{cases} 1, & \text{if BS } l \text{ in AM during time slot } b. \\ 0, & \text{otherwise.} \end{cases} \tag{5.5}$$

Note that in order to ensure that the users can not be connected to a BS in the SM, then, the following condition should be respected

$$\epsilon_{l,u}^b \leq \pi_l^b, \quad \forall l = 1, ., L, \forall u = 1, ., U, \forall b = 1, ., B. \tag{5.6}$$

The constraint given in (5.6) enforces $\epsilon_{l,u}^b = 0, \forall u$ when π_l^b in the SM (i.e., $\pi_l^b = 0$). In this chapter, we always keep the macrocell BS active (i.e., π_0^b, $\forall b = 1, .., B$) to ensure coverage and minimum connectivity in this typical HetNet (i.e., one macrocell BS surrounded by multiple of MBSs and SBSs). In the case of multiple macrocell BSs covering a bigger geographical area, macrocell BSs could be turned off and cell breathing mechanisms can be employed to ensure connectivity [24].

5.1.3 Energy Harvesting Model

It is assumed that each BS can harvest from RE in both AM and SM. We model the RE stochastic energy arrival rate as a random variable Φ Watt defined by a probability density function (pdf) $f(\varphi)$. For example, for photovoltaic energy, Φ can be interpreted as the received amount of energy per time unit with respect to the received luminous intensity in a particular direction per unit solid angle. In general, the energy consumption of the BS l during time slot b can be expressed as

$$E_0^b = T_b \left(\alpha_0 \sum_{u=1}^{U} \epsilon_{0,u}^b P_{0,u} + \beta_0 \right), \quad l = 0 \tag{5.7}$$

$$E_l^b = T_b \left(\pi_l^b \left[\alpha_l \sum_{u=1}^{U} \epsilon_{l,u}^b P_{l,u} + \beta_l \right] + (1 - \pi_l^b)\gamma_l \right), \quad l \geq 1, \tag{5.8}$$

By using (5.6), we can re-write (5.8) as follows

$$E_l^b = T_b \left(\alpha_l \sum_{u=1}^{U} \epsilon_{l,u}^b P_{l,u} + \pi_l^b \beta_l + (1 - \pi_l^b)\gamma_l \right), \quad l \geq 1, \tag{5.9}$$

The harvested energy in BS l and GG at the end of time slot b, are given respectively by

$$H_l^b = T_b \eta_l \varphi_l^b, \tag{5.10}$$

$$H_g^b = T_b \eta_g \varphi_g^b, \tag{5.11}$$

where η_l and η_g are the energy conversion efficiency coefficient of the RE at BS l and GG, respectively, where $0 \leq \eta_l, \eta_g \leq 1$. Notice that the current stored energy in BS l and GG depend on both the current harvested energy during slot time b and the previously stored energy during previous slots. Therefore, the stored energy in BS l at the end of time slot b is given by

$$S_l^b = \left[S_l^{b-1} + H_l^b - E_l^b - E_{le} \right]^+, \tag{5.12}$$

where E_{le} is the leakage energy during T_b.

5.2 Problem Formulation and Solution

In this section, we formulate and solve optimally two optimization problems, based on the knowledge level of the RE generation, aiming to minimize the networks energy consumption

during the B time slots. The first optimization problem corresponds to the zeros knowledge case where the mobile operator manages its BSs time slot by time slot without any prior information about the future RE generation. The second one corresponds to the perfect knowledge case with full information about the future RE generation where all the decisions variables are simultaneously optimized for the B time slots. The perfect knowledge case is a not realistic case. In this study, it is used as a benchmark scenario for comparison with zeros knowledge case or as an approximation of the case where RE energy uncertainty is almost negligible. The achievable data rate of user u served by BS l at a given time b is given by

$$R_{l,u}^{b} = \log_2 \left(1 + \frac{P_{l,u} \left| h_{l,u}^{b} \right|^2}{N_0} \right) \tag{5.13}$$

where N_0 is the noise power density.

5.2.1 Zeros Knowledge Case

In this case, we assume that the mobile operator is not aware about the future RE generation (i.e., φ_l^b and φ_g^b are known during b only). Therefore, the optimization problem that aims to minimize the total consumed energy at each time slot b is formulated as follows

$$\underset{\pi_l^b, \epsilon_{l,u}^b \geq 0}{\text{minimize}} \quad E_c^b = \sum_{l=0}^{L} E_l^b(\pi_l^b, \epsilon_{l,u}^b) - S_l^b(\pi_l^{b-1}, \epsilon_{l,u}^{b-1}) \tag{5.14}$$

subject to:

$$\sum_{u=1}^{U} \epsilon_{l,u}^b P_{l,u} \leq \bar{P}_l, \quad \forall l = 0, .., L, \tag{5.15}$$

$$\sum_{l=0}^{L} \epsilon_{l,u}^b R_{l,u}^b \geq R_0, \quad \forall u = 1, .., U, \tag{5.16}$$

$$S_l^{b-1}(\pi_l^b, \epsilon_{l,u}^b) + H_l^b \leq \bar{S}_l, \quad \forall l = 0, .., L, \tag{5.17}$$

$$\sum_{u=1}^{U} \epsilon_{l,u}^b \leq \bar{U}_l, \quad \forall l = 0, .., L, \tag{5.18}$$

$$\sum_{l=0}^{L} \epsilon_{l,u}^b \leq 1, \quad \forall u = 1, .., U, \tag{5.19}$$

$$\epsilon_{l,u}^b \leq \pi_l^b, \quad \forall l = 1, .., L, \forall u = 1, .., U, \tag{5.20}$$

where constraint (5.15) and (5.16) represent the maximum allowable transmit energy of BS l and user QoS, respectively. Constraint (5.17) forces the total energy stored in the battery of a BS l during the time slot b to be less than the battery capacity denoted by $\bar{S}_l$. Constraints (5.18) and (5.19) are to satisfy the backhauling condition and to ensure that each user is served by at most one BS, respectively.

Notice that, this optimization problem will be solved at the beginning of each time slot. Hence, the optimal solutions for such a problem can be determined optimally using Gurobi/CVX interface [126],[127].

5.2.2 Perfect Knowledge Case

In this case, we assume that the mobile operator can perfectly predict the future RE generation ahead of time. This case can be considered as a useful benchmark to compare with the zeros knowledge case. Therefore, the objective function becomes the minimization of the total energy consumption of the network during all B time slots.

$$\underset{\pi_l^b, \epsilon_{l,u}^b \geq 0}{\text{minimize}} \quad E_c = \sum_{b=1}^{B} \sum_{l=0}^{L} E_l^b(\pi_l^b, \epsilon_{l,u}^b) - S_l^b(\pi_l^{b-1}, \epsilon_{l,u}^{b-1}) \tag{5.21}$$

subject to:

$$\sum_{u=1}^{U} \epsilon_{l,u}^b P_{l,u} \leq \bar{P}_l, \quad \forall l = 0, ., L, \forall b = 1, ., B, \tag{5.22}$$

$$\sum_{l=0}^{L} \epsilon_{l,u}^b R_{l,u}^b \geq R_0, \quad \forall u = 1, .., U, \forall b = 1, .., B, \tag{5.23}$$

$$S_l^{b-1}(\pi_l^b, \epsilon_{l,u}^b) + H_l^b \leq \bar{S}_l, \quad \forall l = 0, .., L, \forall b = 1, .., B, \tag{5.24}$$

$$\sum_{u=1}^{U} \epsilon_{l,u}^b \leq \bar{U}_l, \quad \forall l = 0, .., L, \forall b = 1, .., B, \tag{5.25}$$

$$\sum_{l=0}^{L} \epsilon_{l,u}^b \leq 1, \quad \forall u = 1, .., U, \forall b = 1, .., B, \tag{5.26}$$

$$\epsilon_{l,u}^b \leq \pi_l^b, \quad \forall l = 1, .., L, \forall u = 1, .., U, \forall b = 1, .., B, \tag{5.27}$$

Notice that the constraints (5.22)-(5.27) are similar to the constraints (5.15)-(5.20) except that they have to be satisfied for all time slots $b = 1, .., B$.

The perfect knowledge problem can be also solved optimally with Gurobi/CVX interface [126],[127].

5.2.3 Cost Utility

After solving the optimization problem, the total cost of the non-renewable energy consumed is equal to the cost of the energy consumed by all BSs that exceeding the available harvested energy stored at time b and given by

$$\mathcal{C}^b = \left[\sum_{l=0}^{L} \left[E_l^b - S_l^{b-1}\right]^+ - S_g^{b-1}\right]^+ \tag{5.28}$$

where S_g^{b-1} is the stored energy at the GG at the end of time slot $b-1$. Therefore, the total cost over multiple time slots is given by

$$\mathcal{C} = \sum_{b=1}^{B} \mathcal{C}^b. \tag{5.29}$$

5.2.4 Special case

The communication channel is assumed to be a block fading channel with a coherence time T_c second. Therefore, the scheduling and user-cell association can be assumed to be taken over a short time scale. While, the operational state of the switching ON/OFF of the BSs can be taken over a long time scale, where each long time slot consists of multiple short slots. Hence, the problem can be solved by optimizing only $\epsilon_{l,u}^b$ at the beginning of the short time slot and optimizing both π_l^b and $\epsilon_{l,u}^b$ at the beginning of the long time slot.

5.3 Low Complexity Algorithm

The formulated BLP optimization problems given in Section 5.2 is considered as NP-hard problem due to the existence of the binary variables, hence, we propose to employ a meta-heuristic algorithm, namely BPSO. Then, we propose to compare its performances with the well known evolutionary GA [43].

5.3.1 Binary Particle Swarm Optimization

The BPSO starts by generating N particles $\boldsymbol{\mathcal{N}} = [\pi_1^1, .., \pi_L^B, .., \epsilon_{1,1}^1, .., \epsilon_{L,U}^B]$;$n = 1, .., N$ of size $(L + (L + 1)U) \times 1$ for zeros knowledge case (solved for each time slot b) and $(LB + (L + 1)UB) \times 1$ for perfect knowledge case to form an initial population $\mathcal{S}$. Then, it determines the minimum energy consumed by each particle that satisfy the QoS by solving the optimization problem. Then, it finds the particle that provides the best solution for this iteration, denoted by $\boldsymbol{\mathcal{N}}^{\text{best}}$. In addition, for each particle n, it saves a record of the position of its previous best performance, denoted by $\boldsymbol{\mathcal{N}}^{(\text{n,local})}$. Then, at each iteration i, BPSO computes a velocity term $V_m^{(n)}$ corresponding to element m in $\boldsymbol{\mathcal{N}}$ according to Appendix A. These steps are repeated until reaching convergence by either attaining the maximum number of iterations or stopping the algorithm when no improvement is noticed. Details of the proposed optimization approach are given in Algorithm 5.1.

Algorithm 5.1 Proposed Solution using BPSO Algorithm

1: $q = 1$.
2: Generate an initial population $\mathcal{S}$ composed of N random particles $\boldsymbol{\mathcal{N}}^{(n)}$, $n = 1 \cdots N$.
3: **while** not converged **do**
4: **for** $n = 1 \cdots N$ **do**
5: Compute the corresponding consumed utility function $E_c^{(n)}(q)$.
6: **end for**
7: Find $(n_m, q_m) = \arg\min_{n,q} E_c^{(n)}(q)$ (i.e., n_m and q_m indicate the index and the position of the particle that results in the minimum energy consumption). Then, set $E_c^{\text{best}} = E_c^{(n_m)}(q_m)$ and $\boldsymbol{\mathcal{N}}^{\text{best}} = \boldsymbol{\mathcal{N}}^{(n_m)}(q_m)$.
8: Find $q_n = \arg\min_{q} E_c^{(n)}(q)$ for each particle n (i.e., q_n indicates the position of the particle n that results in best local utility). Then, set $\boldsymbol{\mathcal{N}}^{(\text{n,local})} = \boldsymbol{\mathcal{N}}^{(n)}(q_n)$.
9: Adjust velocities and positions of all particles using (A.4).
10: $q = q + 1$.
11: **end while**

5.3.2 Genetic Algorithm

The performances of the proposed BPSO algorithm is compared to those of the well-know GA. In our genetic based approach, we generate randomly N particles $\boldsymbol{\mathcal{N}}^{(n)}$, $n = 1 \cdots N$ of size $(L+(L+1)U)\times 1$ for zeros knowledge case (solved for each time slot b) and $(LB+(L+1)UB)\times 1$ for perfect knowledge case to form an initial population $\mathcal{S}$. Then, it determines the minimum

energy consumed by each particle that satisfy the QoS by solving the optimization problem. After that, the algorithm selects $\tau(1 \leq \tau \leq N)$ strings that provide the minimum consumed energy and keeps them to the next population while the $N-\tau$ remaining strings are generated by applying crossovers and mutations to the τ survived parents. Crossovers consist in cutting two selected random parent strings at a correspond point which is chosen randomly. The obtained fragments are then swapped and recombined to produce two new strings. Then, mutation (i.e., changing a bit value of the string randomly) is applied with a probability p [128]. This procedure is repeated until reaching convergence or reaching the maximum number of iterations.

5.4 Simulation Results

In this section, selected numerical results are provided to evaluate the performance of the EH HetNets systems. Selected BSs transmit their messages periodically every T_b sec. All the fading channel gains adopted in the framework are assumed to be i.i.d Rayleigh fading gains. The efficiency transmission and conversion ratios are set to $\eta_l = \eta_g = 0.3$, respectively. The target data rate user (R_0), the number of MBSs and SBSs are 10 bits/s/Hz, 4 and 8, respectively, unless otherwise stated. The noise power is taken to be $N_0 = \mathcal{N}_0 W$, where $\mathcal{N}_0 = -174$ dBm/Hz and $W = 180$ KHz. The power consumption parameters are selected according to the energy aware radio and network technologies (EARTH) model for macrocell BS, MBSs, SBSs, are given, respectively [123] as follows: $\alpha_l = \{4.7, 2.6, 4\}$ W and $\beta_l = \{130, 56, 6.8\}$ W. The other power consumption parameters for MBSs and SBSs are given respectively by $\gamma_l = \{39, 2.9\}$ W. The maximum transmit power levels for the for macrocell BS, MBSs, SBSs, are set, respectively, to $\bar{P}_l = \{46, 38, 20\}$ dBm.

At each BS, RE is assumed to be generated following Gamma distributions $\Gamma(20, 2)$, $\Gamma(12, 2)$, and $\Gamma(3, 1)$ for macrocell BS, MBSs, and SBS, respectively, where in $\Gamma(x, y)$, x is the shape parameter and y and scale parameter. While for GG, RE is assumed to be generated following a Gamma distribution $\Gamma(25, 2)$. The total stored energy at macrocell BS, MBSs, and SBSs cannot exceed $\bar{S}_l = \{50, 12, 6\}$ KJ, respectively, and the battery leakage is set to be $E_{le} = 1$ mJ every T_b.

The BPSO is executed with the following parameters: $N = 20$ and $\psi_0 \in [0, 1]$ is a linear decreasing function of the BPSO iterations expressed as follows: $\psi_0 = 0.9 - \frac{n(0.9-0.2)}{I_{\max}}$, where $I_{\max} = 200$ is the maximum number of iterations.

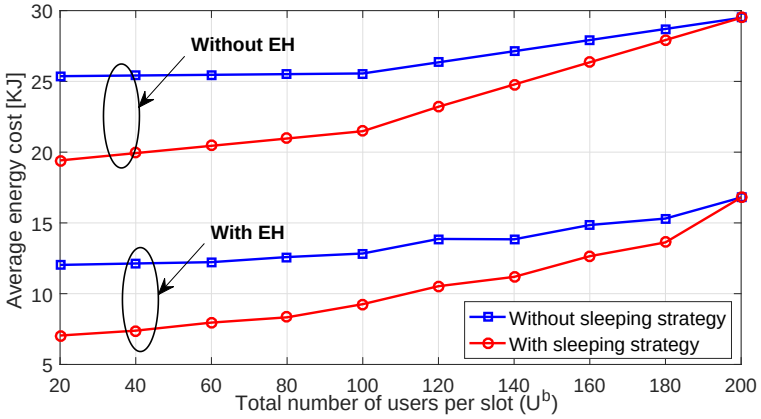

Figure 5.2: Average energy cost of $B = 20$ time slots versus total number of users.

Table 5.1: MBSs and SBSs status during multiple time slots.

Number of users per b	Active MBSs				Active SBSs			
	m_1	m_2	m_3	m_4	s_1	s_2	s_3	s_4
$U^1 = 100$	×	-	-	×	×	-	×	-
$U^2 = 40$	×	-	-	×	×	-	-	×
$U^3 = 200$	×	×	×	×	×	×	×	-
$U^4 = 80$	-	×	-	×	-	-	×	-
$U^5 = 140$	×	-	-	×	×	×	-	×
$U^6 = 220$	×	×	×	×	×	×	×	×
$U^7 = 80$	×	-	-	×	×	-	×	-
$U^8 = 160$	×	×	×	-	-	×	-	×
$U^9 = 160$	×	×	-	×	×	×	×	-
$U^{10} = 60$	-	-	×	-	×	×	×	×

Fig. 5.2 plots the total average energy cost, which is equal to $\frac{\mathcal{C}}{B}$, for $B = 20$ versus number of users (U^b, $\forall b = 1, .., B$), for zeros knowledge case. This figure investigates the impact of RE with two scenarios: 1) with the proposed EH (i.e., hybrid of RE and TG energy), 2) without EH(the energy depends on the TG energy only). It also investigate the impact of the sleeping strategy (i.e., optimizing $\boldsymbol{\pi}$) on the system performance. we can see that the proposed scheme

(with EH and with sleeping strategy) offers a significant amount of energy saving switching over the other scenarios. It should be noted that the sleeping strategy is very useful specially for low traffic period with a considerable energy cost gap. Indeed, for $U^b = 100$ users, the average energy cost can be decreases by around 30% for the EH scenario by going from 13.5 KJ to around 9.5 KJ. However, this gap reduces when number of users increases. This can be justified by the fact that when the number of users are relatively high, most of BSs should be in the AM in order to satisfy the user QoS.

Table 5.1 confirms the sleeping strategy results in Fig 5.2. In general it can be noted that activating the MBSs and SBSs essentially depends on the traffic and BS's battery level. For example, as shown in Table 5.1, during low traffic periods e,g., $b = \{2, 4, 7, 10\}$ (i.e., $U^2 = 40, U^4 = 80, U^7 = 80, U^{10} = 60$), the sleeping strategy activate some of BSs and keeps the others in the SM in order to harvest some energy. On the other hand, when the network is more congested e.g., during slots $b = \{3, 6, 8, 9\}$ (i.e., $U^3 = 200, U^6 = 220, U^8 = 160, U^9 = 160$), most of the BSs are in AM.

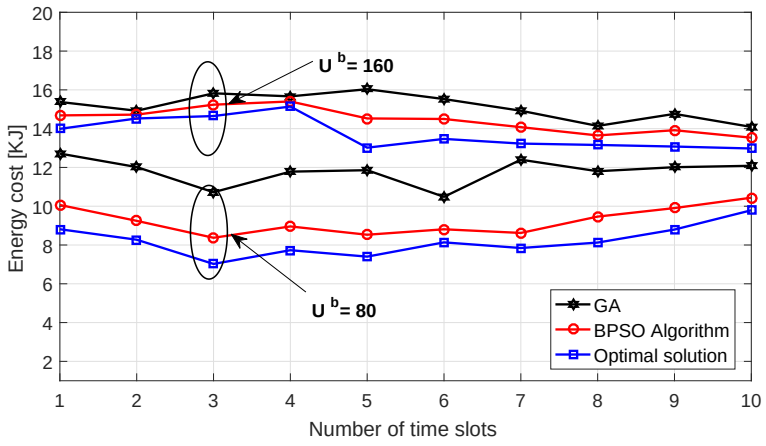

Figure 5.3: Comparison between optimal solution with BPSO algorithm and GA. Energy cost versus number of time slot.

Under the same setup of Fig. 5.2, Fig. 5.3 compares between the optimal solution (obtained by solving the BLP using Gurobi/CVX) with BPSO algorithm and the well known GA for different total number of users $U^b = \{80, 160\}$. It can be seen, that the BPSO achieves better performance than GA and close to the optimal solution in both low and high traffic periods. We

can notice that both algorithms are close to the optimal when the network is more congested. This can be explained, by knowing that during high traffic period, the network needs to keep most of the BSs in AM, hence, optimizing only the association variable (i.e., $\boldsymbol{\epsilon}$). It is also worth to note that optimizing $\boldsymbol{\pi}$ has more weigh in saving energy that optimizing $\boldsymbol{\epsilon}$ due to the high values of offset power parameter β_l compare to the amplified power parameter α_l.

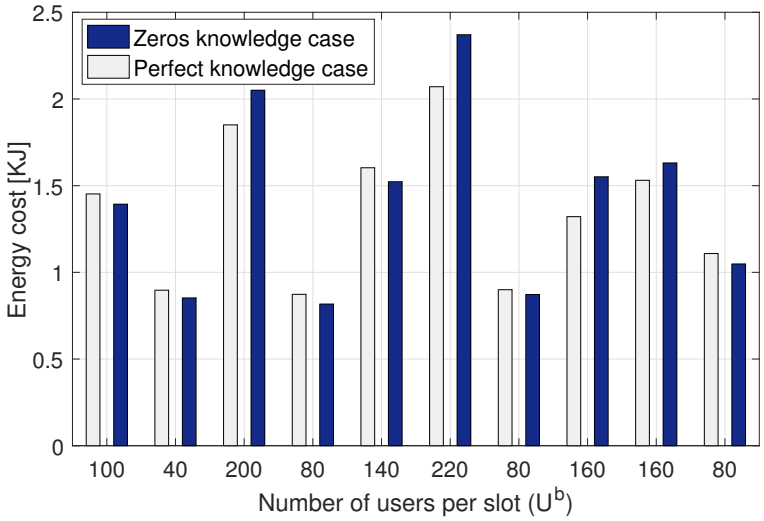

Figure 5.4: Comparison between zeros knowledge and perfect knowledge cases.

Finally, Fig. 5.4 compares the zeros knowledge case to a benchmark case (i.e., perfect knowledge case). Fig. 5.4 plots the total energy cost of the network for both cases versus different numbers of users. Since activating the BSs depends on their battery levels and the traffic status, the perfect knowledge case can manage the available resources globally and more efficiently. For example, during $b = 7$ (i.e., $U^7 = 80$), the perfect knowledge case consume more energy by forcing some BSs to be in SM and activate them where the network is more congested, i.e., $U^8 = U^9 = 160$. Although it consumes more energy than the zeros knowledge case, which is around 0.1 kJ, when $b = 7$, the perfect knowledge case saves more energy, which is around 0.6 kJ, during the next two time slots $b = 8$ and $b = 9$.

5.5 Chapter Summary

In this chapter, the planning and allocation problem of downlink EH in HetNets using hybrid power sources is proposed. All the BSs are equipped with a harvested source and can

get some energy from green grid or/and traditional grid when needed. We formulated a BLP aiming to minimize the consumed energy over multiple time slots. The problem was solved optimally and compared with two low complexity algorithms. After solving the problem, we investigated, via numerical results, the behavior of the proposed scheme versus various system parameters. Finally, the effects of sleeping strategy to the system average energy cost were discussed.

CHAPTER 6. DRONE-BASED COMMUNICATIONS ASSISTED WITH ENERGY HARVESTING

In this chapter, a drone-based communication problem is addressed from a new perspective by investigating the placement of multiple EH DBSs in order to support typical HetNets composed of a single macrocell BS and multiple ground MBSs. The proposed method can be generalized to the context of large-scale HetNets. In this study, we assume that each drone can charge its battery either using traditional electric energy when it is placed in a charging station located at the macrocell BS site or using RE harvested through solar panels placed on top of the drones.

The objective of the framework is to exploit the mobility and quick deployment of these solar-powered drones to support the ground cells whenever it is needed and whenever the drones' batteries permit it. Inactive drones, which are originally placed at the charging station, will be asked to fly to particular locations to serve users and support the overloaded HetNet or replace lightly loaded MBSs during a short period of time. In the latter case, the MBSs can be safely turned off to reduce fossil fuel consumption. Three cases depending on the knowledge level about future RE generation are investigated: (1) The zero knowledge case: in this case, future RE generation statistics are unknown for the mobile operator. A binary linear programming problem is formulated to determine the HetNet and drone statuses based on past and present realizations. (2) The perfect knowledge case: this case assumes that the future statistics of the network are perfectly known and estimated. A non-linear programming problem is formulated to determine the future deployment strategies for the drones. To reduce its complexity, a linearization approach is employed to transform the problem into a binary linear programming optimization problem. (3) The partial knowledge case: in this case, only partial statistics of the future RE generation are known, i.e., probability density function. To

deal with the uncertainty effect, a stochastic programming problem is formulated and solved using the two-stage recourse method. In this case, the uncertainty effect is also considered.

6.1 System Model

In this study, we investigate a time-slotted system of a finite period of time divided into B slots numbered $b = 1, \cdots, B$, of equal duration T_b. The time slots are relatively long compared to the channel coherence time and hence, we focus on the system performance based on its average statistics. Investigating the system performance for instantaneous channel realizations and network statistics is not valid for this framework since we are considering the drones' flying time (seconds) which is very large as compared to the channel coherence time (milliseconds).

6.1.1 Network Model

We consider a typical HetNet consisting of one macrocell BS and L_M MBSs. The HetNet is assisted by D dynamic drones that act as DBSs (i.e., DBS is carried by one drone) as depicted in Fig. 6.1.

In this framework, we aim to optimize the deployment of DBSs in the geographical area covered by the macrocell BS according to the network's need and QoS requirements. We assume that a dynamic drone can be in three different states: 1) the drone is in an idle mode and placed at the charging station assumed to be located in the center of the cell (i.e., in the macrocell BS site.), 2) the drone is placed at a pre-defined location in the cell and acting as a DBS to serve users, or 3) the drone is in motion and flying from a location to another. Placing the charging station at the center of the cell minimizes, in general, the flying time of drones and hence the corresponding energy consumption.

We assume that there are $Z_D + 1$ possible locations available for drones' deployment. These locations, $i = 0, \cdots, Z_D$, can be pre-determined by the mobile operator during the planning phase depending on several factors such as, historical network statistics, location constrains, etc. Each location i is identified by its three dimensional (3D) geographical coordinates (x_i, y_i, h_i). The location $i = 0$ (i.e., $x_0 = y_0 = h_0 = 0$) corresponds to the charging station. Hence, the drone energy consumption depends essentially on its current location (i.e., time slot b) and the

previous one (i.e., time slot $b-1$). Note that once the drone landed in a specific location, it will be in a static state instead of a moving state. This can help in reducing the energy consumption of the drones and improve the battery lifetime.

Denote $\boldsymbol{\epsilon^b}$ as a binary matrix of size $D \times (Z_D + 1)$. Its entries $\epsilon^b_{d_l}(i)$ indicate the location of the drone d_l, where $l = 1, \cdots, D$, and is given by

$$\epsilon^b_{d_l}(i) = \begin{cases} 1, & \text{if the drone } d_l \text{ is placed at location } i \\ & \text{during time slot } b, \\ 0, & \text{otherwise.} \end{cases} \tag{6.1}$$

On the other hand, a dynamic ON/OFF switching mechanism is considered to turn off redundant MBSs whenever it is possible [31],[129]. More specifically, MBS $m_k, k = 1, \ldots, L_M$ can be turned off during low traffic periods and the small number of active users are offloaded to nearby DBSs or macrocell BS. As a result, the energy consumption of lightly loaded MBSs can be eliminated. A binary vector $\boldsymbol{\pi}^b$ is introduced to indicate the status of each ground MBS m_k and is given by:

$$\pi^b_{m_k} = \begin{cases} 1, & \text{if MBS } m_k \text{ is operating during time slot } b. \\ 0, & \text{otherwise.} \end{cases} \tag{6.2}$$

It should be noted that we always keep the macrocell BS active to ensure coverage and minimum connectivity in this typical HetNet (i.e., one macrocell BS surrounded by multiple of MBSs). In the case of multiple macrocell BSs covering a bigger geographical area, macrocell BSs could be turned off and cell breathing mechanisms can be employed to ensure connectivity [24].

We denote by U^b the average total number of users located in the macrocell BS during time slot b and by $\bar{U}_0$, $\bar{U}_m$, and $\bar{U}_d$ the maximum number of users that can be served by macrocell BS, MBS m_k, and DBS d_l, respectively, such that $\bar{U}_d \leq \bar{U}_m \ll \bar{U}_0$. These numbers reflect the BSs' capacities due to available number of frequency carriers and/or hardware and transmit power limitations. We assume that the co-channel interference is ignored and the transmissions are performed in orthogonal basis. Also, we assume that a user is served by at most one BS (either a macrocell BS, MBS, or DBS). We consider that the user distribution during time slot

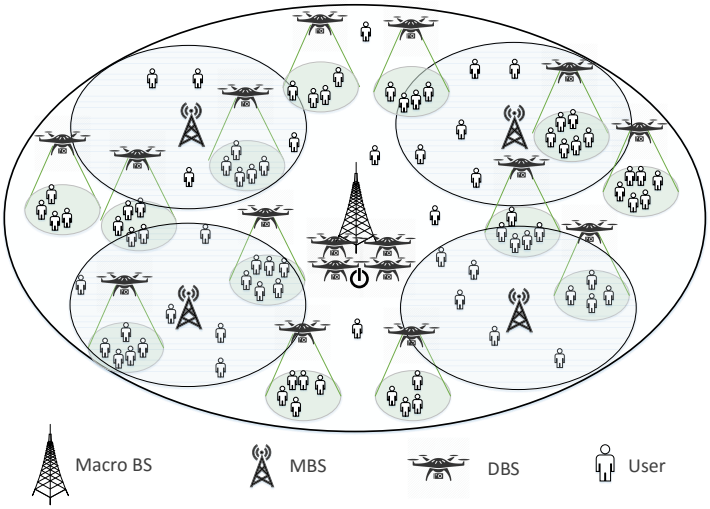

Figure 6.1: Example of a HetNet assisted by DBSs.

b over the macrocell BS area $\mathcal{A}$ follow a certain probability density function (pdf) denoted by $f(x, y, b)$, where (x, y) represents the geographical coordinates of a user. We denote by $\mathcal{A}_{\mathcal{X}}$ ($\mathcal{A}_{\mathcal{X}} \subseteq \mathcal{A}$) the coverage area of an active BS $\mathcal{X}$ where $\mathcal{X} \in \{\{0\}, \{m_k : k = 1, \cdots, L_M\}, \{(d_l, i) : l = 1, \cdots, D, i = 0, \cdots, Z_D\}\}$ referring to the macrocell BS, MBS m_k, and DBS d_l placed at location i, respectively. Hence, the average number of users served by an active BS $\mathcal{X}$ during time slot b is denoted by $U^b_{\mathcal{X}}$ and is given by:

$$U^b_{\mathcal{X}} = \min\left(U^b \iint_{\mathcal{A}_{\mathcal{X}}} f(x, y, b)\ \mathrm{d}x\mathrm{d}y, \bar{U}_{\mathcal{X}}\right), \tag{6.3}$$

for MBSs and DBSs, i.e., $\mathcal{X} \in \{m_k, (d_l, i)\}$

and

$$U^b_0 = \min\left(U^b - \sum_{k=1}^{L_M} \pi^b_{m_k} U^b_{m_k} - \sum_{l=1}^{D}\sum_{i=1}^{Z_D} \epsilon^b_{d_l}(i) U^b_{d_l,i}, \bar{U}_0\right), \tag{6.4}$$

for macrocell BS, i.e, $\mathcal{X} = 0$.

In (6.4), the priority in serving users is given to MBSs and DBSs as macrocell BS's transmit power is usually higher than that of MBS and DBS [130].

6.1.2 Path Loss Model

Sice we are dealing with the average network statistics. Therefore, the channel model is essentially based on the PL model. Fast-fading effects are ignored in this chapter. Two PL models can be distinguished depending on the nature of the transmitter.

6.1.2.1 Ground-to-Ground Path Loss Model

The average PL between a ground BS $\mathcal{X} \in \{0, m_k\}$ and a ground user is given by the average PL for non-line of sight (NLoS) links and is expressed by [101]:

$$PL_{\mathcal{X}}^{\text{NLoS}}[\text{dB}] = 20\log_{10}\left(\frac{4\pi\delta_{\mathcal{X}}}{\lambda_0}\right) + \xi_{\text{NLoS}}, \tag{6.5}$$

where $\delta_{\mathcal{X}}$ is the average distance between the ground BS $\mathcal{X}$ and a served user located within its cell, λ_0 is the carrier wavelength, and ξ_{NLoS} is the average additional loss due to the free space propagation loss for NLoS link.

6.1.2.2 Air-to-Ground Path Loss Model

The PL of the air-to-ground link is a weighted combination of two PL links: LoS and NLoS links. This is due to the ability of the drones to serve users from high altitude as compared to ground BSs. In this case, there will be a probability to obtain a LoS link between the DBS and a user [101]. The average PL between the DBS l positioned at a position i and a served user in urban environments for LoS link is given as [101]:

$$PL_{d_l,i}^{\text{LoS}}[\text{dB}] = 20\log_{10}\left(\frac{4\pi\delta_{d_l,i}}{\lambda_0}\right) + \xi_{\text{LoS}}, \tag{6.6}$$

where $\delta_{d_l,i}$ is the average distance between the DBS l located at position i and the served user located in its cell and ξ_{LoS} is the average additional loss to the free space propagation loss for LoS link.

The LoS probability is given by [98],[131],[132]:

$$p_{d_l,i}^{\text{LoS}} = \frac{1}{1 + \nu_1 \exp(-\nu_2[\theta_{d_l,i} - \nu_1])}, \tag{6.7}$$

where $\theta_{d_l,i}$ is the elevation angle between DBS l positioned at location i and the served user in degree. ν_1 and ν_2 are constant values that depend on the environment. The NLoS probability is, then, equal to $1 - p_{d_l,i}^{\text{LoS}}$. Therefore, the average PL for air-to-ground link is given by:

$$\overline{PL}_{d_l,i} = p_{d_l,i}^{\text{LoS}} PL_{d_l,i}^{\text{LoS}} + (1 - p_{d_l,i}^{\text{LoS}}) PL_{d_l,i}^{\text{NLoS}}. \tag{6.8}$$

6.1.3 Base Stations Power Model

In the active state and to serve its connected users during a time slot b, the BS $\mathcal{X}$ consumes power denoted by $P_{\mathcal{X}}^b$. However, in the idle mode, it consumes constant power equal to $P_{\mathcal{X}}^{\text{idle}} = \gamma_{\mathcal{X}}$. The latter power corresponds to the minimum power required to readily activate BS $\mathcal{X}$. For simplicity, the total power consumption of an active BS $\mathcal{X}$ during a time slot b can be approximated by a linear model as follows [130]:

$$P_{\mathcal{X}}^b = \alpha_{\mathcal{X}} \tilde{P}_{\mathcal{X}}^b + \beta_{\mathcal{X}}, \tag{6.9}$$

where $\alpha_{\mathcal{X}}$ is a parameter that scales with the radiated power, denoted by $\tilde{P}_{\mathcal{X}}^b$, and $\beta_{\mathcal{X}}$ models constant power. The radiated power of a BS $\mathcal{X}$ is expressed as:

$$\tilde{P}_{\mathcal{X}}^b = U_{\mathcal{X}}^b P_{\min} \overline{PL}_{\mathcal{X}}, \tag{6.10}$$

where $\overline{PL}_{\mathcal{X}}$ is the corresponding average PL at the BS cell $\mathcal{X}$. Note that $\overline{PL}_{\mathcal{X}} = PL_{\mathcal{X}}^{\text{NLoS}}$ given in (6.5) in the case of a macrocell BS or MBS and $\overline{PL}_{\mathcal{X}} = \overline{PL}_{d_l,i}$ given in (6.8) in the case of a DBS.

6.1.4 Drone Power Model

Besides the power consumed by the BSs carried by the drones (i.e., DBSs), the drone consumes additional hovering and hardware powers. Without loss of generality, we assume that all drones move with a fixed speed denoted by v_d. The hover and hardware power levels, denoted by P_{hov} and P_{har}, can be expressed, respectively, as [133]:

$$\begin{aligned} P_{\text{hov}} &= \sqrt{\frac{(m_{\text{tot}} g)^3}{2\pi r_p^2 n_p \rho_a}}, \\ &\text{and} \\ P_{\text{har}} &= \frac{P_{\text{full}} - P_s}{v_{\max}} v_d + P_s, \end{aligned} \tag{6.11}$$

where m_{tot}, g, and ρ_a are the drone mass in [Kg], earth gravity in [m/s^2], and air density in [Kg/m^3], respectively. r_p and n_p are the radius and the number of the drone's propellers, respectively. $v_{\max}$ is the maximum speed of the drone. P_{full} and P_s are the hardware power levels when the drone is moving at full speed and when the drone is in idle mode, respectively. Note that, in (6.11), we assume that when serving users at a location i, the drone will be in a static position, hence, it consumes only P_s for hardware power. However, when it is flying to a destination (i.e., one of the $Z_D + 1$ locations), it will consume P_{har}. Finally, the flying power of DBS l can be calculated as:

$$P_f = P_{\text{hov}} + P_{\text{har}}. \tag{6.12}$$

6.1.5 Renewable Energy Model

It is assumed that DBS l can harvest from RE sources selected to be the photovoltaic energy. We model the RE stochastic energy arrival rate as a random variable Φ Watt defined by a pdf $f_\Phi(\varphi^b_{d_l})$. An event $\eta\varphi^b_{d_l}$ in a time slot b can be interpreted as the average received amount of power with respect to the received luminous intensity in a particular direction per unit solid angle. The parameter η denotes the EH efficiency coefficient.

Table 6.1: Consumed and harvested energies of DBS l during time slot b for all possible cases.

Case	Previous location	Current location	Consumed energy	Harvested energy	Charging energy
(1)	$\epsilon^{b-1}_{d_l}(j) = 1,\ j \neq i$	$\epsilon^{b}_{d_l}(i) = 1,\ i \neq 0$	$(P_f + \gamma_d)T_f(j,i) + (P^b_{d_l,i} + P_s)T_r(j,i)$	$\eta\varphi^b_{d_l}(T_f(j,i) + T_r(j,i))$	0
(2)	$\epsilon^{b-1}_{d_l}(j) = 1,\ j = i$	$\epsilon^{b}_{d_l}(i) = 1,\ i \neq 0$	$(P^b_{d_l,i} + P_s)T_b$	$\eta\varphi^b_{d_l}T_b$	0
(3)	$\epsilon^{b-1}_{d_l}(j) = 1,\ j \neq 0$	$\epsilon^{b}_{d_l}(i) = 1,\ i = 0$	$(P_f + \gamma_d)T_f(j,i) + \gamma_d T_r(j,i)$	$\eta\varphi^b_{d_l}(T_f(j,i) + T_r(j,i))$	$P_{ch}T_r(j,i)$
(4)	$\epsilon^{b-1}_{d_l}(j) = 1,\ j = 0$	$\epsilon^{b}_{d_l}(i) = 1,\ i = 0$	$\gamma_d T_b$	$\eta\varphi^b_{d_l}T_b$	$P_{ch}T_b$

In general, the RE generation matrix $\mathbf{\Phi}$, of size $D \times B$, with elements $\varphi^b_{d_l}, \forall l = 1, \cdots, D, \forall b = 1, \cdots, B$ can be modeled as follows:

$$\mathbf{\Phi} = \bar{\Phi} + \tilde{\Phi}, \tag{6.13}$$

where $\bar{\Phi}$ is the deterministic portion of the RE generation that can be estimated from historical data and $\tilde{\Phi}$ is a matrix of random variables representing the stochastic portion of the RE generation and models its uncertainty.

To summarize, Table 6.1 presents the consumed and harvested energies of the drone for all possible cases: 1) when the drone is moving from a location $j \neq 0$ to a new location $i \neq 0$, 2) when the drone remains at the same location $i \neq 0$, 3) when the drone decides to go to the charging station (i.e., $i = 0$) while it was positioned at location $j \neq 0$ during time slot $b-1$, and 4) when the drone decides to stay in the charging station $i = 0$. In Table 6.1, $T_f(j,i)$ corresponds to the drone trip duration from a location j to a location i and it is computed as follows:

$$T_f(j,i) = \frac{d_{j,i}}{v_d}, \tag{6.14}$$

where $d_{j,i}$ is the euclidean distance separating the two locations i and j. On the other hand, $T_r(j,i) = T_b - T_f(j,i)$ corresponds to the time spent by a drone at a location i to serve users (i.e., $i \neq 0$) or to charge its battery (i.e., $i = 0$) such that $T_f(j,i) \ll T_r(j,i)$. P_{ch} denotes the charging power per drone of the charging station.

6.2 Problem Formulation

In this section, three optimization problems are formulated, based on the knowledge level of the RE generation, aiming to minimize the network's energy consumption during the B time slots. Choosing this metric reduces at maximum the use of drones and hence, sends them only when needed. The first optimization problem corresponds to the zero knowledge case where the mobile operator manages its BSs time slot by time slot without any prior information about the future RE generation. The second one corresponds to the perfect knowledge case with full information about the future RE generation where all the decision variables are simultaneously optimized for the B time slots. The perfect knowledge case is a not realistic case. In this study, it is used as a benchmark scenario for comparison with other cases or as an approximation of the case where RE energy uncertainty is close to negligible. The third one assumes the availability of statistical information about the future RE generation. Hence, the network's management based on RE uncertainty will be investigated under this partial knowledge case. In general, the total energy consumption of the network during time slot b can be expressed as

$$E^b_{\text{tot}} = E^b_0 + E^b_M + E^b_D, \tag{6.15}$$

where, using (6.4) and (6.9), $E_0^b = \left(\alpha_0 \tilde{P}_0^b \left(\boldsymbol{\pi}^b, \boldsymbol{\epsilon}^b\right) + \beta_0\right) T_b$ and represents the energy consumption of the macrocell BS during time slot b. E_M^b is the total energy consumption of L_M MBSs during time slot b which is expressed as:

$$E_M^b = \sum_{k=1}^{L_M} \left[\pi_{m_k}^b (\alpha_m \tilde{P}_{m_k}^b + \beta_m) + (1 - \pi_{m_k}^b)\gamma_m\right] T_b. \tag{6.16}$$

Finally, $E_D^b = \sum_{l=1}^{D} E_{d_l}^b$ corresponds to the total energy consumption of all D drones during time slot b. Using Table 6.1 and knowing that $T_f(i,i) = 0$, the total energy consumption of a drone d_l during time slot b is expressed as follows:

$$\begin{aligned} E_{d_l}^b = \epsilon_{d_l}^b(0) \sum_{j=0}^{Z_D} \epsilon_{d_l}^{b-1}(j) \left[(P_f + \gamma_d) T_f(j,0) + \gamma_d T_r(j,0)\right] + \\ \sum_{i=1}^{Z_D} \sum_{j=0}^{Z_D} \epsilon_{d_l}^b(i) \epsilon_{d_l}^{b-1}(j) \left[(P_f + \gamma_d) T_f(j,i) + (P_{d_l} + P_s) T_r(j,i)\right]. \end{aligned} \tag{6.17}$$

On the other hand and again using Table 6.1, the total harvest-plus-charging energy of DBS l during time slot b due to EH and P_{ch}, denoted by $H_{d_l}^b$, is given as follows:

$$\begin{aligned} H_{d_l}^b = & \epsilon_{d_l}^b(0) \sum_{j=0}^{Z_D} \epsilon_{d_l}^{b-1}(j) \left[\eta \varphi_{d_l}^b T_f(j,0) + (\eta \varphi_{d_l}^b + P_{ch}) T_r(j,0)\right] \\ & + \sum_{i=1}^{Z_D} \sum_{j=0}^{Z_D} \epsilon_{d_l}^b(i) \epsilon_{d_l}^{b-1}(j) \eta \varphi_{d_l}^b \left[T_b\right]. \end{aligned} \tag{6.18}$$

It is assumed that the DBSs are battery powered devices. Therefore, the stored energy by DBS l at the end of time slot b, denoted by $S_{d_l}^b$, is given by:

$$S_{d_l}^b = S_{d_l}^{b-1} + H_{d_l}^b - E_{d_l}^b. \tag{6.19}$$

We assume that, initially, each battery is charged by an amount of energy denoted by $S_{d_l}^0$.

6.2.1 Zero Knowledge Case

In this case, the mobile operator is not aware of the future RE generation process, i.e., $\varphi_{d_l}^b$ is unknown during any future time slots, where $\boldsymbol{\Phi}$ in (6.13) is known during b only.

The optimization problem minimizing the total energy consumption at each time slot b with EH drones is given as:

$$\underset{\boldsymbol{\epsilon}^b\in\{0,1\},\boldsymbol{\pi}^b\in\{0,1\}}{\text{minimize}} \quad E^b_{\text{tot}} = E^b_0 + E^b_M + E^b_D \tag{6.20}$$

subject to:

$$E^b_{d_l} \leq S^{b-1}_{d_l}, \quad \forall l, \tag{6.21}$$

$$S^{b-1}_{d_l} + H^b_{d_l} \leq \bar{S}, \quad \forall l, \tag{6.22}$$

$$\sum_{i=0}^{Z_D} \epsilon^b_{d_l}(i) = 1, \quad \forall l, \tag{6.23}$$

$$\sum_{l=1}^{D} \epsilon^b_{d_l}(i) \leq 1, \quad \forall i = 1, \cdots, Z_D, \tag{6.24}$$

$$U^b - \sum_{k=1}^{L_M} \pi^b_{m_k} U^b_{m_k} - \sum_{l=1}^{D}\sum_{i=1}^{Z_D} \epsilon^b_{d_l}(i) U^b_{d_l,i} \leq \bar{U}_0. \tag{6.25}$$

Constraint (6.21) indicates that the total energy consumed by a drone d_l during the time slot b has to be less than the energy stored at the beginning of this time slot. Constraint (6.22) forces the total energy stored in the battery of a drone d_l during the time slot b to be less than the battery capacity denoted by $\bar{S}$.

Note that $\bar{S}$ is chosen such that the required energy to return a drone to the charging station ($i = 0$) is guaranteed. This energy is simply equal to $P_f T_f(i_{\max}, 0)$ where $i_{\max}$ is the farthest location from $i = 0$. Constraints (6.23) and (6.24) prevent the optimization problem from positioning a drone in two or more different locations during the same time slot and positioning at maximum one drone in the locations $i = 1, \cdots, Z_D$, respectively.

Note that multiple drones can be located simultaneously at the charging station $i = 0$. Finally, constraint (6.25) ensures that the macrocell BS's capacity is not violated. This constraint encourages the activation of MBSs and the deployment of DBSs during high traffic time slots.

Notice that this optimization problem will be solved at the beginning of each time slot which is possible due to the knowledge of the status of the network during the previous time slot $\boldsymbol{\epsilon}^{\boldsymbol{b-1}}$. Hence, the problem can be converted to the standard form of a binary linear programming optimization problem. Optimal solutions for such a problem can be determined optimally with Gurobi/CVX interface [134],[126],[127].

6.2.2 Perfect Knowledge Case

In this case, the mobile operator can perfectly predict the future RE generation $\varphi_{d_l}^b, \forall l = 1, \cdots, D, \forall b = 1, \cdots, B$, ahead of time (i.e., $\tilde{\Phi} = 0$). This case can be considered as a useful benchmark to compare with other cases. Therefore, the objective function becomes the minimization of the total energy consumption of the network during all B time slots. The decision variables are identified as $\boldsymbol{\epsilon}$ and $\boldsymbol{\pi}$ that correspond to the vertical concatenation of the matrices $\boldsymbol{\epsilon}^b$ and $\boldsymbol{\pi}^b, \forall b = 1, \cdots, B$, respectively. Hence, the problem becomes a binary non-linear programming problem due to the existence of the binary products $\epsilon_{d_l}^{b-1}(j)\epsilon_{d_l}^b(i)$ in the energy expressions given in (6.17) and (6.18). To linearize the problem, we introduce for each link the parameter $\zeta_{d_l}^b(j,i)$ such that $\zeta_{d_l}^b(j,i) = \epsilon_{d_l}^{b-1}(j)\epsilon_{d_l}^b(i)$ where the following inequalities have to be respected:

$$\begin{aligned} &\zeta_{d_l}^b(j,i) \leq \epsilon_{d_l}^{b-1}(j), \\ &\zeta_{d_l}^b(j,i) \leq \epsilon_{d_l}^b(i), \\ &\text{and} \\ &\zeta_{d_l}^b(j,i) \geq \epsilon_{d_l}^{b-1}(j) + \epsilon_{d_l}^b(i) - 1. \end{aligned} \tag{6.26}$$

The first two inequalities ensure that $\zeta_{d_l}^b(j,i) = 0$ if $\epsilon_{d_l}^{b-1}(j)$ or $\epsilon_{d_l}^b(i)$ is zero. The third inequality guarantees that $\zeta_{d_l}^b(j,i) = 1$ if $\epsilon_{d_l}^{b-1}(j) = \epsilon_{d_l}^b(i) = 1$. It can be deduced from (6.26) that when $\zeta_{d_l}^b(j,i) = 1$, the drone d_l will move from location j to location i during time slot b. Hence, the expressions (6.17) and (6.18) become depending on $\zeta_b(d_l, n)$ and the decision variables turn into $\boldsymbol{\zeta}$, $\boldsymbol{\epsilon}$, and $\boldsymbol{\pi}$ that have the following number of elements: $BD(Z_D+1)^2$, $BD(Z_D+1)$, and BM, respectively. Accordingly, the optimization problem that minimizes the network energy consumption during all B time slots is given by

$$\underset{\substack{\boldsymbol{\epsilon}\in\{0,1\},\boldsymbol{\pi}\in\{0,1\},\\ \boldsymbol{\zeta}\in\{0,1\}}}{\text{minimize}} \quad E_{\text{tot}} = \sum_{b=1}^{B} E_0^b + E_M^b + E_D^b \tag{6.27}$$

subject to:

$$\sum_{t=1}^{b} E_{d_l}^t - \sum_{t=1}^{b-1} H_{d_l}^t \leq S_{d_l}^0, \quad \forall l, \forall b, \tag{6.28}$$

$$S_{d_l}^0 + \sum_{t=1}^{b} H_{d_l}^t - \sum_{t=1}^{b-1} E_{d_l}^t \leq \bar{S}, \forall l, \forall b, \tag{6.29}$$

$$\sum_{i=0}^{Z_D} \epsilon_{d_l}^b(i) = 1, \quad \forall l, \forall b, \tag{6.30}$$

$$\sum_{l=1}^{D} \epsilon_{d_l}^b(i) \leq 1, \quad \forall i = 1, \cdots, Z_D, \forall b, \tag{6.31}$$

$$U^b - \sum_{k=1}^{L_M} \pi_{m_k}^b U_{m_k}^b - \sum_{l=1}^{D} \sum_{i=1}^{Z_D} \epsilon_{d_l}^b(i) U_{d_l,i}^b \leq \bar{U}_0, \quad \forall b, \tag{6.32}$$

$$\zeta_{d_l}^b(j,i) \leq \epsilon_{d_l}^b(i), \quad \forall l, \forall i, \forall j, \forall b, \tag{6.33}$$

$$\zeta_{d_l}^b(j,i) \leq \epsilon_{d_l}^{b-1}(j), \quad \forall l, \forall i, \forall j, \forall b, \tag{6.34}$$

$$\zeta_{d_l}^b(j,i) \geq \epsilon_{d_l}^{b-1}(j) + \epsilon_{d_l}^b(i) - 1, \quad \forall l, \forall i, \forall j, \forall b, \tag{6.35}$$

Notice that the constraints (6.28)-(6.32) are similar to the constraints (6.21)-(6.25) except that they have to be satisfied for all time slots $b = 1, \cdots, B$. The constraints (6.28)-(6.29) are obtained by replacing $S_{d_l}^b$ by its expression given in (6.19). The constraints (6.33)-(6.35) correspond to the linearization process as indicated in (6.26).

In terms of complexity, the linearized perfect knowledge optimization problem is largely more complex than the one of the zero knowledge case due to the higher number of binary decision variables and constraints. The linearized perfect knowledge problem can be also solved optimally with Gurobi/CVX interface [134],[126],[127].

6.2.3 Partial Knowledge Case

In this case, the mobile operator has only partial knowledge about future RE generation (i.e., the RE generation is uncertain). One of the ways to deal with the RE uncertainty is to

solve the optimization problem using stochastic programming. Stochastic programming is a mathematical framework for modeling optimization problems in which some or all optimization variables are presented by random variables that involve uncertainty. The goal of such framework is to provide useful analytical or numerical information to a decision maker by finding a feasible policy that optimizes the expectation of some functions of the deterministic and the random decision variables [135]. In this case, we use two-stage recourse stochastic programming to represent the impacts of uncertainty in the partial knowledge case due to its simplicity.

This approach includes two stages. In the first stage, the decision is made before observing the stochastic variables. Once the uncertain events have been unfolded, further decision on the operation of the system can be made through the second stage [90]. The first stage in stochastic programming is to optimize other variables, given that the output variables are known, for any given value of Φ. Then, the decision needs to be updated once the actual realization of Φ has been obtained. More specifically, we choose to fix feasible values of $\boldsymbol{\pi}$ since it does not directly depend on the RE generation. This allows us to compute the best combination of other variables (i.e., $\boldsymbol{\zeta}$ and $\boldsymbol{\epsilon}$) provided that Φ is known.

The objective function given in (6.27) can be re-written as

$$E_{\text{tot}} = \hat{E} + E^*, \tag{6.36}$$

where $\hat{E}$ does not depend on the RE directly while E^* does.

Therefore, the problem can be written as a two-stage recourse problem as follows [136]:

$$\underset{\boldsymbol{\pi}\in\{0,1\}}{\text{minimize}} \qquad E_{\text{tot}} = \hat{E} + \mathbb{E}_{\Phi}[E^*], \tag{6.37}$$

where $\mathbb{E}_{\Phi}[.]$ represents the expectation function with respect to Φ and E^* can be obtained as follows:

$$E^* = \underset{\boldsymbol{\epsilon}\in\{0,1\},\boldsymbol{\zeta}\in\{0,1\}}{\text{minimize}} \quad f(\boldsymbol{\epsilon},\boldsymbol{\zeta}) \tag{6.38}$$

subject to:

$$\sum_{t=1}^{b} E_{d_l}^t - \sum_{t=1}^{b-1} H_{d_l}^t(\varphi_{d_l}^b) \leq S_{d_l}^0, \quad \forall l, \forall b, \tag{6.39}$$

$$S_{d_l}^0 + \sum_{t=1}^{b} H_{d_l}^t(\varphi_{d_l}^b) - \sum_{t=1}^{b-1} E_{d_l}^t \leq \bar{S}, \forall l, \forall b, \tag{6.40}$$

$$\sum_{i=0}^{Z_D} \epsilon_{d_l}^b(i) = 1, \quad \forall l, \forall b, \tag{6.41}$$

$$\sum_{l=1}^{D} \epsilon_{d_l}^b(i) \leq 1, \quad \forall i = 1, \cdots, Z_D, \forall b, \tag{6.42}$$

$$U^b - \sum_{k=1}^{L_M} \pi_{m_k}^b U_{m_k}^b - \sum_{l=1}^{D}\sum_{i=1}^{Z_D} \epsilon_{d_l}^b(i) U_{d_l,i}^b \leq \bar{U}_0, \quad \forall b, \tag{6.43}$$

$$\zeta_{d_l}^b(j,i) \leq \epsilon_{d_l}^b(i), \quad \forall l, \forall i, \forall j, \forall b, \tag{6.44}$$

$$\zeta_{d_l}^b(j,i) \leq \epsilon_{d_l}^{b-1}(j), \quad \forall l, \forall i, \forall j, \forall b, \tag{6.45}$$

$$\zeta_{d_l}^b(j,i) \geq \epsilon_{d_l}^{b-1}(j) + \epsilon_{d_l}^b(i) - 1, \quad \forall l, \forall i, \forall j, \forall b, \tag{6.46}$$

where $f(\boldsymbol{\epsilon},\boldsymbol{\zeta})$ is a function of $\boldsymbol{\epsilon}$ and $\boldsymbol{\zeta}$. In this case, $\boldsymbol{\epsilon}$ and $\boldsymbol{\zeta}$ are considered the second stage decision variables.

The solution of the first stage problem can be solved efficiently by evaluating the expectation over $\boldsymbol{\Phi}$, in case the solution of the second stage problem can be obtained in its closed-form expression. However, in most cases, obtaining a closed-form solution may either be impossible or requires the computation of very complicated and intractable expressions.

In order to simplify the problem, we propose to discretize the random variables to solve the two stage problem recourse efficiently [137]. This allow the achievement of near optimal solutions for continuous random variables with an accuracy level dependent on the discretization scale.

It is assumed that the random variables $\varphi_{d_l}^b, \forall l = 1, \cdots, D, \forall b = 1, \cdots, B$ is discretized to take a set of V possible values. We denote by $\mathcal{V}$ the set that includes all the possible combinations of the RE generation over the drones. Its size is given as $|\mathcal{V}| = V^{DB}$, where $|.|$

denotes the cardinality of a set, and depends on the number of drones D and the number of time slots B. We consider that each possibility of V is realized with a probability $\mathcal{P}_v, v = 1, \cdots, |\mathcal{V}|$ where $\mathcal{P}_v$ indicates the probability mass function of $\varphi^b_{d_l}$ which can be determined from the discretization process. Therefore, the two stage recourse optimization problem can be formulated as the following large binary linear programming problem:

$$\underset{\substack{\boldsymbol{\epsilon}_v \in \{0,1\}, \boldsymbol{\pi} \in \{0,1\}, \\ \boldsymbol{\zeta}_v \in \{0,1\}}}{\text{minimize}} \quad \hat{E} + \mathbb{E}_{\Phi}[f(\boldsymbol{\epsilon}_v, \boldsymbol{\zeta}_v)] \tag{6.47}$$

subject to:

$$\sum_{t=1}^{b} E^t_{d_l,v} - \sum_{t=1}^{b-1} H^t_{d_l,v}(\varphi^b_{d_l}) \leq S^0_{d_l}, \quad \forall l, \forall b, \forall v, \tag{6.48}$$

$$S^0_{d_l} + \sum_{t=1}^{b} H^t_{d_l,v}(\varphi^b_{d_l}) - \sum_{t=1}^{b-1} E^t_{d_l,v} \leq \bar{S}, \forall l, \forall b, \forall v, \tag{6.49}$$

$$\sum_{i=0}^{Z_D} \epsilon^b_{d_l,v}(i) = 1, \quad \forall l, \forall b, \forall v, \tag{6.50}$$

$$\sum_{l=1}^{D} \epsilon^b_{d_l,v}(i) \leq 1, \quad \forall i = 1, \cdots, Z_D, \forall b, \forall v, \tag{6.51}$$

$$U^b - \sum_{k=1}^{L_M} \pi^b_{m_k} U^b_{m_k} - \sum_{l=1}^{D} \sum_{i=1}^{Z_D} \epsilon^b_{d_l,v}(i) U^b_{d_l,i} \leq \bar{U}_0, \forall b, \forall v, \tag{6.52}$$

$$\zeta^b_{d_l,v}(j,i) \leq \epsilon^b_{d_l,v}(i), \quad \forall l, \forall i, \forall j, \forall b, \forall v, \tag{6.53}$$

$$\zeta^b_{d_l,v}(j,i) \leq \epsilon^{b-1}_{d_l,v}(j), \quad \forall l, \forall i, \forall j, \forall b, \forall v, \tag{6.54}$$

$$\zeta^b_{d_l,v}(j,i) \geq \epsilon^{b-1}_{d_l,v}(j) + \epsilon^b_{d_l,v}(i) - 1, \quad \forall l, \forall i, \forall j, \forall b, \forall v, \tag{6.55}$$

where $\mathbb{E}_{\Phi}[f(\boldsymbol{\epsilon}_v, \boldsymbol{\zeta}_v)] = \sum_{v=1}^{|\mathcal{V}|} \mathcal{P}_v f(\boldsymbol{\epsilon}_v, \boldsymbol{\zeta}_v)$. The optimal solution for the binary linear optimization problem given in (6.47)-(6.55) can be determined using Gurobi/CVX interface [134],[126],[127].

Notice that this problem becomes very complex compared to the other scenarios as the number of its constraints exponentially scales with the number of possibilities V^{DB}.

6.3 Numerical Results

In this section, selected numerical results are provided to investigate the benefits of utilizing dynamic DBSs in HetNets. Firstly, the results are investigating the zero knowledge and perfect

knowledge cases to show the performance and advantages of the proposed drone-assisted HetNet model. Then, a comparison with the partial knowledge case is performed to evaluate the impact of uncertainty on the system performance.

6.3.1 Simulation Parameters

Table 6.2: System parameters.

Parameter	Value	Parameter	Value	Parameter	Value
λ_0 (m)	0.125	$P_{\min}(dBm)$	-70	T_b (minute)	10
ν_1	9.6	ν_2	0.29	ξ_{LoS} (dB)	1
ξ_{NLoS} (dB)	12	α_0	4.7	β_0 (W)	130
α_m	2.6	β_m (W)	56	γ_m (W)	39
α_d	4	β_d (W)	6.8	γ_d (W)	2.9
$\bar{S}$ (kJ)	10	$v_d = v_{\max}$ (m/s)	15	m_{tot} (g)	750
r_p (cm)	20	n_p	4	P_s (W)	0.5
P_{ch} (W)	10	η	0.3	$\bar{U}_0$	130

Assume a HetNet consisting of one macrocell BS with radius of one km, four MBSs ($L_M = 4$) with a coverage of 250 meters, and six identical drones ($D = 6$), unless otherwise stated, that can potentially be placed in sixteen different locations ($Z_D = 16$) in addition to the charging station location. We consider that these 16 locations have the same altitude $h_i = 60$ meters, $\forall i = 1, \ldots, 16$ and that each drone has a coverage of 150 meters to meet the minimum required receiving power $P_{\min} = -70$ dBm. The $Z_D + 1$ pre-planned locations are indicated as depicted in Fig 6.2. We assume that the drones are initially charged with $S_{d_l}^0 = 6$ kJ of energy and placed at the charging station. The average received amount of photovoltaic power $\phi_{d_l}^b$ is assumed to be generated following a Gamma distribution with shape and scale parameters equal to 1 and 2, respectively. We assume that $U^b = 140, \forall b = 1, \cdots, B$ users exist within the macrocell BS unless otherwise stated. In case of cell overlap between the MBS and an active DBS, we assume that the drone has the priority in serving the users in the intersection region once deployed. In Table 6.2, we present the values of the remaining parameters used in the simulations [130],[133].

6.3.2 System Performance

In Fig. 6.2, we start by investigating the behavior of two randomly selected drones, drone d_1 and drone d_3 respectively, for two different user distributions but for the same number of users and RE generation per drone and time slot. In Fig. 6.2(a,c), we consider a uniform user distribution and hence, if a drone is placed in a location $i \neq 0$, it will serve, on average, exactly the same number of users as another drone placed in another location $j \neq i$. In Fig. 6.2(b,d), another non-uniform distribution is considered and hence, the number of users to be served differs from a location to another. It is shown that with the uniform distribution, once the drone is sent to a location i then, it has two possibilities for the next slot, either to stay at the same location (e.g., d_1 during $b = 3, 4$) if it has enough energy, otherwise, it returns back to the charging station (e.g., d_1 during $b = 2$). On the other hand, with the random distribution, the drone can go from one location to another to serve the users without passing by the charging station. For instance, d_1 goes to $i = 5$ in $b = 3$, then moves to $i = 2$. It is also worth to note that the drones avoid long distance trip when selecting the locations unless they are forced to do it due to high user density in these locations (e.g., d_3 with random distribution moves to $i = 2, 15$ during $b = 3, 1, 5$).

In Fig. 6.3, we plot the energy consumption and number of active drones per time slot for $B = 20$ and different number of users uniformly distributed (i.e., $U^b = 140$ and $U^b = 160, \forall b$). This figure investigates the impact of RE for two cases: 1) when the drones are supported by solar panels and 2) when the drones are charged by the central station only. It is shown that EH does not only help in reducing the total fossil fuel consumption of the network but also, it helps in avoiding (or decreasing) the outage risk (i.e., where not all users can be simultaneously served). Indeed, when the number of users in the network is relatively large (e.g., U^b=160), two outage periods are detected $b = \{9, 10\}$ and $b = 18$. These outages are due to two reasons: Firstly, the non-EH drones need to go to the central station to charge their batteries more frequently than the solar-powered drones. Secondly, the EH drones can harvest energy when flying and serving users which contributes to the increase of their battery levels and hence, get more flexibility to move to other locations without passing by the charging station. This is

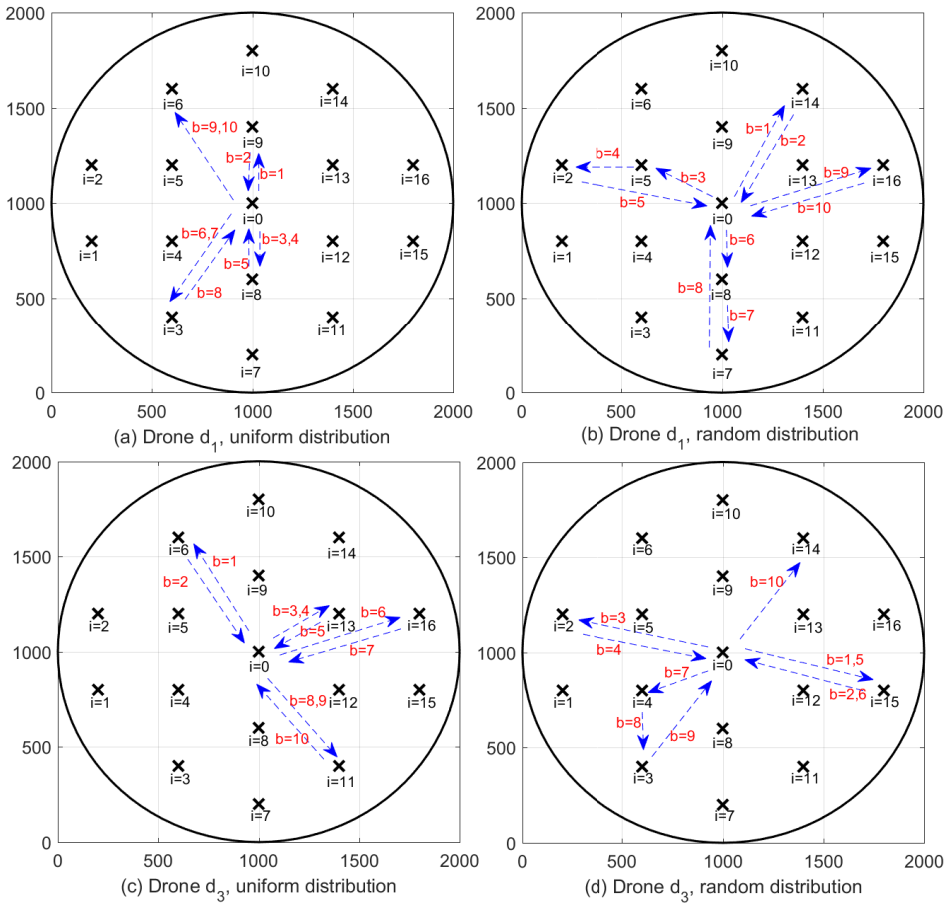

Figure 6.2: The behavior of two drones, drone d_1 (a,b), drone d_3 (c,d) for different user distributions with $D = 6$.

deduced from the number of active drones of each case which is higher for the EH case.

Fig. 6.4 compares between the zero and perfect knowledge cases presented in Section 6.2 for different number of drones while increasing the total number of users per time slot. It is noticed that increasing the number of drones help in avoiding network outage and reducing the total energy consumption specially when the network becomes more and more congested. For example, in the traditional case without drone, the network becomes overloaded for a number of users higher than $U^b > 160$. Furthermore, the perfect knowledge case achieves a more important energy saving due to its efficient management of the harvested energy compared to the zero knowledge case. Nevertheless, the achieved performance of the zero knowledge case follows the same trend of the one of the perfect knowledge case.

In Fig. 6.5 and Table 6.3, another scenario is investigated for time varied number of users

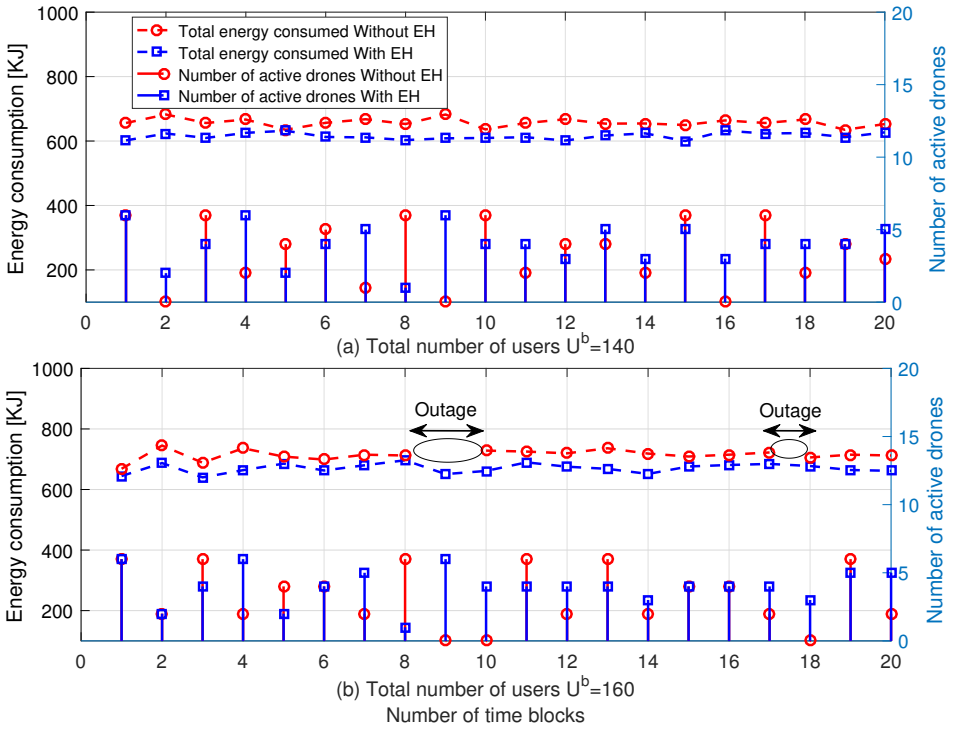

Figure 6.3: Total energy consumption and number of active drones during the trial period for (a) $U^b = 140, \forall b$ and (b) $U^b = 160, \forall b$.

over $B = 10$ time slots and with $D = 4$ drones and $L_M = 4$ MBSs. The behavior of the drones and the statuses of MBSs are illustrated for each time slot using the zero and perfect knowledge cases. Fig. 6.5(a)-(c) plot the total energy consumption of the drones, MBSs, and macrocell BS, respectively. Also, the total energy consumption per time slot is presented in Fig. 6.5(d). It can be noticed that, in general, activating the MBSs and/or DBSs essentially depends on the traffic and drones' battery level. Fig. 6.5 also, shows the advantages of using the MBSs along with the drones in order to reduce the macrocell BS energy, thus, reduce the total consumed energy. For example, although the macrocell BS can handle all the users during $b = 3$ (i.e., $U^3 = 120$), the optimization suggests to activate 3 MBSs and 4 drones for both zero and perfect knowledge cases in order to reduce the total transmit power of the macrocell BS and hence, the total energy consumption. Another important notice can be deduced from Table 6.3, although the number of users during $b = 4$ (i.e., $U^b = 80$) is greater than the number of users during $b = 7$ (i.e., $U^b = 60$), we activate only one drone during $b = 4$ instead of 3 drones during $b = 7$. This is can be justified by the fact that since the network was more congested during $b = 3$

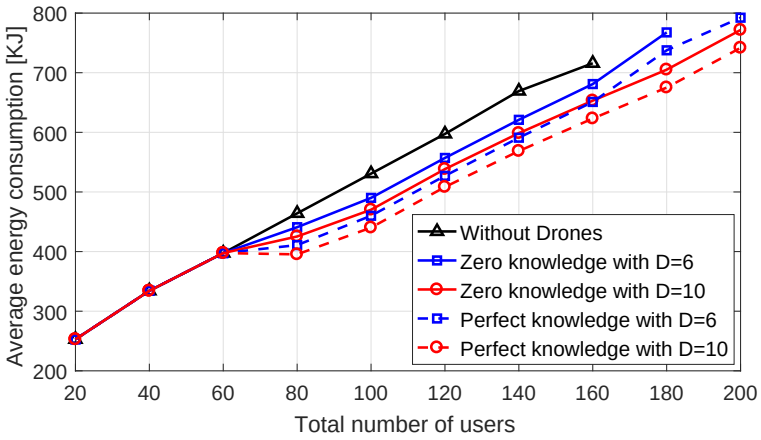

Figure 6.4: Comparison between the zero knowledge and perfect knowledge cases for different values of D.

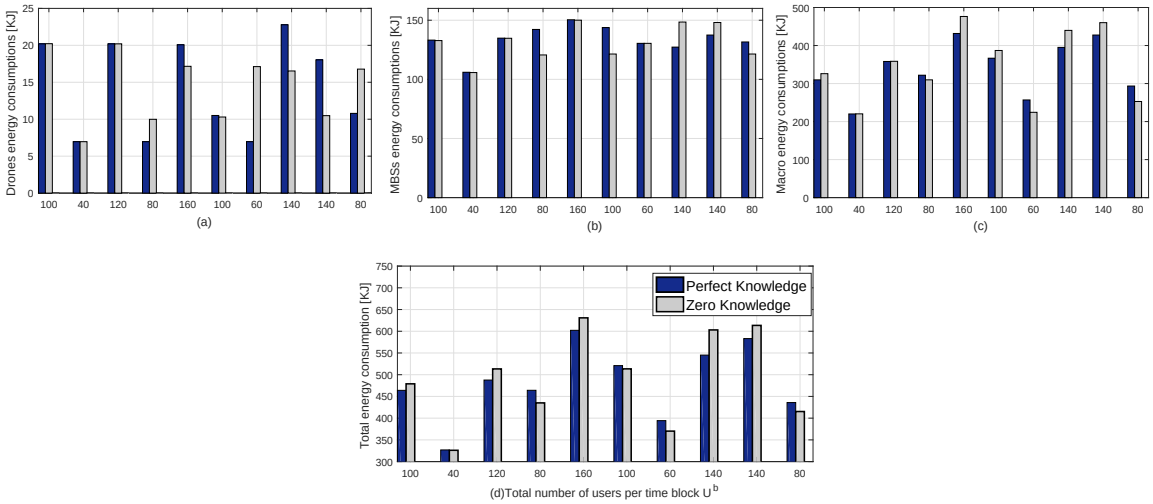

Figure 6.5: Comparison between zero and perfect knowledge cases for $D = 4$ and $B = 10$.

compared to $b = 6$ where more drones were sent then, due to the drones' battery limitation, one drone is activated during $b = 4$.

It is also worth to note that there is a kind of alternation between the activation of MBSs and the drones' deployment. If the network is partially congested, we notice that the system decides either to deploy drones or activate MBSs depending on the battery levels. For example, for the perfect knowledge, during $b = 7$, 3 MBSs are activated while no drone is used. However, during $b = 8$, 2 MBSs are turned off and all drones are employed.

On the other hand, it can be shown that the prefect knowledge case achieves better performance than the one of the zero knowledge case by managing the available resource more

Table 6.3: Drones and MBSs status during multiple time slots.

	Number of users per b	Active MBSs				Active drones			
		m_1	m_2	m_3	m_4	d_1	d_2	d_3	d_4
Perfect knowledge case	$U^1 = 100$	×	-	×	×	×	×	×	×
	$U^2 = 40$	×	×	-	-	-	-	-	-
	$U^3 = 120$	-	×	×	×	×	×	×	×
	$U^4 = 80$	×	×	×	×	-	-	-	-
	$U^5 = 160$	×	×	×	×	×	×	×	×
	$U^6 = 100$	×	×	×	×	-	-	-	×
	$U^7 = 60$	-	×	×	×	-	-	-	-
	$U^8 = 140$	×	-	×	-	×	×	×	×
	$U^9 = 140$	×	-	×	×	×	×	-	×
	$U^{10} = 80$	-	×	×	×	-	-	×	-
Zero knowledge case	$U^1 = 100$	×	-	×	×	×	×	×	×
	$U^2 = 40$	-	-	-	×	-	-	-	-
	$U^3 = 120$	×	×	×	-	×	×	×	×
	$U^4 = 80$	×	×	-	-	×	-	-	-
	$U^5 = 160$	×	×	×	×	-	×	×	×
	$U^6 = 100$	×	×	-	-	×	-	-	-
	$U^7 = 60$	×	-	×	×	-	×	×	×
	$U^8 = 140$	×	×	×	×	×	×	×	-
	$U^9 = 140$	×	×	×	×	-	-	-	×
	$U^{10} = 80$	×	×	-	-	×	×	×	-

efficiently such as drones' available batteries. For example, as shown in Table 6.3, during $b = 7$ (i.e., $U^7 = 160$), the perfect knowledge case keeps all the drones in the charging station in order to charge the batteries and hence, it becomes possible to send most of them during the next two time slots (i.e., d_1, d_2, d_3, and d_4 are active during $b = 8$ and d_1, d_2, and d_4 are active during $b = 9$) where the network is more congested, i.e., $U^8 = U^9 = 140$ as shown in Table 6.3. As shown in Fig. 6.5, although it consumes more energy than the zero knowledge case, which is around 20 kJ, when $b = 7$, the perfect knowledge case saves more energy, which is around 75 kJ, during the next two time slots $b = 8$ and $b = 9$.

Finally, Fig. 6.6 plots the average energy consumption per time slot b (i.e., E_{tot}/B) versus the total number of users for $D = 3$. The results compare between the different RE knowledge cases: zero, perfect, and partial knowledge cases, where different deviation values from the

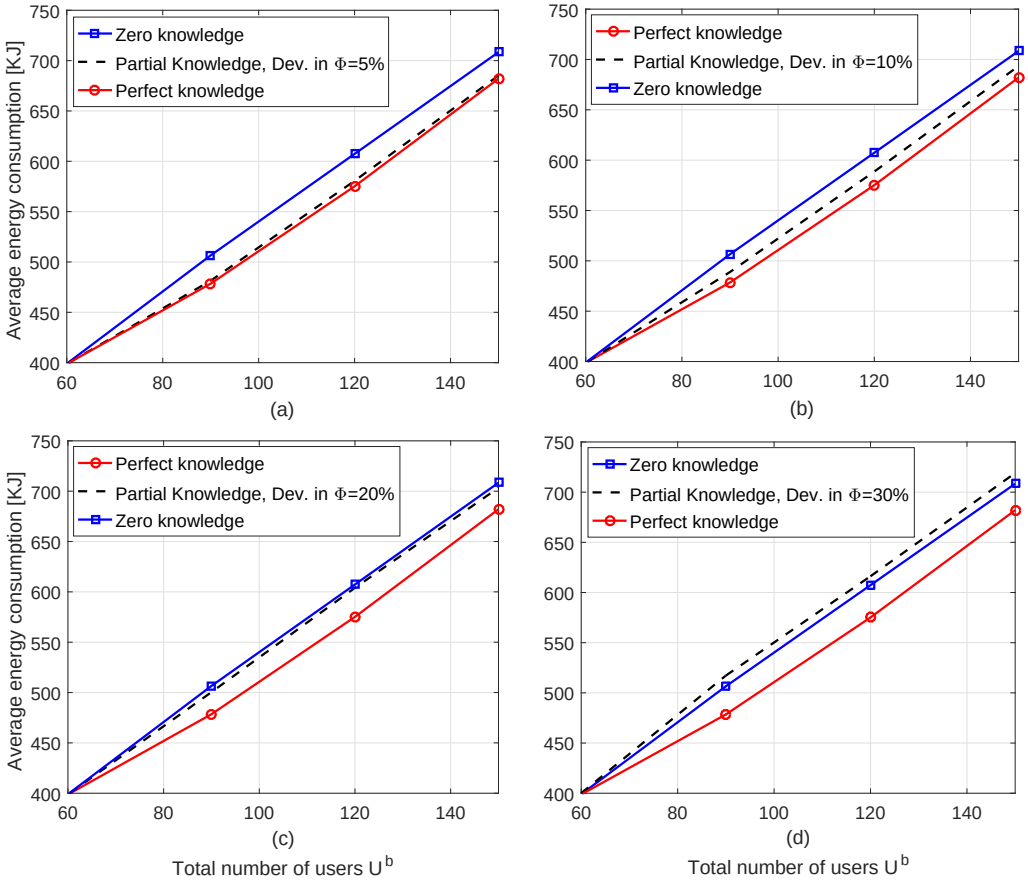

Figure 6.6: Comparison of the average energy consumption per time slot versus the total number of users for $D = 3$ and three drone management cases (i.e., zero, partial, perfect) with different deviation values in Φ.

mean of RE generations Φ are considered in the partial knowledge case. In other words, we consider a discrete decision variable with 2 possibilities where $\tilde{\Phi} \in \{-x\%\bar{\Phi}, x\%\bar{\Phi}\}$. In the figure, we set $x = \{5, 10, 20, 30\}$. The obtained results confirm that the perfect knowledge case always achieves the lowest energy consumption compared to the other cases (zero and partial knowledge cases) as it represents the benchmark solution. On the other hand, the partial knowledge case achieves better performance compared to the zero knowledge case and the obtained energy consumption remains close to the perfect case when the uncertainty is relatively small (e.g., $5\%, 10\%, 20\%$). However, when the uncertainty is relatively large, (e.g., 30%), the zero knowledge case outperforms the partial knowledge case since the drones in the latter case can not consume the available power in their batteries efficiently. Indeed, when the uncertainty level becomes high, the stochastic programming solution reduces the risk of failing

in an outage scenario (either in terms of battery depletion or in terms of network outage). Therefore, it forces the drones to return to the charging station more frequently than the zero knowledge case. Hence, more MBSs are activated and a major part of the users are served by the macrocell BS. This happens clearly, when the number of users is relatively large.

6.4 Chapter Summary

In this chapter, we proposed an energy management framework for cellular heterogeneous networks assisted by solar-powered drone small cells. A BLP problem is formulated in order to minimize the total energy consumption of the networks over a time-slotted period while maintaining the network coverage and connectivity. Multiple drone base stations are optimally placed in order to support overloaded cells while taking into account their photovoltaic energy generation and battery capacity. In order to deal with the uncertainty in the renewable energy generation, two cases are investigated in our analysis. The first case, identified as the zero knowledge case, manages the system time slot per time slot without considering future renewable energy generation. The second case exploits the partial knowledge about future renewable energy generation and devises a pre-planned network management while considering the level of uncertainty in its optimization. These two cases are compared to a benchmark case assuming perfect knowledge of future renewable energy generation, i.e., zero uncertainty.

Through several numerical results, we investigated the behavior of the dynamic drones as well as the ON/OFF switching operation applied to the micro cell BSs for different scenarios. Our results show the notable impacts of employing dynamic drones mainly during peak-hour periods in ensuring connectivity and supporting overloaded cells with minimum energy consumption. As expected the perfect knowledge case outperforms the other cases which provides close solutions for low levels of uncertainty. However, for high uncertainty level, the partial knowledge case will be more risk-aware and generates safer solutions to avoid battery depletion and network outage.

CHAPTER 7. CONCLUSIONS AND FUTURE WORK

7.1 Conclusions and Summary of Contributions

In this thesis, all research efforts have focused on proposing and analyzing energy efficient planning and operation models for wireless communication systems. A brief summary of the main contributions of this thesis is outlined.

- Chapter 3 proposed an overlay CR relaying problem using TWR system assisted with multiple antennas. A meta-heuristic approach based on particle swarm optimization algorithm was developed to solve the formulated optimization problem. In this setup multiple AF relays are used where the primary and cognitive terminal powers were optimized adaptively with the bandwidth and amplification gains. The objective was based on maximizing the cognitive utility while satisfying a certain primary target rate. Starting with expressions of primary and cognitive powers for fixed bandwidths and amplification gains, a meta-heuristic approach based on PSO algorithm was developed to reach a near-optimal solution. Moreover, in addition to the sum rate objective function, other utilities are investigated to introduce more fairness among cognitive users.

- Chapter 4 proposed a multiple-relay selection scheme for PS protocol-based EH TWR system. The relays harvest energy from RE and RF sources. An optimization problem was formulated aiming to maximize the rate utility over multiple time slots. Due to the non-convexity of the optimization problem, a joint-optimization approach based on BPSO and geometric programming is adopted. The proposed solution enables the system to achieve near optimal solutions with a significant gain compared to dual problem-based solution.

- Chapter 5 proposed a green downlink EH framework in three tier HetNets using hybrid power sources. All the BSs are equipped with a harvested source and can get some energy from GG or/and TG when needed. A binary linear optimization problem was formulated aiming to minimize the energy cost over multiple time slots. The problem was solved optimally and compared with two low complexity algorithms.

- Chapter 6 proposed an energy management framework for cellular HetNets assisted by solar-powered DBSs. Multiple drones are optimally placed in order to support overloaded cells while taking into account their photovoltaic energy generation and battery capacities. In order to deal with the uncertainty in the renewable energy generation, two cases are investigated in our analysis. The first case, identified as the zero knowledge case, manages the system time slot per time slot without considering future renewable energy generation. The second case exploits the partial knowledge about future renewable energy generation and devises a pre-planned network management while considering the level of uncertainty in its optimization. These two cases are compared to a benchmark case assuming perfect knowledge of future renewable energy generation, i.e., zero uncertainty. The results show notable impacts of employing dynamic drones mainly during peak-hour periods in ensuring connectivity and supporting overloaded cells with minimum energy consumption. As expected the perfect knowledge case outperforms the other cases which provides close solutions for low levels of uncertainty. However, for high uncertainty level, the partial knowledge case will be more risk-aware and generates safer solutions to avoid battery depletion and network outage.

7.2 Future Works

The future and ongoing works of this thesis will deal with new research directions that can improve our work and lead to better performance

- **Internet of Things with 5G Support and Energy Harvesting**

  In the close future, each physical object/machine will be connected to the internet and able to identify itself to other devices. Actually 4G is good enough for now, however in

few years, 4G will obviously not be able to meet requirements for new devices. Therefore, 5G is considered as the backbone of the IoT that links the fixed devices with moving devices. In addition to energy consumption, one of the challenges is the interference management between devices. Interestingly, most of IoT devices are low power devices and require relatively low data rates such as bio-sensors and environmental monitoring sensors.

I intend to propose optimization problems that use efficient multiple access protocols to squeeze in a lot of IoT devices with different QoS requirements into the same time slot or bandwidth. On the other hand, each IoT will be equipped with a harvester that harvests from RE and RF sources to power its communication points.

Therefore, the objective will be to minimize the total energy consumption and reduce the carbon footprint of the network while achieving different QoS for different users under the 5G IoT framework.

- **Self Healing Assisted with Drone-based Communications**

  The drone-based communications has represented a novel and interesting area of research in communications, where drones-based communications provides more degrees of freedom in time (available on demand) and space (mobile) and they can be located according to uses need.

  When a failure occurs in any BS tier, the conventional and well-known self-healing technique for compensating this failure is to change the BSs antenna power and tilt to serve the users of the failed BS. The disadvantage of this technique is that the users of the neighboring cells will be affected by this change in their BSs antenna power and tilt.

  On the other hand, if the network is supported by DBSs, when the failure occurs, the conventional technique will be used to serve the users of the failed BS until the drones reach the predetermined locations. When the drones reach this locations, the neighboring BSs will return to serve their own users only and the users of the failed BS will be served by the DBSs.

Therefore, the next task is to investigate drone-based communication under a multiple failure BSs scenario by optimizing the location of these drones, managing their limited energy consumption, and evaluating their achieved performance to help failed BSs in healing some of their users.

APPENDIX A. PARTICLE SWARM OPTIMIZATION ALGORITHM

PSO algorithm can be employed to optimize $\boldsymbol{\mathcal{N}}$ vector variable. The PSO algorithm was introduced in 1995 [138] and it is inspired by swarm intelligence, social behavior, and food searching by a flock birds and a school of fish. This approach is widely used in several wireless communication fields due to its simplicity and efficiency [139],[140],[141]. Due to the following advantages of PSO compared with the other heuristic approaches, we apply it for solving some problem: (i) simple search process and easy to implement by manipulating few numerical parameters (e.g., such as the number of particles and acceleration factors for PSO), (ii) it requires low computational cost attained from small number of agents, and (iii) it provides a good convergence speed [142].

Although PSO's application has been proved to be effective, convergence to its most optimistic solution cannot be guaranteed in theory [143].

First, the PSO generates N random particles $\boldsymbol{\mathcal{N}}^{(n)},\ n = 1, \cdots, N$, to form an initial population set $\mathcal{S}$. The algorithm computes the achieved utility of all particles for this $\boldsymbol{\mathcal{N}}^{(n)}$. Then, it finds the particle that provides the global optimal utility for this iteration, denoted $\boldsymbol{\mathcal{N}}^{(\text{global})}$. In addition, for each particle n, it memorizes the position of its previous best performance, denoted $\boldsymbol{\mathcal{N}}^{(\text{n,local})}$. After finding these two best values, PSO updates its velocity $\boldsymbol{\nu}_j^{(n)}$ and its particle positions $\boldsymbol{\mathcal{N}}_j^{(n)}$. These steps are repeated until reaching convergence by either attaining the maximum number of iterations or stopping the algorithm when no improvement is noticed.

Particle Swarm Optimization Algorithm

For the continuous variables case, the updated velocity $\boldsymbol{\nu}_j^{(n)}$ and particle positions $\boldsymbol{\mathcal{N}}_j^{(n)}$ at each iteration q are given respectively as follows

$$\begin{aligned}\boldsymbol{\nu}_j^{(n)}(q+1) = \psi_0 \boldsymbol{\nu}_j^{(n)}(q) + c_1\psi_1(q)\left(\boldsymbol{\mathcal{N}}_j^{(\mathrm{n,local})}(q) - \boldsymbol{W}_j^{(n)}(q)\right) \\ + c_2\psi_2(q)\left(\boldsymbol{\mathcal{N}}_j^{(\mathrm{global})}(q) - \boldsymbol{\mathcal{N}}_j^{(n)}(q)\right),\end{aligned} \tag{A.1}$$

$$\boldsymbol{\mathcal{N}}_j^{(n)}(q+1) = \left(\boldsymbol{\mathcal{N}}_j^{(n)}(q) + \boldsymbol{\nu}_j^{(n)}(q+1)\right)^{+}, \tag{A.2}$$

where ψ_0 is the inertia weight used to control the convergence speed ($0.8 \leq \psi_0 \leq 1.2$). ψ_1 and ψ_2 are two random positive numbers generated for iteration q ($\psi_1, \psi_2 \in [0, 2]$) [109]. Finally, c_1 and c_2 are the step size that a particle takes towards the best individual candidate solution $\boldsymbol{\mathcal{N}}^{(\mathrm{n,local})}$ and the global best solution $\boldsymbol{\mathcal{N}}^{(\mathrm{global})}$. This procedure is repeated until convergence (i.e., the utility remains constant for a certain number of iterations or reaching maximum number of iterations).

Binary Particle Swarm Optimization Algorithm

For the binary variables case the, updated velocity $\boldsymbol{\nu}_j^{(n)}$ and particle positions $\boldsymbol{\mathcal{N}}_j^{(n)}$ at each iteration q are given respectively as follows

$$\begin{aligned}\boldsymbol{\nu}_{l,b}^{(n)}(q+1) =& \psi_0 \boldsymbol{\nu}_{l,b}^{(n)}(q) + \psi_1(q)\left(\boldsymbol{\mathcal{N}}_j^{(\mathrm{n,local})}(q) - \boldsymbol{\mathcal{N}}_j^{(n)}(q)\right) \\ &+ \psi_2(q)\left(\boldsymbol{\mathcal{N}}_j^{\max}(q) - \boldsymbol{\mathcal{N}}_j^{(n)}(q)\right),\end{aligned} \tag{A.3}$$

$$\boldsymbol{\mathcal{N}}_j^{(n)}(q+1) = \begin{cases} 1 \text{ if } r_{\mathrm{rand}} < \Psi_{\mathrm{BPSO}}\left(\boldsymbol{\nu}_{l,b}^{(n)}(q+1)\right), \\ 0 \text{ otherwise.} \end{cases} \tag{A.4}$$

where r_{rand} is a pseudo-random number selected from a uniform distribution in $[0, 1]$ and Ψ_{BPSO} is a sigmoid function for transforming the velocity to probabilities and is given as:

$$\Psi_{\mathrm{BPSO}}(x) = \frac{1}{1 + e^{-x}}. \tag{A.5}$$

APPENDIX B. GEOMETRIC PROGRAMMING

GP is a class of nonlinear and nonconvex optimization problems that can be efficiently solved after converting them to a nonlinear but convex problems [107]. The interior-point method can be applied to GP with a polynomial time complexity [144]. The standard form of GP is defined as the minimization of a posynomial function subject to inequality posynomial constraints and equality monomial constraints as given below:

$$\underset{\boldsymbol{z}}{\text{minimize}} \qquad f_0(z) \tag{B.1}$$

subject to:

$$f_i(z) \leq 1, \quad \forall i = 1, .., m, \tag{B.2}$$

$$\tilde{f}_j(z) = 1, \quad \forall j = 1, .., M, \tag{B.3}$$

where $f_i(z)$, $i = 0, .., m$, are posynomials and $\tilde{f}_j(z)$, $j = 1, ..., M$ are monomials. Monomial are defined as a function $f : \mathbf{R}^n_{++} \rightarrow \mathbf{R}$ as follows

$$f(z) = z_0 z_1^{\bar{c_1}} z_2^{\bar{c_2}} ... z_n^{\bar{c_n}}, \tag{B.4}$$

where the multiplicative constant $z_0 \geq 0$, and the exponential constants $\bar{c}_i \in \mathbf{R}$, $i = 1, ..., n$. A posynomial is a nonnegative sum of monomials.

In general, GP in its standard form is a non-convex optimization problem, because posynomials and monomials functions are not convex functions. However, with a logarithmic change of the variables, objective function, and constraint functions, it can be turned into an equivalent convex form using the property that the logarithmic sum of exponential function is a convex (see [107] for more details). From a relaxed GP, we propose an approximation to solve out the original non-convex problem.

APPENDIX C. PUBLICATIONS

Book Chapters

1. **A. Alsharoa**, A. Celik, and A.E. Kamal,, "Energy Efficient 5G Networks Using Joint Energy Harvesting and Scheduling", accepted in 5G Networks: Fundamental Requirements, Enabling Technologies, and Operations Management, IEEE Wiley Book on 5G Networks, to appear, 2017.

Journal Papers

1. **A. Alsharoa**, H. Ghazzai, A. Kadri, and A.E. Kamal, "Spatial and Time Management of Multiple Solar Powered Drones Assisting Cellular HetNets", submitted to IEEE Transactions on Mobile Computing.

2. **A. Alsharoa**, H. Ghazzai, A.E. Kamal, and A. Kadri, "Optimization of the Power Splitting Protocol for Two Way Multiple Energy Harvesting Relay System", submitted to IEEE Transactions on Green Communications and Networking, 2nd round.

3. M. Selim, **A. Alsharoa**, A.E. Kamal, and M. Alnuem, "SURE: A Novel Approach for Self Healing Battery Starved Users using Energy Harvesting", accepted in IEEE Access.

4. A. Celik, **A. Alsharoa**, and A.E. Kamal, "Hybrid Energy Harvesting-Based Cooperative Spectrum Sensing and Access in Heterogeneous CRNs", IEEE Transactions on Cognitive Communications and Networking, vol. 3, no. 1, pp. 37-48, Mar. 2017.

5. **A. Alsharoa**, H. Ghazzai, E. Yaacoub, M.-S. Alouini, A.E. Kamal, "Joint Bandwidth and Power Allocation for MIMO Two-Way Relays-Assisted Overlay Cognitive Radio Sys-

tems", IEEE Transactions on Cognitive Communications and Networking, vol. 1, no. 4, pp. 383-393, Dec. 2015.

Conference Papers

1. **A. Alsharoa**, A. Celik, and A.E. Kamal, "Energy Harvesting in Heterogenous Networks with Hybrid Powered Communication Systems", submitted to IEEE 86th Vehicular Technology Conference (VTC-fall), Toronto, Canada.(*invited paper*).

2. **A. Alsharoa**, H. Ghazzai, A. Kadri, and A.E. Kamal "Energy Management in Cellular HetNets Assisted by Solar Powered Drone Small Cells", in proceeding of the IEEE Wireless Communication and Networking Conference (WCNC), San Francisco, CA, USA, Mar. 2017.

3. **A. Alsharoa**, H. Ghazzai, A.E. Kamal, and A. Kadri, "Near-Optimal Power Splitting Protocol for Energy Harvesting-based Two-Way Multiple-Relay Systems", in proceeding of the IEEE Wireless Communication and Networking Conference (WCNC), San Francisco, CA, USA, Mar. 2017.

4. H. Ghazzai, **A. Alsharoa**, A.E. Kamal, and A. Kadri, "A Multi-Relay Selection Scheme for Time Switching Energy Harvesting Two-Way Relaying Systems", in proceedings of the IEEE International Conference on Communications (ICC), Kuala Lumpur, Malaysia, May 2016.

5. **A. Alsharoa**, H. Ghazzai, A.E. Kamal, and A. Kadri, "Wireless RF-based Energy Harvesting for Two-Way-Relaying Systems", in proceedings of the IEEE Wireless Communication and Networking Conference (WCNC), Doha, Qatar, Apr. 2016.

6. **A. Alsharoa** and A.E. Kamal, "Green Downlink Radio Management Based Cognitive Radio LTE HetNets", in proceedings of the IEEE Global Telecommunications Conference (GLOBECOM), San Diego, CA, USA, Dec. 2015.

7. Y. Jie, **A. Alsharoa**, A.E. Kamal, and M. Alnuem, "Self-Healing Solution To Heterogeneous Networks Using CoMP", in the proceedings of the IEEE Global Telecommunications Conference (GLOBECOM), San Diego, CA, USA, Dec. 2015.

BIBLIOGRAPHY

[1] J. G. Andrews, S. Buzzi, W. Choi, S. V. Hanly, A. Lozano, A. C. K. Soong, and J. C. Zhang, "What will 5G be?," *IEEE Journal on Selected Areas in Communications*, vol. 32, pp. 1065–1082, June 2014.

[2] C. Bazelon and G. McHenry, "Substantial licensed spectrum deficit: Updating the FCCs mobile data demand projections," *Brattle Spectrum Deficit Report*, June 2015.

[3] Cisco VNI Mobile, "Cisco visual networking index: Global mobile data traffic forecast update, 2016-2021," 2017.

[4] H. Bogucka and O. Holland, "Multi-layer approach to future green mobile communications," *IEEE Intelligent Transportation Systems Magazine*, vol. 5, pp. 28–37, winter 2013.

[5] V. Chamola and B. Sikdar, "Solar powered cellular base stations: current scenario, issues and proposed solutions," *IEEE Communications Magazine*, vol. 54, pp. 108–114, May 2016.

[6] J. Yang, *Spatial channel characterization for cognitive radios.* Master thesis, University of California, Berkeley, 2004.

[7] S. Haykin, "Cognitive radio: Brain-empowered wireless communications," *IEEE Journal on Selected Areas in Communications*, vol. 23, no. 2, pp. 201–220, Feb. 2005.

[8] A. Goldsmith, S. Jafar, I. Maric, and S. Srinivasa, "Breaking spectrum gridlock with cognitive radios: An information theoretic perspective," *Proceedings of the IEEE*, vol. 97, no. 5, pp. 894–914, May 2009.

[9] J. Mitola III, *Cognitive Radio: An Integrated Agent Architecture for Software Defined Radio*. Ph.D. Dissertation, Royal Institute of Technology (KTH), Stockholm, Sweden, 2000.

[10] I. F. Akyildiz, W. y. Lee, M. C. Vuran, and S. Mohanty, "A survey on spectrum management in cognitive radio networks," *IEEE Communications Magazine*, vol. 46, pp. 40–48, Apr. 2008.

[11] A. Alsharoa, F. Bader, and M. Alouini, "Relay selection and resource allocation for two-way DF-AF cognitive radio networks," *IEEE Wireless Communications Letters*, vol. 2, no. 4, pp. 427–430, Aug. 2013.

[12] Y. Zou, Y.-D. Yao, and B. Zheng, "Cooperative relay techniques for cognitive radio systems: Spectrum sensing and secondary user transmissions," *IEEE Communications Magazine*, vol. 50, no. 4, pp. 98–103, Apr. 2012.

[13] Y. Zou, J. Zhu, B. Zheng, and Y.-D. Yao, "An adaptive cooperation diversity scheme with best-relay selection in cognitive radio networks," *IEEE Transactions on Signal Processing*, vol. 58, no. 10, pp. 5438–5445, Oct. 2010.

[14] W. Su, J. Matyjas, and S. Batalama, "Active cooperation between primary users and cognitive radio users in heterogeneous Ad-Hoc networks," *IEEE Transactions on Signal Processing*, vol. 60, no. 4, pp. 1796–1805, Apr. 2012.

[15] M. Hasna and M.-S. Alouini, "Optimal power allocation for relayed transmissions over Rayleigh-fading channels," *IEEE Transactions on Wireless Communications*, vol. 3, pp. 1999–2004, Nov. 2004.

[16] K. Jitvanichphaibool, R. Zhang, and Y.-C. Liang, "Optimal resource allocation for two-way relay-assisted OFDMA," *IEEE Transactions on Vehicular Technology*, vol. 58, no. 7, pp. 3311–3321, Sept. 2009.

[17] B. Rankov and A. Wittneben, "Spectral efficient protocols for half-duplex fading relay channels," *IEEE Journal on Selected Areas in Communications*, vol. 25, no. 2, pp. 379–389, Feb. 2007.

[18] G. Amarasuriya, C. Tellambura, and M. Ardakani, "Two-way amplify-and-forward multiple-input multiple-output relay networks with antenna selection," *IEEE Journal on Selected Areas in Communications*, vol. 30, no. 8, pp. 1513–1529, Sept. 2012.

[19] T. Cui, F. Gao, T. Ho, and A. Nallanathan, "Distributed space-time coding for two-way wireless relay networks," in *Proc. of the IEEE International Conference on Communications (ICC'2008), Beijing, China*, May 2008.

[20] H. Park, J. Chun, and R. Adve, "Computationally efficient relay antenna selection for af MIMO two-way relay channels," *IEEE Transactions on Signal Processing*, vol. 60, no. 11, pp. 6091–6097, Nov 2012.

[21] J. Xu and R. Zhang, "Throughput optimal policies for energy harvesting wireless transmitters with non-ideal circuit power," *IEEE Journal on Slected Areas in Communications*, vol. 32, no. 2, pp. 322–332, Feb. 2014.

[22] S. Ulukus, A. Yener, E. Erkip, O. Simeone, M. Zorzi, P. Grover, and K. Huang, "Energy harvesting wireless communications: A review of recent advances," *IEEE Journal on Selected Areas in Communications*, vol. 33, pp. 360–381, Mar. 2015.

[23] H. Tabassum, E. Hossain, A. Ogundipe, and D. I. Kim, "Wireless-powered cellular networks: Key challenges and solution techniques," *IEEE Communications Magazine*, vol. 53, no. 6, pp. 63–71, June 2015.

[24] Z. Hasan, H. Boostanimehr, and V. Bhargava, "Green cellular networks: A survey, some research issues and challenges," *IEEE Communications Surveys & Tutorials*, vol. 13, no. 4, pp. 524–540, Fourth 2011.

[25] V. Raghunathan, S. Ganeriwal, and M. Srivastava, "Emerging techniques for long lived wireless sensor networks," *IEEE Communications Magazine*, vol. 44, no. 4, pp. 108–114, Apr. 2006.

[26] X. Lu, P. Wang, D. Niyato, D. I. Kim, and Z. Han, "Wireless networks with RF energy harvesting: A contemporary survey," *IEEE Communications Surveys Tutorials*, vol. 17, no. 2, pp. 757–789, May 2015.

[27] B. Medepally and N. Mehta, "Voluntary energy harvesting relays and selection in cooperative wireless networks," *IEEE Transactions on Wireless Communications*, vol. 9, no. 11, pp. 3543–3553, Nov. 2010.

[28] F. Yuan, S. Jin, K. Wong, and H. Zhu, "Optimal harvest-use-store policy for energy-harvesting wireless systems in frequency-selective fading channels," *EURASIP Journal on Wireless Communications and Networking*, vol. 2015, no. 1, Mar. 2015.

[29] A. Ghosh, N. Mangalvedhe, R. Ratasuk, B. Mondal, M. Cudak, E. Visotsky, T. A. Thomas, J. G. Andrews, P. Xia, H. S. Jo, H. S. Dhillon, and T. D. Novlan, "Heterogeneous cellular networks: From theory to practice," *IEEE Communications Magazine*, vol. 50, pp. 54–64, June 2012.

[30] E. Yaacoub, "Green communications in lte networks with environmentally friendly small cell base stations," in *Proc. of the 2012 IEEE Online Conference on Green Communications (GreenCom)*, pp. 110–115, Sept. 2012.

[31] C. Liu, B. Natarajan, and H. Xia, "Small cell base station sleep strategies for energy efficiency," *IEEE Transactions on Vehicular Technology*, vol. 65, no. 3, pp. 1652–1661, Mar. 2016.

[32] S. Hayat, E. Yanmaz, and R. Muzaffar, "Survey on unmanned aerial vehicle networks for civil applications: A communications viewpoint," *IEEE Communications Surveys Tutorials*, vol. 18, pp. 2624–2661, Fourthquarter 2016.

[33] L. Gupta, R. Jain, and G. Vaszkun, "Survey of important issues in uav communication networks," *IEEE Communications Surveys Tutorials*, vol. 18, Secondquarter 2016.

[34] I. Bucaille et al., "Rapidly deployable network for tactical applications: Aerial base station with opportunistic links for unattended and temporary events absolute example," in *Proc. of the IEEE Military Communications Conference (MILCOM), San Diego, CA, USA*, pp. 1116–1120, Nov. 2013.

[35] AT&T/Qualcomm, "Qualcomm and AT&T to trial drones on cellular network to accelerate wide-scale deployment," http://about.att.com/story/qualcomm_and_att_to_trial_drones_on_cellular_network.html.

[36] AT&T/Intel, "AT&T and Intel to test drones on LTE network," http://about.att.com/story/att_and_intel_to_test_drones_on_lte_network.html.

[37] Nokia, "Nokia showcases power of drones and LTE connectivity for public safety at D4G award event in Dubai," https://www.nokia.com/en_int/news/releases/2017/02/17/nokia-showcases-power-of-drones-and-lte-connectivity-for-public-safety-at-d4g-award-event-in-dubai,.

[38] Y. Zeng, R. Zhang, and T. J. Lim, "Wireless communications with unmanned aerial vehicles: Opportunities and challenges," *IEEE Communications Magazine*, vol. 54, pp. 36–42, May 2016.

[39] T. Schouwenaars, B. DeMoor, E. Feron, and J. How, "Mixed integer programming for multi-vehicle path planning," in *Proc. of the European Controls Conference, Orlando, Florida, USA*, p. 26032608, Dec. 2011.

[40] S. Ulukus, A. Yener, E. Erkip, O. Simeone, M. Zorzi, P. Grover, and K. Huang, "Energy harvesting wireless communications: A review of recent advances," *IEEE Journal on Selected Areas in Communications*, vol. 33, no. 3, pp. 360–381, Mar. 2015.

[41] S. Mirjalili, S-M. Mirjalili, and A. Lewis, "Grey wolf optimizer," *Elsevier Advances in Engineering Software*, vol. 69, no. 1, pp. 46–61, Mar. 2014.

[42] M. Chiang, C. W. Tan, D. P. Palomar, D. O'Neill and D. Julian, "Power control by geometric programming," *IEEE Transactions on Wireless Communications*, vol. 6, no. 7, pp. 2640–2651, July 2007.

[43] M. Mitchell, *An Introduction to Genetic Algorithms*. Cambridge, MA, USA: MIT Press, 1998.

[44] S. Chandrasekharan, K. Gomez, A. Al-Hourani, S. Kandeepan, T. Rasheed, L. Goratti, L. Reynaud, D. Grace, I. Bucaille, T. Wirth, and S. Allsopp, "Designing and implementing future aerial communication networks," *IEEE Communications Magazine*, vol. 54, pp. 26–34, May 2016.

[45] R. D'Sa, D. Jenson, T. Henderson, J. Kilian, B. Schulz, M. Calvert, T. Heller, and N. Papanikolopoulos, "SUAV:Q - An improved design for a transformable solar-powered UAV," in *Proc. of the IEEE/RSJ International Conference on Intelligent Robots and Systems (IROS 2016), Daejeon, Korea*, pp. 1609–1615, Daejeon, South Korea, Oct. 2016.

[46] S. Toroujeni, S. Sadough, and S. Ghorashi, "Spectrum leasing for OFDM-Based cognitive radio networks," *IEEE Transactions on Vehicular Technology*, vol. 62, no. 5, pp. 2131–2139, June 2013.

[47] S. Jayaweera and T. Li, "Dynamic spectrum leasing in cognitive radio networks via primary-secondary user power control games," *IEEE Transactions on Wireless Communications*, vol. 8, no. 6, pp. 3300–3310, June 2009.

[48] F. Gomez-Cuba, R. Asorey-Cacheda, F. Gonzalez-Castano, and H. Huang, "Application of cooperative diversity to cognitive radio leasing: Model and analytical characterization of resource gains," *IEEE Transactions on Wireless Communications*, vol. 12, no. 1, pp. 40–49, Jan. 2013.

[49] O. Simeone, I. Stanojev, S. Savazzi, Y. Bar-Ness, U. Spagnolini, and R. Pickholtz, "Spectrum leasing to cooperating secondary Ad Hoc networks," *IEEE Journal on Selected Areas in Communications*, vol. 26, no. 1, pp. 203–213, Jan. 2008.

[50] E. Biglieri, A. Goldsmith, L. Greenstein, N. Mandayam, and H. Poor, *Principles of cognitive radio*. New York, NY, USA: Cambridge University Press, 2012.

[51] Y. Pei and Y.-C. Liang, "Resource allocation for device-to-device communications overlaying two-way cellular networks," *IEEE Transactions on Wireless Communications*, vol. 12, no. 7, pp. 3611–3621, July 2013.

[52] Q. Li, S. H. Ting, A. Pandharipande, and Y. Han, "Cognitive spectrum sharing with two-way relaying systems," *IEEE Transactions on Vehicular Technology*, vol. 60, no. 3, pp. 1233–1240, Mar. 2011.

[53] A. Hyadi, E. Driouch, W. Ajib, and M.-S. Alouini, "Overlay cognitive radio systems with adaptive two-way relaying," in *Proc. of the IEEE Global Communications Conference (GLOBECOM'2013), Atlanta, Georgia, USA*, pp. 937–942, Nov. 2013.

[54] A. Alizadeh, S.-S. Sadough, and N. Khajavi, "Optimal beamforming in cognitive two-way relay networks," in *Proc. of the IEEE 21st International Symposium on Personal Indoor and Mobile Radio Communications (PIMRC'2010), Istanbul, Turkey*, pp. 2331–2335, Sept. 2010.

[55] A. Alsharoa, H. Ghazzai, E. Yaacoub, and M.-S. Alouini, "Bandwidth and power allocation for two-way relaying in overlay cognitive radio systems," in *Proc. of the IEEE Global Communications Conference (GLOBECOM'2014), Austin, Texas, USA*, pp. 911–916, Dec. 2014.

[56] A. Nasir, X. Zhou, S. Durrani, and R. Kennedy, "Relaying protocols for wireless energy harvesting and information processing," *IEEE Transactions on Wireless Communications*, vol. 12, no. 7, pp. 3622–3636, July 2013.

[57] Y. Gu and S. Aissa, "RF-based energy harvesting in decode-and-forward relaying systems: Ergodic and outage capacities," *IEEE Transactions on Wireless Communications*, vol. 14, no. 11, pp. 6425–6434, Nov. 2015.

[58] Y. Luo, J. Zhang, and K. Letaief, "Relay selection for energy harvesting cooperative communication systems," in *Proc. of the IEEE Global Communications Conference (GLOBECOM 2013), Atlanta, GA, USA*, Dec. 2013.

[59] A. Nasir, X. Zhou, S. Durrani, and R. Kennedy, "Wireless-powered relays in cooperative communications: Time-switching relaying protocols and throughput analysis," *IEEE Transactions on Communications*, vol. 63, no. 5, pp. 1607–1622, May. 2015.

[60] S. Gupta, R. Zhang, and L. Hanzo, "Throughput maximization for a buffer-aided successive relaying network employing energy harvesting," *IEEE Transactions on Vehicular Technology*, vol. 65, no. 8, pp. 6758–6765, Aug. 2016.

[61] S. Atapattu and J. Evans, "Optimal energy harvesting protocols for wireless relay networks," *IEEE Transactions on Wireless Communications*, vol. 15, no. 8, pp. 5789–5803, Aug. 2016.

[62] K. H. Liu, "Performance analysis of relay selection for cooperative relays based on wireless power transfer with finite energy storage," *IEEE Transactions on Vehicular Technology*, vol. 65, pp. 5110–5121, July 2016.

[63] Y. Liu, L. Wang, M. Elkashlan, T. Duong, and A. Nallanathan, "Two-way relaying networks with wireless power transfer: Policies design and throughput analysis," in *Proc. of the IEEE Global Communications Conference (GLOBECOM 2014), Austin, TX, USA*, Dec. 2014.

[64] K. Tutuncuoglu, B. Varan, and A. Yener, "Throughput maximization for two-way relay channels with energy harvesting nodes: The impact of relaying strategies," *IEEE Transactions on Communications*, vol. 63, no. 6, pp. 2081–2093, June 2015.

[65] M.-L. Ku and W. Li, Y. Chen and K. J. Ray Liu, "Advances in energy harvesting communications: Past, present, and future challenges," *IEEE Communications Surveys & Tutorials*, vol. 18, no. 2, pp. 1384–1412, First Quarter 2016.

[66] L. Roselli et al., "Smart surfaces: Large area electronics systems for Internet of things enabled by energy harvesting," *Proceedings of the IEEE*, vol. 102, no. 11, pp. 1723–1746, Nov. 2014.

[67] K. Niotaki, A. Collado, A. Georgiadis, S. Kim, and M. M. Tentzeris, "Solar/electromagnetic energy harvesting and wireless power transmission," *Proceedings of the IEEE*, vol. 102, no. 11, pp. 1712–1722, Nov. 2014.

[68] S. Kim, R. Vyas, J. Bito, K. Niotaki, A. Collado, A. Georgiadis, and M. M. Tentzeris, "Ambient RF energy-harvesting technologies for self-sustainable standalone wireless sensor platforms," *Proceedings of the IEEE*, vol. 102, no. 11, pp. 1649–1666, Nov. 2014.

[69] J. Bito, R. Bahr, J. G. Hester, S. A. Nauroze, A. Georgiadis, and M. M. Tentzeris, "A novel solar and electromagnetic energy harvesting system with a 3-D printed package for energy efficient Internet-of-things wireless sensors," *to appear in IEEE Transactions on Microwave Theory and Techniques*, 2017.

[70] F. Wang, S. Guo, Y. Yang, B. Xiao, "Relay selection and power allocation for cooperative communication networks with energy harvesting," *to appear in IEEE Systems Journal*, 2017.

[71] G. Fettweis and E. Zimmermann, "ICT energy consumption trends and challenges," in *Proc. of the 11th International Symposium on Wireless Personal Multimedia Communications (WPMC 2008), Oulu, Filand*, Sept. 2008.

[72] E. Oh, K. Son, and B. Krishnamachari, "Dynamic base station switching-on/off strategies for green cellular networks," *IEEE Transactions on Wireless Communications*, vol. 12, no. 5, pp. 2126–2136, May 2013.

[73] G. Koudouridis, H. Gao, and P. Legg, "A centralised approach to power on-off optimisation for heterogeneous networks," in *Proc. of the 76nd IEEE Vehicular Technology Conference (VTC Fall 2012), Qubec City, Canada*, Quebec, Canada, Sept. 2012.

[74] H. Ghazzai, E. Yaacoub, M.-S. Alouini, and A. Abu-Dayya, "Optimized smart grid energy procurement for LTE networks using evolutionary algorithms," *IEEE Transactions on Vehicular Technology*, vol. 63, no. 9, pp. 4508–4519, Nov. 2014.

[75] Y. S. Soh, T. Q. S. Quek, M. Kountouris, and H. Shin, "Energy efficient heterogeneous cellular networks," *IEEE Journal on Selected Areas in Communications*, vol. 31, no. 5, pp. 840–850, May 2013.

[76] I. Ashraf, F. Boccardi, and L. Ho, "Sleep mode techniques for small cell deployments," *IEEE Communications Magazine*, vol. 49, no. 8, pp. 72–79, Aug. 2011.

[77] L. Falconetti, P. Frenger, H. Kallin, and T. Rimhagen, "Energy efficiency in heterogeneous networks," in *Proc. of the IEEE Online Conference on Green Communications (GreenCom)*, Sept. 2012.

[78] H. Liang, A. K. Tamang, W. Zhuang, and X. S. Shen, "Stochastic information management in smart grid," *IEEE Communications Surveys Tutorials*, vol. 16, pp. 1746–1770, Third Quarter 2014.

[79] J. Leithon, S. Sun, and T. J. Lim, "Energy management strategies for base stations powered by the smart grid," in *Proc. of the IEEE Global Communications Conference (GLOBECOM), Atlanta, GA, USA*, pp. 2635–2640, Dec. 2013.

[80] T. Han and N. Ansari, "On optimizing green energy utilization for cellular networks with hybrid energy supplies," *IEEE Transactions on Wireless Communications*, vol. 12, pp. 3872–3882, Aug. 2013.

[81] H. A. H. Hassan, A. Pelov, and L. Nuaymi, "Integrating cellular networks, smart grid, and renewable energy: Analysis, architecture, and challenges," *IEEE Access*, vol. 3, pp. 2755–2770, 2015.

[82] T. Han and N. Ansari, "Powering mobile networks with green energy," *IEEE Wireless Communications*, vol. 21, pp. 90–96, Feb. 2014.

[83] V. Chamola and B. Sikdar, "Solar powered cellular base stations: current scenario, issues and proposed solutions," *IEEE Communications Magazine*, vol. 54, pp. 108–114, May 2016.

[84] J. Leithon, T. J. Lim, and S. Sun, "Online energy management strategies for base stations powered by the smart grid," in *2013 IEEE International Conference on Smart Grid Communications (SmartGridComm)*, pp. 199–204, Oct. 2013.

[85] S. Bu, F. R. Yu, Y. Cai, and X. P. Liu, "When the smart grid meets energy-efficient communications: Green wireless cellular networks powered by the smart grid," *IEEE Transactions on Wireless Communications*, vol. 11, pp. 3014–3024, Aug. 2012.

[86] J. Xu, L. Duan, and R. Zhang, "Cost-aware green cellular networks with energy and communication cooperation," *IEEE Communications Magazine*, vol. 53, pp. 257–263, May 2015.

[87] V. K. Bhargava and A. Leon-Garcia, "Green cellular networks: A survey, some research issues and challenges," in *2012 26th Biennial Symposium on Communications (QBSC)*, pp. 1–2, May 2012.

[88] P. S. Yu, J. Lee, T. Q. S. Quek, and Y. W. P. Hong, "Traffic offloading in heterogeneous networks with energy harvesting personal cells-network throughput and energy efficiency," *IEEE Transactions on Wireless Communications*, vol. 15, pp. 1146–1161, Feb. 2016.

[89] M. B. Ghorbel, T. Touzri, B. Hamdaoui, M. Guizani, and B. Khalfi, "Joint user-channel assignment for efficient use of renewable energy in hybrid powered communication systems," in *Proc. of the IEEE Global Communications Conference (GLOBECOM 2015), San Diego, CA, USA*, pp. 1–6, Dec. 2015.

[90] M. J. Farooq, H. Ghazzai, A. Kadri, H. ElSawy, and M. S. Alouini, "A hybrid energy sharing framework for green cellular networks," *IEEE Transactions on Communications*, vol. 65, pp. 918–934, Feb. 2017.

[91] S. Rohde and C. Wietfeld, "Interference aware positioning of aerial relays for cell overload and outage compensation," in *Proc. of the IEEE Vehicular Technology Conference (VTC Fall), Quebec, QC, Canada*, pp. 1–5, Sept. 2012.

[92] P. Zhan, K. Yu, and A. L. Swindlehurst, "Wireless relay communications using ann unmanned aerial vehicle," in *IEEE Workshop on Signal Processing Advances in Wireless Communications, Cannes, France*, pp. 1–5, July 2006.

[93] J. Komerl and A. Vilhar, "Base stations placement optimization in wireless networks for emergency communications," pp. 200–205, June 2014.

[94] Z. Han, A. L. Swindlehurst, and K. J. R. Liu, "Optimization of MANET connectivity via smart deployment/movement of unmanned air vehicles," *IEEE Transactions on Vehicular Technology*, vol. 58, pp. 3533–3546, Sept. 2009.

[95] I. Bekmezci, M. Ermis, and S. Kaplan, "Connected multi UAV task planning for flying ad hoc networks," in *Proc. of the IEEE International Black Sea Conference on Communications and Networking (BlackSeaCom), Odessa, Ukraine*, pp. 28–32, May 2014.

[96] J. Scherer and B. Rinner, "Persistent multi-UAV surveillance with energy and communication constraints," in *Proc. of the IEEE International Conference on Automation Science and Engineering (CASE), Fort Worth, TX, USA*, pp. 1225–1230, Aug. 2016.

[97] T. Schouwenaars, J. How, and E. Feron, "Receding horizon path planning with implicit safety guarantees," in *Proc. of the American Control Conference, Boston, MA, USA*, pp. 5576–5581, June 2004.

[98] M. Mozaffari, W. Saad, M. Bennis, and M. Debbah, "Drone small cells in the clouds: Design, deployment and performance analysis," in *Proc. of the IEEE Global Communications Conference (GLOBECOM), San diego, CA, USA*, pp. 1–6, Dec. 2015.

[99] Q. Feng, E. K. Tameh, A. R. Nix, and J. McGeehan, "Modelling the likelihood of line-of-sight for air-to-ground radio propagation in urban environments," in *Proc. of the IEEE Global Communications Conference (GLOBECOM), San Francisco, CA, USA*, pp. 1–5, Nov.- Dec 2006.

[100] Q. Feng, J. McGeehan, E. K. Tameh, and A. R. Nix, "Path loss models for air-to-ground radio channels in urban environments," in *Proc. of the 63rd IEEE Vehicular Technology Conference (VTC Spring), Melbourne, VIC, Australia*, pp. 2901–2905, May 2006.

[101] A. Al-Hourani, S. Kandeepan, and A. Jamalipour, "Modeling air-to-ground path loss for low altitude platforms in urban environments," in *Proc. of the IEEE Global Communications Conference (GLOBECOM), Austin, TX, USA*, pp. 2898–2904, Dec. 2014.

[102] M. Mozaffari, W. Saad, M. Bennis, and M. Debbah, "Unmanned aerial vehicle with underlaid device-to-device communications: Performance and tradeoffs," *IEEE Transactions on Wireless Communications*, vol. 15, pp. 3949–3963, June 2016.

[103] S. Chang and B. Kelley, "An efficient time synchronization scheme for broadband two-way relaying networks based on physical-layer network coding," *IEEE Communications Letters*, vol. 16, no. 9, pp. 1416–1419, Sept. 2012.

[104] X. Bi, J. Zhang, Y. Wang, and P. Viswanath, "Fairness improvement of maximum C/I scheduler by dumb antennas in slow fading channel," in *Proc. of the 72nd IEEE Vehicular Technology Conference (VTC Fall 2010), Ottawa, Ontario, Canada*, Sept. 2010.

[105] Y. Song, G.and Li, "Cross-layer optimization for OFDM wireless networks-Part I: Theoretical framework," *IEEE Transactions on Wireless Communications*, vol. 4, no. 2, pp. 614–624, Apr. 2005.

[106] T. Zhang, Z. Zeng, and Y. Qiu, "A subcarrier allocation algorithm for utility proportional fairness in OFDM systems," in *Proc. of the 67th IEEE Vehicular Technology Conference (VTC Spring 2008), Singapore City, Singapore*, May 2008.

[107] S. Boyd and L. Vandenberghe, *Convex Optimization*. New York, NY, USA: Cambridge University Press, 2004.

[108] S. Boyd and A. Mutapcic, "Stochastic Subgradient Methods." *Notes for EE364, Stanford University*, Winter. 2006-07.

[109] J. Kennedy and R. Eberhart, "A discrete binary version of the particle swarm algorithm," in *Proc. of the IEEE International Conference on Systems, Man, and Cybernetics. Computational Cybernetics and Simulation*, vol. 5, pp. 4104–4108, Orlando, FL, USA, Oct. 1997.

[110] A. Alsharoa, H. Ghazzai, A. E. Kamal, A. Kadri, "Wireless RF-based energy harvesting for two-way relaying systems," in *Proc. of the IEEE Wireless Conference and Networking Conference (WCNC 2016), Duha, Qatar*, Doha, Qatar, Apr. 2016.

[111] X. Zhou, R. Zhang, and C. K. Ho, "Wireless information and power transfer: Architecture design and rate-energy tradeoff," *IEEE Transactions on Communications*, vol. 61, no. 11, pp. 4754–4767, Nov. 2013.

[112] A. Alsharoa, F. Bader, and M. Alouini, "Relay selection and resource allocation for two-way DF-AF cognitive radio networks," *IEEE Wireless Communications Letters*, vol. 2, no. 4, pp. 427–430, Aug. 2013.

[113] M. O. Hasna and M. S. Alouini, "End-to-end performance of transmission systems with relays over rayleigh-fading channels," *IEEE Transactions on Wireless Communications*, vol. 2, pp. 1126–1131, Nov. 2003.

[114] M. Ju and I. M. Kim, "Relay selection with ANC and TDBC protocols in bidirectional relay networks," *IEEE Transactions on Communications*, vol. 58, pp. 3500–3511, Dec. 2010.

[115] L. Liu, R. Zhang, and K.-C. Chua, "Wireless information and power transfer: A dynamic power splitting approach," *IEEE Transactions on Communications*, vol. 61, no. 9, pp. 3990–4001, Sept. 2013.

[116] J. Papandriopoulos and J. S. Evans, "SCALE: A low-complexity distributed protocol for spectrum balancing in multiuser DSL networks," *IEEE Transactions on Information Theory*, vol. 55, no. 8, pp. 3711–3724, Aug. 2009.

[117] A. H. Land and A. G. Doig, "An automatic method of solving discrete programming problems," *Econometrica*, vol. 28, pp. 497–520, July 1960.

[118] S. R. Douglas, "On the computational complexity of branch and bound search strategies," *Monterey, California: Naval Postgraduate School*, vol. 63, no. 6, pp. 2081–2093, Nov. 1979.

[119] M. J. Brusco, S. Stahl, *Branch-and-Bound Applications in Combinatorial Data Analysis*. Springer New York, 2005.

[120] F. Shahin, *ZigBee Wireless Networks and Transceivers*. USA: Newnes PAP/COM edition, 2008.

[121] Y. Chen, K. T. Sabnis, and R. A. Abd-Alhameed, "New formula for conversion efficiency of rf eh and its wireless applications," *IEEE Transactions on Vehicular Technology*, vol. 65, pp. 9410–9414, Nov. 2016.

[122] A. W. Manyonge, R. M. Ochieng, F. N. Onyango, and J. M. Shichikha, "Mathematical modeling of wind turbine in a wind energy conversion system: Power coefficient analysis," *Applied Mathematical Sciences*, vol. 6, pp. 4527–4536, Jan. 2012.

[123] B. Dusza, C. Ide, L. Cheng, and C. Wietfeld, "An accurate measurement-based power consumption model for LTE uplink transmissions," in *Proc. of the IEEE Computer Communications Workshops in conjunctions of IEEE International Conference on Computer Communications (INFOCOM 2013), Turin, Italy*, pp. 49–50, Apr. 2013.

[124] B.-M. Hodge and D. L. M. Milligan, "Short-term load forecasting error distributions and implications for renewable integration studies," in *Proc. of the IEEE Green Technologies Conference, Denver, CO, USA*, Apr. 2013.

[125] M. Mureddu and H. Meyer-Ortmanns, "Extreme prices in electricity balancing markets from an approach of statistical physics," in *arXiv:1612.05525*, Dec. 2016.

[126] "Gurobi optimizer reference manual," 2016. Available [online]: http://www.gurobi.com/.

[127] CVX Research, Inc., "CVX: MATLAB Software for disciplined convex programming, version 2.0," Aug. 2012. Available [online]: http://cvxr.com/cvx/.

[128] D. Beasley, D. R. Bull, and R. R. Martin, "An overview of genetic algorithms: Part 2, Research topics," *University Computing*, vol. 15, no. 4, pp. 170–181, 1993.

[129] H. Ghazzai, M. J. Farooq, A. Alsharoa, E. Yaacoub, A. Kadri, and M. S. Alouini, "Green networking in cellular hetnets: A unified radio resource management framework with base station ON/OFF switching," *to appear in IEEE Transactions on Vehicular Technology*, 2017.

[130] "Energy efficiency analysis of the reference systems, areas of improvements and target breakdown." *Energy Aware Radio and neTwork tecHnologies*, Dec. 2010.

[131] Y. W. Y. Zheng and F. Meng, "Modeling and simulation of pathloss and fading for air-ground link of haps within a network simulator," in *Proc. of the IEEE International Conference on Cyber-Enabled Distributed Computing and Knowledge Discovery (CyberC), Beijing, China*, Oct. 2013.

[132] A. Al-Hourani, S. Kandeepan, and S. Lardner, "Optimal LAP altitude for maximum coverage," *IEEE Wireless Communications Letters*, vol. 3, no. 6, pp. 569–572, Dec. 2014.

[133] J. V. Dries Hulens and T. Goedeme, "How to choose the best embedded processing platform for onboard UAV image processing," in *Proc. of the International Joint Conference Computer Vision, Imaging and Computer Graphics Theory and Applications (VISIGRAPP), Berlin, Germany*, Mar. 2015.

[134] R. Zakaria, M. Dib, L. Moalic, and A. Caminada, "Car relocation for carsharing service: Comparison of CPLEX and greedy search," in *Proc. of the IEEE Symposium on Computational Intelligence in Vehicles and Transportation Systems, Orlando, Florida, USA*, pp. 51–58, Dec. 2014.

[135] P. Kall and J. Mayer, *Stochastic Linear Programming: Models, Theory, and Computation. International series in operations research and management science*. New York: Springer, 2005.

[136] S. Kwon, L. Ntaimo, and N. Gautam, "Optimal day-ahead power procurement with renewable energy and demand response," *IEEE Transactions on Power Systems*, vol. PP, no. 99, pp. 1–1, 2016.

[137] C. I. Fabian and Z. Szoke, "Solving two-stage stochastic programming problems with level decomposition," *Computational Management Science*, vol. 4, no. 4, p. 313353, Oct. 2007.

[138] J. Kennedy and R. Eberhart, "Particle swarm optimization," in *Proc. of the IEEE International Conference on Neural Networks, Perth, Australia*, pp. 1942–1948, Nov/Dec. 1995.

[139] H. Chen, C. Tse, and J. Feng, "Minimizing effective energy consumption in multi-cluster sensor networks for source extraction," *IEEE Transactions on Wireless Communications*, vol. 8, no. 3, pp. 1480–1489, Mar. 2009.

[140] J. Zhang, S. Chen, X. Mu, and L. Hanzo, "Evolutionary-algorithm-assisted joint channel estimation and turbo multiuser detection/decoding for OFDM/SDMA," *IEEE Transactions on Vehicular Technology*, vol. 63, no. 3, pp. 1204–1222, Mar. 2014.

[141] S. Efazati and P. Azmi, "Effective capacity maximization in multirelay networks with a novel cross-layer transmission framework and power-allocation scheme," *IEEE Transactions on Vehicular Technology*, vol. 63, no. 4, pp. 1691–1702, May 2014.

[142] M. Clerc and J. Kennedy, "The particle swarm-explosion, stability, and convergence in a multidimensional complex space," *IEEE Transactions on Evolutionary Computation*, vol. 6, no. 3, pp. 58–73, Feb. 2002.

[143] Q. Bai, "Analysis of particle swarm optimization algorithm," *Computer and Information Science*, vol. 3, no. 1, pp. 180–184, Feb. 2010.

[144] Y. Nesterov and A. Nemirovskii, *Interior-Point Polynomial Algorithms in Convex Programming*. Society for Industrial and Applied Mathematics, 1994.